

8-2002

Numerical Wave Simulations on Different Oceanic Scales

Khalid M. Zubier

Follow this and additional works at: <http://digitalcommons.library.umaine.edu/etd>

 Part of the [Oceanography Commons](#)

Recommended Citation

Zubier, Khalid M., "Numerical Wave Simulations on Different Oceanic Scales" (2002). *Electronic Theses and Dissertations*. 175.
<http://digitalcommons.library.umaine.edu/etd/175>

This Open-Access Dissertation is brought to you for free and open access by DigitalCommons@UMaine. It has been accepted for inclusion in Electronic Theses and Dissertations by an authorized administrator of DigitalCommons@UMaine.

NUMERICAL WAVE SIMULATIONS ON DIFFERENT OCEANIC SCALES

By

Khalid M. Zubier

B.S. King Abdulaziz University, 1990

M.S. University of Maine, 1997

A THESIS

**Submitted in Partial Fulfillment of the
Requirements for the Degree of
Doctor of Philosophy
(in Oceanography)**

**The Graduate School
The University of Maine**

August, 2002

Advisory Committee:

Vijay G. Panchang, Professor of Oceanography, Advisor

Neal Pettigrew, Associate Professor of Oceanography

Huijie Xue, Associate Professor of Oceanography

Fei Chai, Associate Professor of Oceanography

Zeki Demirbilek, Senior Research Engineer

LIBRARY RIGHTS STATEMENT

In presenting this thesis in partial fulfillment of the requirements for an advanced degree at The University of Maine, I agree that the Library shall make it freely available for inspection. I further agree that permission for "fair use" copying of this thesis for scholarly purposes may be granted by the Librarian. It is understood that any copying or publication of this thesis for financial gain shall not be allowed without my written permission.

Signature:

A handwritten signature in black ink, appearing to be 'C. J. ...' with a stylized flourish at the end.

Date:

August 23, 2002

NUMERICAL WAVE SIMULATIONS ON DIFFERENT OCEANIC SCALES

By Khalid M. Zubier

Thesis Advisor: Dr. Vijay G. Panchang

An Abstract of the Thesis Submitted
in Partial Fulfillment of the Requirements for the
Degree of Doctor of Philosophy
(in Oceanography)
August, 2002

In practical applications, numerical wave models are used as reliable tools to provide near future wave predictions and wave climatology for specific region. Obviously models first should go through extensive validation/verification procedures. Once validated, models can be used in scientific applications to investigate methods for improving performance and to develop better understanding of wave associated physical mechanisms and their interactions in specific field experiments.

Two wave transformation models, SWAN and CGWAVE, are used to simulate wave conditions at the Field Research Facility, Duck (North Carolina). The motivation is to examine how well these models reproduce observations and to determine the level of consistency between the two models. Stationary wave conditions pertaining to three different storm-induced bathymetric representations are modeled. It was found that SWAN and CGWAVE reproduced the observed wave behavior to a large extent, but

CGWAVE results tended to be somewhat smaller than the SWAN results and the measurements. The differences were attributed to wave-wave interactions and breaking. Otherwise the models showed a high level of consistency. SWAN and CGWAVE were also used to explore other mechanisms reported in the recent literature; the results were either consistent with some observations (in the case of the nonlinear mechanisms) or they shed more light on others (in case of the role of the research pier legs).

An operational high resolution wave prediction system for the Gulf of Maine was experimentally developed. Attempts were then made to improve the quality of the SWAN model predictions through the assimilation of observed wave data into the model simulations. It was demonstrated that a simple data assimilation scheme that uses only the observed significant wave height to correct the energy level of the predicted full 2D wave spectrum may improve the quality of wave forecasting model predictions for up to 2 days. Shorter relaxation times were attributed to inaccurate predictions of the wind field and/or inadequate representation of the boundary conditions. The results suggests that a simple and computationally inexpensive assimilation scheme is sufficient and would be of a greater benefit to high resolution operational wave prediction systems for the Gulf of Maine.

DEDICATION

THIS DISSERTATION IS DEDICATED TO:

MY PARENTS,

MY WIFE,

AND MY CHILDREN

ACKNOWLEDGEMENTS

I would like to thank my research advisor, Dr. Vijay Panchang, for his consistent and invaluable support, guidance and friendship throughout the last five years of my graduate study at the University of Maine. I would also like to express my thanks to my research committee members for all the advices and suggestions they offered during the course of my research. I am grateful to Dr. Kewal Puri, for his continuous encouragement. I also would like to express my appreciation to my fellow graduate students for their team work spirit and their helpful discussions.

A special note of thanks goes to the Saudi Arabian Ministry of Higher Education represented by King Abdulaaziz University for sponsoring my graduate studies in the United States. Thanks are also due to my professors, friends and colleagues at the Faculty of Marine Sciences, King Abdulaziz University for their continous support. The support and encouragement by the faculty members of the School of Marine Scinces, University of Maine is also appreciated. I am also thankful to all my friends here in the United States and back in Saudi Arabia for offering me their precious friendship and for their effort to make my life easier.

The endless support and encouragement by my parents, my wife, my son and daughter made the completion of this dissertation possible.

TABLE OF CONTENTS

DEDICATION	ii
ACKNOWLEDGEMENTS	iii
LIST OF TABLES	vi
LIST OF FIGURES	viii

Chapter

1. INTRODUCTION	1
1.1 Numerical Wave Modeling (Background)	1
1.2 General Characteristics of Numerical Wave Models	3
1.3 SWAN Model	8
1.4 Thesis Layout	10
2. SIMULATION OF WAVES AT DUCK (NORTH CAROLINA) USING TWO NUMERICAL MODELS	13
2.1 Introduction	13
2.2 Description of Models	16
2.3 Study Area and Modeling Details	21
2.4 Results and Discussion	33
2.4.1 Quantitative Model Performance	34
2.4.2 Qualitative Model Performance	50
2.4.3 Effect of the Pilings	59
2.5 Concluding Remarks	63

3.	OPERATIONAL WAVE PREDICTION AND WAVE DATA ASSIMILATION AT THE GULF OF MAINE	66
3.1	Introduction	66
3.2	Wind and Wave Climates in the Gulf of Maine	70
3.2.1	General Background	70
3.2.2	Description of Storms	74
3.3	Modeling Details	81
3.3.1	SWAN Model	81
3.3.2	Modeling Schemes	82
3.3.3	Data Assimilation Scheme	84
3.3.4	Boundary Conditions Schemes	91
3.4	Results and Discussion	93
3.4.1	Sample Case	94
3.4.2	Test Case	99
3.4.3	Simulations of Year 2001 Seasonal Maximum Wave Conditions	105
3.4.4	Spatial scale of assimilation impact	129
3.5	Summary and Conclusions	136
4.	SUMMARY AND CONCLUDING REMARKS	143
	REFERENCES	149
	APPENDIX A. Statistical Parameters	156
	BIOGRAPHY OF THE AUTHOR	157

LIST OF TABLES

Table 1.1	Relative importance of the physical mechanisms associated with wave evolution in different domains	4
Table 2.1	Observed wave conditions at FRF during three storm events	23
Table 2.2	SWAN-computed significant wave heights and peak wave periods for three storm events with different physics incorporated	39
Table 2.3	CGWAVE-computed significant wave heights for three storm events with and without breaking	42
Table 2.4	Significant wave height comparison between wave gauge G625 and near the location of the wave gauge (GM83) used by Miller et al. (1983)	60
Table 3.1	Simulation period and approximate storm period for year 2001 seasonal maximum wave conditions simulated in this study	75
Table 3.2	Modeling schemes used in three different operational wave prediction systems	83
Table 3.3	Longitudinal and Latitudinal ranges of influence used in assimilation of wave data from 5 NDBC buoys into the model simulations	90
Table 3.4	Statistical analysis of computed wind speeds and significant wave heights at three buoy locations for 48 hours forecast in February 2001	101
Table 3.5	Statistical analysis of computed wind speeds and significant wave heights at three buoy locations for 48 hours forecast in February 2001	113
Table 3.6	Statistical analysis of computed wind speeds and significant wave heights at three buoy locations for 48 hours forecast in September 2001	124

Table 3.7	Statistical analysis of computed wind speeds and significant wave heights at three buoy locations for 48 hours forecast in November 2001	131
------------------	---	------------

LIST OF FIGURES

Figure 2.1	Plan view of the Field Research Facility (FRF)	22
Figure 2.2	Wind and wave data observed for three storms	24
Figure 2.3	Model domains and bathymetries for SWAN and CGWAVE simulations	28
Figure 2.4	Input directional wave spectra for SWAN simulations	30
Figure 2.5	CGWAVE-produced phase diagram and SWAN-produced peak wave directions for a monochromatic wave	35
Figure 2.6	SWAN and CGWAVE computed significant wave heights for the May 1998 storm	37
Figure 2.7	Significant wave height comparisons for SWAN and CGWAVE for three storm events	40
Figure 2.8	Water depth profiles and significant wave heights obtained with SWAN and CGWAVE along three cross-shore sections	45
Figure 2.9	SWAN- and CGWAVE- computed significant wave heights, with and without breaking along pier line section for three storm events	48
Fig.2.10	Water depth profile and CGWAVE-computed significant wave heights comparison	49
Figure 2.11:	Difference between “all on” and “triad off” significant wave heights obtained from SWAN for the May 1998 simulation	52

Figure 2.12	Spectra and significant wave heights obtained using SWAN with all physical mechanisms turned on and with the triad wave-wave interaction turned off at nearshore locations	53
Figure 2.13	Water depth profiles and the wave directional spreadings observed along cross-shore transects for three storm events in 1994	54
Figure 2.14	Water depth profiles and directional wave spreading with breaking and with no breaking, along cross-shore transects for three simulations	55
Figure 2.15	Observations of Elgar et al. (2001) and modeled significant wave heights along two cross-sections for the 1997 case	61
Figure 2.16	Elgar et al. (2001) observed and SWAN-computed wave energy spectra at three gauge locations for the 1997 case	64
Figure 3.1	The model region with NDBC buoy locations indicated	71
Figure 3.2	Observed and predicted atmospheric parameters at three buoy locations during different 8-day periods in year 2001	77
Figure 3.3	SWAN wave model computational domain	85
Figure 3.4	Observed and predicted wind speeds, significant wave heights and mean wave periods for a 7-day period in February 2001 at three buoy locations with and without wave data assimilation	96
Figure 3.5	February 2001 inter-comparisons of observed and computed wind speeds, significant wave heights for 48 hours	100

Figure 3.6	Observed and predicted wind speeds, significant wave heights and mean wave periods for a 7-day period in February 2001 at three buoy locations with two different boundary conditions	102
Figure 3.7	Observed and predicted wind speeds, significant wave heights and mean wave periods for an 8-day period in February 2001 at three buoy locations with and without wave data assimilation	106
Figure 3.8	Observed and predicted atmospheric parameters at buoy 44005 during an 8-day period in February 2001	111
Figure 3.9	February 2001 inter-comparisons of observed and computed wind speeds and significant wave heights for 48 hours	112
Figure 3.10	Observed and predicted wind speeds, significant wave heights and Mean wave periods for an 8-day period in April 2001 at three buoy locations	114
Figure 3.11	Observed and predicted wind speeds, significant wave heights and mean wave periods for an 8-day period in September 2001 at three buoy locations with and without wave data assimilation	119
Figure 3.12	September 2001 inter-comparisons of observed and computed wind speeds and significant wave heights for 48 hours	123

Figure 3.13	Observed and predicted wind speeds, significant wave heights and mean wave periods for an 8-day period in November 2001 at three buoy locations with and without wave data assimilation	125
Figure 3.14	November 2001 inter-comparisons of observed and computed wind speeds and significant wave heights for 48 hours	130
Figure 3.15	Differences between “with assimilation” and “without assimilation” significant wave heights at different times	132

Chapter One

INTRODUCTION

1.1 Numerical Wave Modeling (Background)

Despite the fact that the history of the study of ocean wave dynamics goes back several centuries, reasonable understanding of the physical properties of ocean waves did not start to develop before the late nineteenth century. With the progress in the understanding of the wave dynamics that took place in the early twentieth century, some attention has been paid to modeling the ocean waves. Interests in the prediction of the sea state started to grow by the middle of the last century especially after the concepts of wave spectrum and its evolution were recognized. Nowadays, despite the fact that many aspects of the physics of wind generated waves are still not fully understood (e.g. wave breaking), the several numerical wave models that currently exist do, indeed, have the ability to predict the wave conditions on geographical scales ranging from coastal to global.

Numerical wave models constitute the most efficient and cost effective tools that can provide essential wave information for purposes such as navigational safety and coastal protection. Wave measurements are expensive to obtain and yet limited in their spatial and/or temporal coverage. Conventional wave measurements from wave buoys are largely limited in their spatial coverage. Measurements of the waves obtained from satellite mounted instruments have substantially higher spatial coverage but are somewhat limited in their temporal coverage and are not always reliable (e.g. near coastal areas). Nevertheless, these wave measurements, regardless of their coverage, do not provide near future wave predictions.

Applications of the several existing numerical wave models, nowadays, fall under two major categories: one is practical and the other is scientific. In practical applications models are used as reliable tools to provide near future wave predictions, wave climatology or extreme wave statistics for specific regions. Obviously, models have to go through extensive validation/verification procedures before they can be used in practical applications. Scientific applications of wave models involve the investigation of methods to improve the model performance, the simulations of extreme cases that rarely occur in the real world and the development of better understanding of physical mechanisms associated with the waves and the way they interact in specific field experiments.

The research presented in this thesis mainly involves the application of the-state-of-the-art numerical wave model SWAN in both scientific and practical aspects. The overall objectives of this thesis are as follows:

1. Verification of the SWAN model on both coastal and marginal sea scales.
2. Using the SWAN model to investigate the effect of physical mechanisms that significantly affect the wave evolution at a coastal area.
3. Developing an operational wave prediction system for a marginal sea that is based on the SWAN model.
4. Investigating the impact of a simple data assimilation scheme on the quality of the SWAN model predictions.

The outline of the remainder of this introductory chapter is as follows. The general characteristics of numerical wave models are provided in subsection 1.2. This is followed, in subsection 1.3, by a detailed description of the numerical wave model SWAN. The layout of this thesis is given in section 1.4.

1.2 General Characteristics of Numerical Wave Models

Numerical wave models strive to simulate the various physical mechanisms that can be associated with generation and/or propagation of the waves. However the

Physics	Deep Oceans	Shelf Seas	Shoaling Zones	Harbors
Refraction (Bottom)	⊗	•	•	•
Refraction (Current)	⊗	○	•	⊗
Diffraction	⊗	⊗	○	•
Quad Interactions	•	•	○	⊗
Triad Interactions	⊗	○	•	○
Atmospheric Wind Input	•	•	○	⊗
Whitecapping	•	•	○	⊗
Depth Breaking	⊗	○	•	⊗
Bottom Friction	⊗	•	•	⊗

⊗ Negligible; ○ Minor Importance; • Significant; ● Dominant

Table 1.1: The relative importance of the physical mechanisms associated with wave evolution in different domains [after Young (1999)].

significance of these mechanisms largely varies with respect to the different oceanic scales (Table 1.1). For instance, the effect of the winds is not significant on waves propagating into a harbor but is significant on waves on a marginal sea. The case is exactly the opposite when considering the effect of diffraction. Due to the differences in the physical nature of the mechanisms shown in Table 1.1, it is almost impossible to have all these mechanisms implemented into a single wave model. Even if such model can exist, our current computational resources are not sufficient to operate such an expensive model which after all will not be always worthwhile. Therefore, the variety of numerical wave models that exist, nowadays, differ in the types of physics that they account for based on their nature and their scale of applications for which they were developed.

According to the spatial scale of their applications, numerical wave models can be classified to large and small scale models. The large scale models focus on phenomenon that occur on large scales such as the wave generated by extra-tropical storms in the North Atlantic Ocean and the swells that travel for thousands of kilometers in the Pacific Ocean. Such models are typically applied on global and ocean scales. The small scale models mainly focus on the small scale variabilites in the wave conditions that result from wave interaction with the local bathymetric and geometric features. Typical applications of such models include simulating waves in harbors, coastal and near-shore areas.

Both large and small scale models are, therefore, based on different levels of assumptions and simplifications in the physics and numerics that limit their applications

to the purposes they were developed for. In fact, small scale models widely vary in the types of physics that they account for and therefore might not be used interchangeably. Variabilities among the large scale models are much less profound. Another aspect on which these models vary is their grid resolution. In order to resolve small scale variabilites in the wave conditions, the small scale models use much finer resolution grid sizes than those used in the large scale models.

Based on their physical nature, numerical wave models can (loosely) be divided into two major types:

1. Energy Balance Models: Models that are based on energy balance predict the spatial and temporal evolution of the full 2D wave energy spectrum. Since models of this type resolve only averaged wave properties such as the wave energy spectrum or its integral properties (e.g. wave heights, wave periods, etc.) and not the phase of individual waves, these models are also known as phase averaging models.

Models of this class should be used only where wave properties vary slowly within few lengths. Domains of application for this model class range from global to coastal scales, hence, this model class includes both large scale models such as WAM (Komen et al. 1994) and WAVEWATCH (Tolman 1989); and relatively small scale models such as SWAN(Booij et al. 1999) and STWAVE (Resio 1993). These models include the effects of wind, bathymetric and current induced refractions, bottom friction,

whitecapping and nonlinear wave-wave interactions. Additionally, the small scale models of this type include the effect of bottom induced breaking.

2. Mass and Momentum Conservation models: Models that are based on the conservation of mass and momentum predict the amplitude and the phase of the individual waves and therefore are also referred to as phase resolving models. This model type includes models that are based on the Mild Slope equation and models that are based on the Boussinesq equations.

Models of this class are computationally demanding and therefore should be only used where wave properties vary rapidly within few wavelengths. Domains of application for this model include regions where wave-structure interactions are significant (e.g. harbors) and coastal and nearshore areas with complex geometric and/or bathymetric structures such that diffraction is significant. This class includes models like RCPWAVE (Ebersole et al. 1986), REFDIR (Kirby and Ozkan 1994), CGWAVE (Dimerbilek and Panchang 1998) and HARBD (Chen and Houston 1987).

The above brief descriptions are intended to provide the very general characteristics of numerical wave models. For extensive reviews of existing numerical wave models reader is referred to Battjes, (1994), Panchang et al., (1998) and Young, (1999). However, detailed description of the energy balance model SWAN, which is the focus of this research, is provided in the next section of this chapter. The mass and momentum balance model CGWAVE is described in Chapter 2 of this thesis.

1.3 SWAN Model

SWAN (Simulating Waves Nearshore) is a numerical wave model developed at the Technical University of Delft in the Netherlands (Booij et al. 1999; Ris et al. 1999; Holthuijsen et al. 2000). The model is based on the following spectral action balance equation:

$$\frac{\partial}{\partial t} N + \frac{\partial}{\partial x} c_x N + \frac{\partial}{\partial y} c_y N + \frac{\partial}{\partial \sigma} c_\sigma N + \frac{\partial}{\partial \theta} c_\theta N = \frac{S}{\sigma} \quad (1.1)$$

where $N(\sigma, \theta, x, y, t)$ is the action density which equals to the energy density $E(\sigma, \theta, x, y, t)$ divided by the relative wave frequency σ , θ is the wave direction, and c_x and c_y are components of the wave propagation velocity. The first term on the left hand side of (1.1) represents the rate of change of action in time and the second and the third terms represent the propagation of action in the (x, y) space. The fourth and fifth terms represent, respectively, the frequency shift and refraction induced by depth and currents. The source/sink term (S), on the right hand side of (1.1), which represents the effects of generation, dissipation and nonlinear wave-wave interactions is given by:

$$S = S_{inp} + S_{brk} + S_{frc} + S_{wcp} + S_{nl3} + S_{nl4} \quad (1.2)$$

where,

S_{inp} = generation due to wind Input

S_{brk} = dissipation due to bottom-induced breaking

S_{frc} = dissipation due to bottom friction

S_{wcp} = dissipation due to whitecapping

S_{nl3} = triad nonlinear wave-wave interaction

S_{nl4} = quadruplet nonlinear wave-wave interaction

The terms of the above equations implies that SWAN is a third generation wave model that accounts for the following physical mechanisms:

- Wave propagation in spatial and temporal domains
- Shoaling and refraction due to depth effect
- Shoaling and refraction due to current effect
- Wave generation by atmospheric input (wind)
- Wave dissipation due to depth-induced breaking
- Wave dissipation due to bottom friction
- Wave dissipation due to whitecapping
- Triad nonlinear wave-wave interaction
- Quadruplet nonlinear wave-wave interaction

Currently SWAN does not account for diffraction although reasonable ad hoc assumptions (e.g. Booij et al., 1997) might be able to remedy this limitation in the future. Although, wave transmission through and reflection against obstacles is accounted for in the recent SWAN version, the computed wave field in the immediate vicinity of obstacles

is not accurate. These limitations imply that SWAN is not suitable for modeling the waves in harbors or in areas with complex bathymetric or geometric structures.

SWAN is formulated in terms of the wave action density (Equation 1.1) instead of the wave energy density, because in the presence of currents, the wave energy density is not conserved whereas the action density spectrum is conserved. The action balance equation (1.1) is integrated in SWAN using finite-difference schemes in all five dimensions (time(t), geographical space(x,y), spectral space(σ,θ)). The source/sink terms (Equation 1.2) are numerically estimated with explicit or implicit approximations (Booij et al. 1999).

Although, Equation (1.1) is written in Cartesian spatial coordinates (x,y), in the current SWAN version the user can also use spherical spatial coordinates. This allows the model to be easily nested in the coarse grid wave models WAM and WAVEWATCH. The more accurate and less diffusive propagation schemes, now implemented in SWAN recent version, allow the model to be used on spatial scales from laboratory conditions to shelf seas.

1.4 Thesis Layout

The research work is presented in chapters 2 and 3 of this thesis. Each one of the two chapters was written in a journal article format. Although this has led to occasional

repetitions of some basic definitions, governing equations, etc., each chapter stands alone and may be read with less effort.

In Chapter 2, two wave transformation models, SWAN and CGWAVE, are used to simulate wave conditions at the Field Research Facility (FRF), Duck (North Carolina). The motivation is to examine how well these models reproduce observations and to determine the level of consistency between the two models. The use of the two models, in which some components of the wave physics are similar and others are different, allows the isolation of these components and to examine their significance. The qualitative performance of the two models is examined by comparing the model results for three simulated storm events with some field observations made by other researchers at FRF during different time periods. The results of the two models are also used in a quantitative-qualitative sense to investigate the effect of the piles of the FRF research pier on obliquely approaching waves as they pass under the pier during an event that has been studied by other researchers.

In chapter 3, the principal motivation is to develop a high resolution operational wave forecasting system for the Gulf of Maine that is based on the numerical wave model SWAN, which accounts for the physical mechanisms associated with the wave generation and propagation in both deep and shallow waters. The major goal of this research is to investigate the extent to which wave buoy data can be cross validated and assimilated using the model SWAN. The research is intended to provide answers for two major questions, which are very relevant to the future of high resolution wave forecasting in the

Gulf of Maine. The two questions are: (1) How significant is the impact of the used wave data assimilation technique on the quality of SWAN model predictions?, and (2) Is the assimilation of the observed wave height data sufficient or is the assimilation of other types of observation (e.g. spectral data), which requires higher level of sophistication, needed?.

Chapter 4 contains concluding remarks that summarizes the studies presented in this thesis.

Chapter Two

SIMULATION OF WAVES AT DUCK (NORTH CAROLINA) USING TWO NUMERICAL MODELS

2.1 Introduction

In the United States and Europe, the development of ocean observing systems is receiving increased attention. These systems are intended to procure and disseminate data regarding various ocean parameters to user communities at regular intervals (See special issues of *Coastal Engineering* (Sept 2000, "Operational Oceanography in Coastal Waters") and *Oceanography* (v.13, 1, 2000)). Mathematical modeling methods constitute an integral component of such systems. In the context of waves, models like WAM (Komen et al. 1994) and WAVEWATCH (Tolman 1989) are now routinely operational and produce ongoing forecasts for much of the global oceans. However, the resolution used in these systems is too coarse for obtaining reliable wave information in coastal regions. (For example, around the US, the National Weather Service uses grids varying between 0.5 and 1.25 degrees) and the models are not intended to handle complex geometric features and the resulting wave-scattering effects such as reflections, diffraction, etc. that may be important in nearshore areas.

A suite of models may therefore be needed to perform operational simulations in coastal regions and one component may consist of the local use of specialized models in the intermediate region between the grid points of the outer-ocean WAM or WAVEWATCH operations and the very nearshore areas. This intermediate domain, which may be of the order of about 50 km, may experience wave growth due to wind and call for the use of energy balance models. Much closer to the coast (e.g. in regions like harbors) where wave transformation is governed by the domain geometry, it may be necessary to model the wave motion itself using phase-resolving models (as opposed to modeling merely the energy transport). Panchang et al. (1998) provides a review of coastal wave modeling tools that have been developed in the last two decades.)

One difficulty with operational modeling of waves in coastal areas pertains to the reliability of the predictions. For the outer ocean wave models, the length scale of the wind-induced changes is large and the combination of the available buoy and satellite data in the domain are generally sufficient for model validation. In coastal areas, however, spatial variability induced by geometric irregularities can be greater and more complex. Yet, most model domains will have little or no data for validation/calibration. Satellite data close to the coast are not reliable (Siddabathula and Panchang 1996) and buoys, if at all present, are too localized to provide a proper representation of the complete wave scattering problem. (Zhao et al. (2001) discuss the effects of undersampling while making model-data comparisons.) Even when data are available, they would most likely contain the effects of physical mechanisms not modeled. It is obvious that unlike regional tidal/circulation models, it is difficult to validate or calibrate

a regional coastal wave model used in an ocean observing system. Based on their examination of several coastal engineering models, Thielert et al. (2000) complain that assumptions and predictions associated with many currently-used models are either poor or totally invalid. In order to invest faith in the predictions, it is therefore necessary to validate the models whenever the opportunity exists and, if satisfactory results are obtained, to apply them at other desired sites in the hope that the predictions are reliable. The purpose of this paper is to examine the performance of two models, the energy balance model SWAN (Booij et al. 1999) and the phase-resolving model CGWAVE (Demirbilek and Panchang 1998; Panchang and Demirbilek, 2001) in a field application. The domain of interest, the Field Research Facility (FRF) at Duck (North Carolina, USA), contains a greater number of measurements than are normally available. The use of the two models, in which some components of the wave physics are similar and others are different, allows one to isolate these components and to examine their effects.

The research presented in this paper consists of three parts. First, a comparison is made, in a quantitative sense, between the results of the two models themselves and between the model results and the observations at two FRF wave gauges. In this part we also try to quantify the significance of some of the physical mechanisms that the models account for. In the second part, the qualitative performance of the two models is examined by comparing the model results for the three storm events with some field observations made by other researchers at FRF during different time periods. Finally, we use the results of the two models in a quantitative-qualitative sense to investigate the

effect of the piles of the FRF research pier on obliquely approaching waves as they pass under the pier during an event that has been studied by other researchers.

The layout of this paper is as follows. In Section 2.2, a brief description of the two models is given. This is followed, in Section 2.3, by some details about the study area and the modeling schemes. The results are discussed in Section 2.4. Concluding remarks are given in Section 2.5.

2.2 Description of Models

The model CGWAVE (Demirbilek and Panchang 1998) is a two-dimensional model developed at the University of Maine (USA). It is based on the following extension of the “combined refraction-diffraction” equation:

$$\nabla \cdot (CC_g \nabla \Phi) + (k^2 CC_g + i\sigma w + iC_g \sigma \gamma) \Phi = 0 \quad (2.1)$$

where, for a given wave frequency σ , $\Phi(x,y)$ is the wave potential from which the wave height and phase may be estimated, C is the wave velocity, C_g is the group velocity, k is the wave number, w is a bottom friction factor, and γ is the wave breaking parameter. This equation is applicable to both long and short waves and hence finds wide application. (See Mei (1983) and Panchang et al. (1999) for details.) The mild-slope assumption associated with (2.1) requires that for local depth d , $(|\nabla d| / kd) \ll 1$, a criterion that is usually met in practice. Being elliptic, the equation represents a boundary

value problem, which can accommodate internal non-homogeneities and boundaries. It hence forms a well-accepted basis for performing wave simulations in regions with arbitrarily-shaped (manmade or natural) boundaries and arbitrary depth variations without limitations on the angle of wave incidence or the degree and direction of wave reflection and scattering that can be modeled. In essence, it represents the complete two-dimensional wave-scattering problem for the non-homogeneous Helmholtz equation. Irregular wave conditions may be simulated using (2.1) by superposition of monochromatic simulations (e.g. Chawla et al. 1998; Panchang et al. 1990a; Zhao et al. 2001.)

CGWAVE uses a triangular finite-element formulation with grid sizes varying throughout the domain based on the local wavelength. The model allows one to specify the desired reflection properties along the coastline and other internal boundaries via a Robbins' type boundary condition ($\delta\Phi/\delta n = \alpha\Phi$, where α is related to the reflection coefficient). The model also uses a semi-circle (as an open boundary) to separate the model domain from the outer sea. Examples of typical CGWAVE model domains are described later (e.g. Fig. 2.3). The input conditions are provided at the offshore ends of two one-dimensional cross-shore sections. (In practice, the input condition is known at the end of one of the transects. The condition at the offshore end of the other transect is obtained by appropriate phase translation.) A combination of the incident and reflected waves is computed along these transects using a one-dimensional version of (2.1); this partial solution is then mapped on to the semicircle to force the two-dimensional model. The remainder of the solution on the boundary consists of a scattered wave that emanates

from within the domain; this component is allowed to radiate out through the use of an impedance boundary condition. (For detailed descriptions, see Panchang et al. 2000; Zhao et al. 2001; and Panchang and Demirebilek, 2001).

The model SWAN is a third generation wave model developed at the Technical University of Delft in the Netherlands (Booij et al. 1999; Ris et al. 1998; and Ris et al. 1999). The model is based on the following spectral action balance equation:

$$\frac{\partial}{\partial t} N + \frac{\partial}{\partial x} c_x N + \frac{\partial}{\partial y} c_y N + \frac{\partial}{\partial \sigma} c_\sigma N + \frac{\partial}{\partial \theta} c_\theta N = \frac{S}{\sigma} \quad (2.2)$$

where N is the action density (= spectral energy/ σ), θ is the wave direction, and c_x and c_y are components of the wave propagation velocity. The first term on the left hand side of (2.2) represents the rate of change of action in time and the second and the third terms represent the propagation of action in the (x, y) space. The fourth and fifth terms represent, respectively, the frequency shift and refraction induced by depth and currents. The source/sink term (S) on the right hand side of (2.2) represents the effects of generation, dissipation (due to breaking, bottom-friction, and whitecapping), and nonlinear wave-wave interactions. In the present study, we have used the following steady state version of (2.2):

$$\frac{\partial}{\partial x} c_x N + \frac{\partial}{\partial y} c_y N + \frac{\partial}{\partial \theta} c_\theta N = \frac{S}{\sigma} \quad (2.3)$$

where it has been assumed that over the length scales of interest, the propagation times are small enough so that unsteady effects may be ignored (e.g. Booij et al. 1996). This makes the model compatible with CGWAVE, which is a quasi-steady (time-harmonic) model. Further, in an ocean observing system, computational efficiency may demand that these models be run in the steady mode at frequent time intervals (say 3 hours), forced by the output from the outer ocean WAM/WAVEWATCH simulations. (The domains for coastal models such as CGWAVE often involve about half a million nodes, making unsteady or more frequent simulations impractical.) The effects of currents are also not considered in the present study ($c_\sigma = 0$). The governing equation is solved using finite differences for a spectral or parametric input specified along the boundaries (Booij et al. 1999; Ris 1997).

SWAN can use either a rectilinear or curvilinear computational grids with a uniform grid size in either case. Although, unlike CGWAVE, the grid size in SWAN is independent of the water depth, it should be small enough to resolve the changes in bathymetric, wind, and wave fields. The boundaries of SWAN computational grid are either land or water. The land boundary absorbs all incoming waves (reflection is not accounted for). The wave input conditions are defined along one of the three water boundaries while along the other two, waves cannot enter the domain but can only leave freely. This assumption is obviously a source of error and therefore it is necessary to select such lateral boundaries to be sufficiently far away from where reliable computations are needed in order to minimize the lateral boundary effect on the model results at that area of interest.

The major differences in the two models lie in the fact that (2.1) is based on the Laplace equation and hence models the wave motion, while (2.2) models the transport of energy. As a consequence, the effects of wind generation cannot be included in the former, while the effects of reflection and diffraction cannot be included in the latter. (*Ad hoc* attempts to remedy these limitations have been described by Booij et al. (1997) and Pearce and Panchang (1985).) Thus, CGWAVE is not appropriate for cases where wave generation by wind is significant, and simulation with SWAN in areas with complex bathymetry, around islands or structures, and in semi-closed areas such as harbors and inlets may be difficult. (It is noted that despite such limitations, Bondzie and Panchang (1993) found that the wave model HISWA (the predecessor of SWAN) provided reasonable simulations in one test involving complex caustic-causing bathymetry.) The grid resolution is also generally different: phase resolving models require a resolution that is a fraction of the wavelength, while energy balance model grids can be much larger. Other differences also exist; these are due to the fact that (unlike SWAN) the version of CGWAVE used in this study does not include whitecapping and non-linear wave-wave interactions. However, such limitations can be remedied in the future. (To elucidate, whitecapping may be regarded as a modification to γ , and nonlinear resonant interactions can be included in the governing equation (2.1) following Tang and Oullet (1997) and Kaihatu and Kirby (1995).) In general, however, the modeler does not *a priori* know how significant these mechanisms are in a given application. If the physics are similar, the models should produce similar results despite the difference in their genesis.

2.3 Study Area and Modeling Details

The Field Research Facility (FRF) is a unique facility that is operated by the US Army Corps of Engineers to study coastal processes and has been internationally recognized for its coastal studies. FRF (Fig. 2.1), which faces the North Atlantic Ocean, is located near the town of Duck (North Carolina) and is subject to frequent storms and hurricanes. A nearshore sand bar, which often forms during the moderate phase of a storm, migrates offshore as the storm intensifies. The bottom slope at the FRF varies on average between 1:20 offshore of the sand bar and a steep 1:5 near the beach. The FRF research pier extends 561 m offshore and is supported by 108 concrete-filled steel piles, each with diameter of approximately 0.85 m. Under the pier a permanent bathymetric trough exists, but its shape and depth changes with the wave conditions. Specialized equipment and instruments constantly monitor the changing bathymetry, winds, waves, tides, and currents. All measurements made at the FRF can be downloaded from the FRF web-site (<http://www.frf.usace.army.mil>).

Simulations were performed for wave conditions observed during three different storm events that occurred at FRF (Table 2.1 and later in Fig. 2.4). These events, which occurred in 1994, 1996, and 1998, were selected as a consequence of both the availability of the data (mainly bathymetric) and the severity of the storm conditions. Data pertaining to the bathymetry, waves, winds, and sea levels were used in this study. During the peak of the storms, the conditions were largely steady, as illustrated in Fig. 2.2.

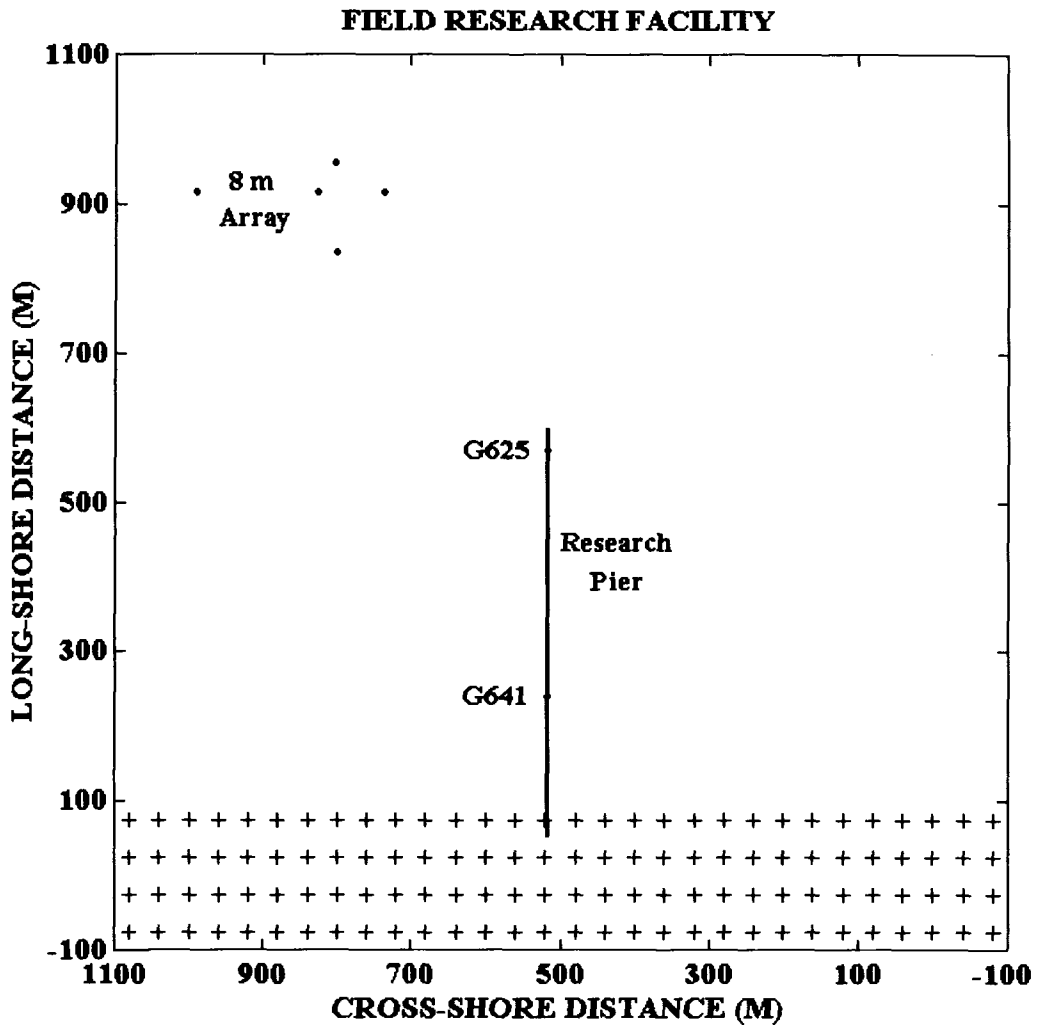


Figure 2.1: Plan view of the Field Research Facility (FRF), showing the locations of instruments. + represents land areas.

Date Time	Location	Hs (m)	Tp (sec)	Dp (deg)	Ds (deg)
Nov. 18, 1994 04:00 – 06:16	<u>8-m Array</u>	<u>5.140</u>	<u>13.563</u>	<u>80.0</u>	<u>21.4</u>
	Gauge625	3.135	14.238		
	Gauge641	1.442	14.745		
Sep. 06, 1996 01:00 – 03:16	<u>8-m Array</u>	<u>3.270</u>	<u>8.866</u>	<u>94.0</u>	<u>20.9</u>
	Gauge625	2.708	8.891		
	Gauge641	1.628	8.790		
May 13, 1998 13:00 – 15:16	<u>8-m Array</u>	<u>3.280</u>	<u>11.976</u>	<u>64.0</u>	<u>20.6</u>
	Gauge625	2.673	12.434		
	Gauge641	1.276	12.019		

Table 2.1: Observed wave conditions at FRF during three storm events. Hs, Tp, Dp, and Ds represent significant wave height, peak wave period, peak wave direction and averaged wave directional spreading, respectively. All directions are from true north. The underlined values at the 8-m array location also represent the spectral parameters of the input conditions used for simulating each storm event.

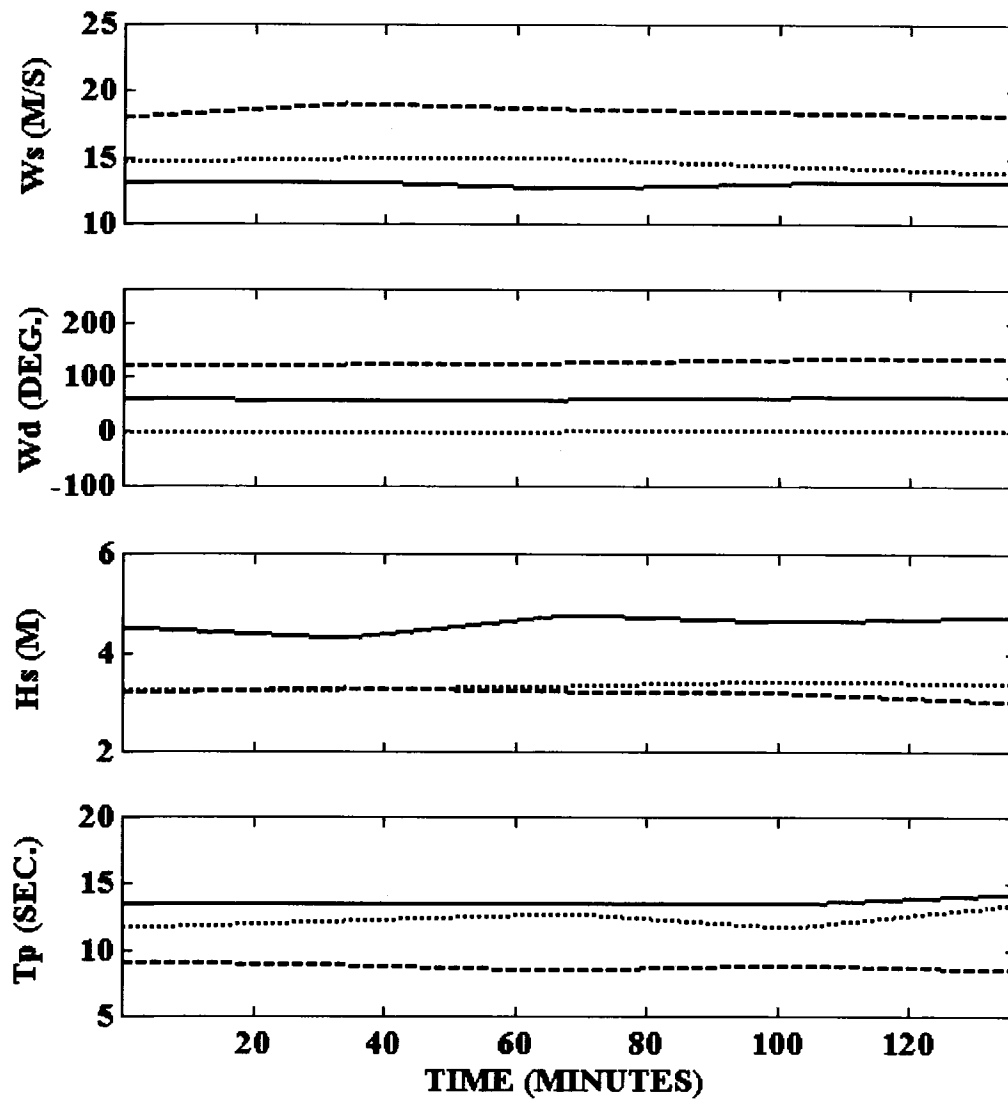


Figure 2.2: Wind speed (Ws), wind direction (Wd), significant wave height (Hs), and peak wave period (Tp) data for the time periods investigated (8192 Seconds) for the three storm events, 1994 (solid lines), 1996 (dashed lines) and 1998 (dotted lines).

The changing bathymetry at FRF is monitored using the "Coastal Research Amphibious Buggy" which records, at irregular intervals, bathymetric data along cross-shore sections separated by about 40 m. On each cross-shore transect, measurements are made at a spacing of 0.5-0.75 meters. Temporal changes in the bathymetry at FRF are quite significant (Howd and Birkemeier 1987) due to the wave action during storm events. For instance, Gallagher et al. (1998) observed a 130 m movement of the crest of the nearshore sand bar during a two-month period in the fall of 1994 that included three storms. As a consequence of such changes, each of the three cases investigated in this study is unique and requires a different model grid. Further difficulties arise due to the fact that SWAN and CGWAVE use different kinds of grids, so that two different model grids must be generated for each storm event.

For SWAN, a rectilinear computational grid is generated with grid size of 8 m x 8 m for each case. The three different computational grids extend for 800 m in the cross-shore direction between $y = 100$ m and 900 m (Fig. 2.1). In the long-shore direction, the computational domains were extended on each side sufficiently beyond our area of interest, which is between 100 m and 900 m long-shore coordinate, in order to minimize any effect of the lateral boundaries. (Sensitivity analyses were also performed by using even larger domains to check that the area of interest was unaffected by possible spurious boundary effects). The generated computational grids contained 13750, 15000, and 14300 grids for 1994, 1996 and 1998 events respectively. In SWAN, the coastline absorbs all the incoming waves. For CGWAVE, grid-generation is more complicated since the resolution is based on the wavelength, which is a function of water depth. For

each case, a mesh of non-equal size triangular finite elements was generated for the domain with a semi-circular open boundary using the grid-generation package contained in the "Surface-Water Modeling System" (Zundell et al. 1998). The alongshore extents of the three CGWAVE domains were almost equal to those used in SWAN domains. For each event, a model grid was generated such that there were at least 10 nodes per wavelength, and resulted in 72440, 88629, and 76180 finite elements for the three cases. Since small features can be more readily accommodated with finite elements, the pilings of the FRF research pier were included in the CGWAVE grid (but not in the SWAN simulations). This was done because recently Elgar et al. (2001) have investigated the effects of the research pier on the data collected at FRF. The 76 research pier pilings that were accommodated were considered to be fully reflective. The coastline was assumed to be fully absorbing boundary.

It must be noted here that since all non-homogeneities are enclosed in domains of different shapes for the SWAN and CGWAVE simulations, the modeled scenarios are similar but not identical. An example of the two different domains is shown in Fig. 3 for the bathymetry used for the 1998 storm event. Because of differences in grid resolution, the bathymetric representation in the two model domains is somewhat different.

Another feature in which the simulations differ pertains to the open boundary conditions used by each model. Input conditions to SWAN are defined along the offshore boundary of the rectangular domain (i.e. at $y = 900$ m). For CGWAVE, the input conditions are provided at the offshore ends of the two one-dimensional cross-shore

sections (Fig. 2.3) that also extends to $y = 900$ m. The input wave conditions were based on frequency-direction spectra, Fig. 2.4, obtained from the 9-element linear array of pressure gauges located on the 8 m depth contour about 900 m offshore (Fig. 2.1). Each spectrum is based on an 8192-second time-series of data collected at 2 Hz. Each spectrum consists of 29 frequency components between 0.04443 Hz and 0.31787 Hz with frequency resolution of about 0.00977 Hz and 90 directional components distributed into 45 directional bins on either side of the research pier with a resolution of 2 degrees. The resulting 2610 spectral components were used to force SWAN. However, the much larger number of grids in CGWAVE simulations precluded the inclusion of such a large number of components. The spectral discretization provided to CGWAVE was based on eliminating components containing energy less than a prespecified threshold (9% of the total energy) and enhancing the energy content of the remaining components to reproduce the desired incident wave conditions.

Uniform winds were assumed over the SWAN domain based on averaged wind measurements at the end of the FRF research pier. Tidal measurements, collected by a tide gauge located at the offshore end of the research pier, were also used to adjust the water depths in the domains. The observed wave conditions at the two gauges located under the FRF research pier (denoted by "G641" and "G625" in Fig. 2.1) are compared to the model output to determine the quantitative performance of the two models. At these two gauges the wave conditions are measured every 34 minutes; therefore, for each case a total of five measurements were averaged at each wave gauge.

a.

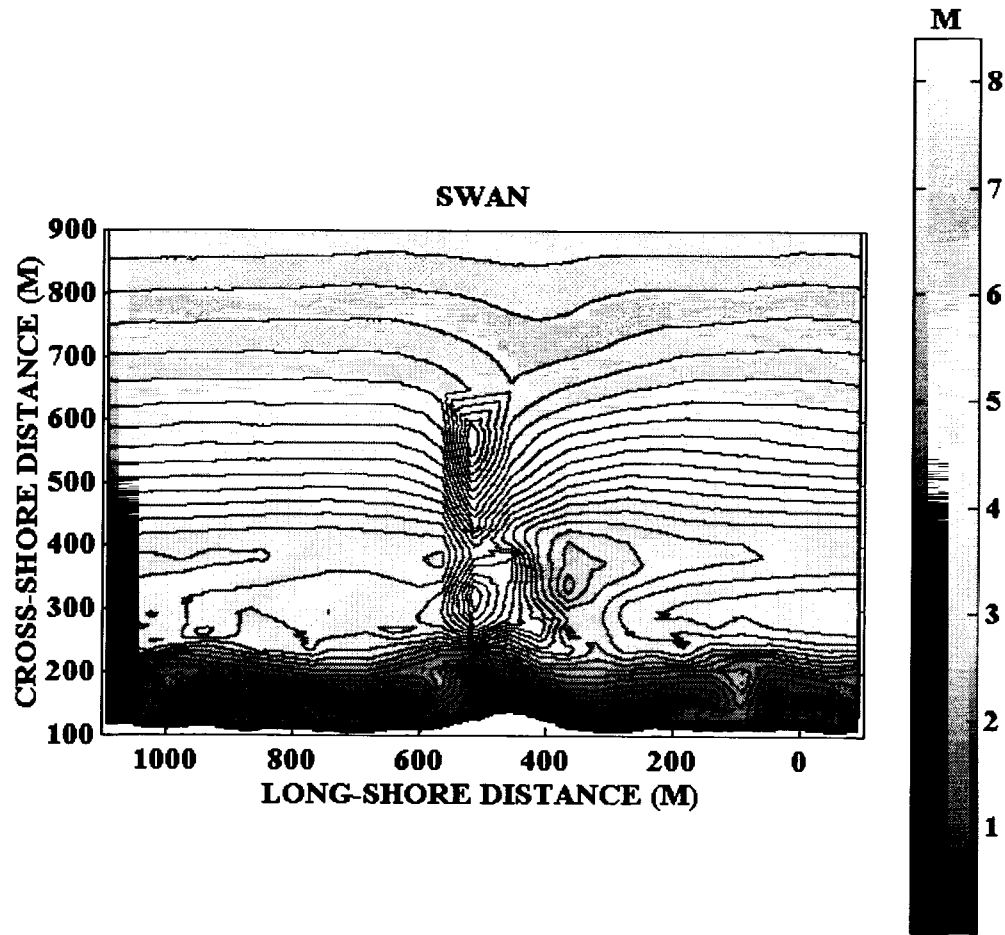
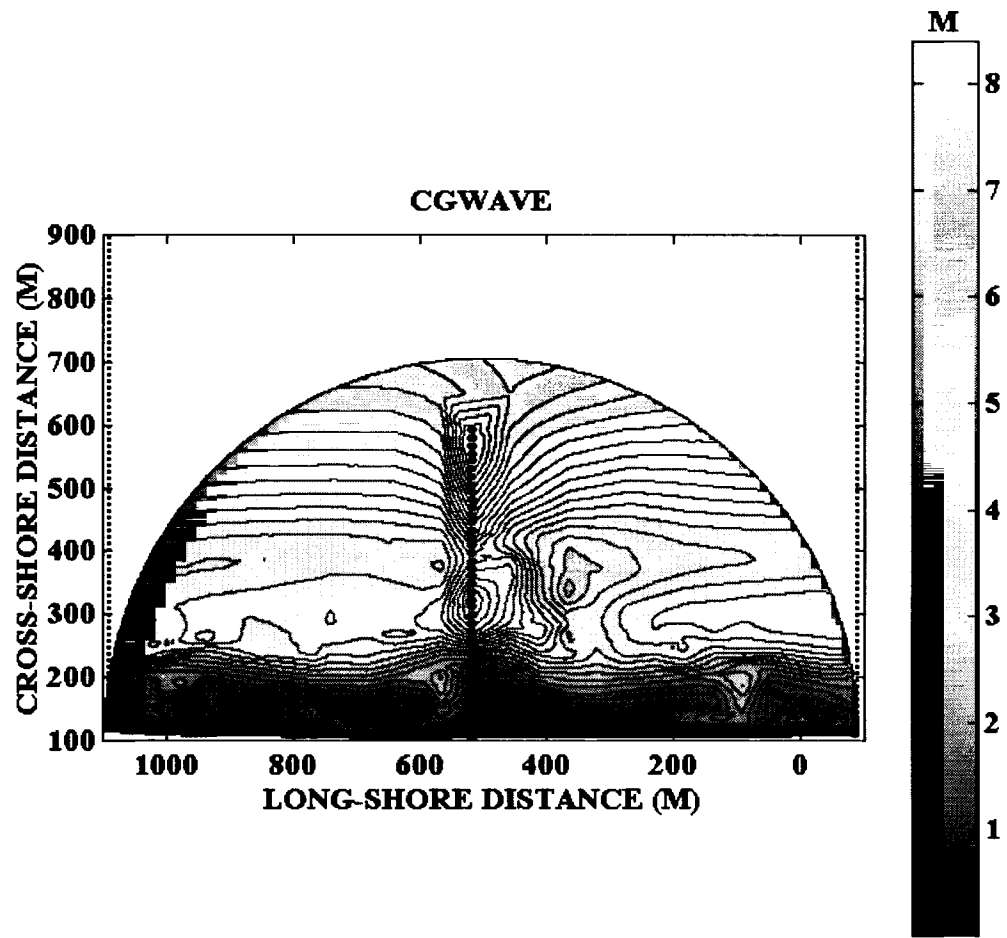


Figure 2.3: Model domains and bathymetries for (a) SWAN and (b) CGWAVE simulations.

- a. Model domain and bathymetry for SWAN simulation of the May 1998 storm event.

b.



b. Model domain and bathymetry for CGWAVE simulation of the May 1998 storm event.

(a) NOVEMBER 18th, 1994 ; 04:00 - 06:16

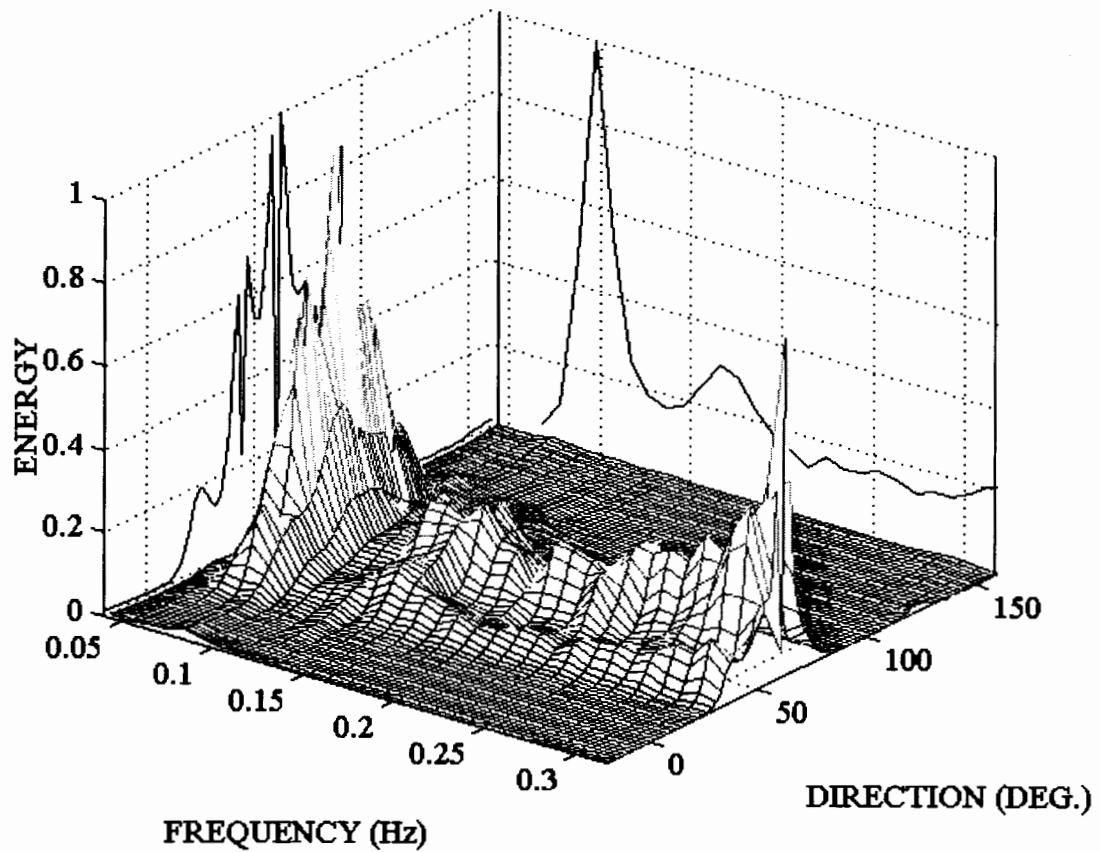
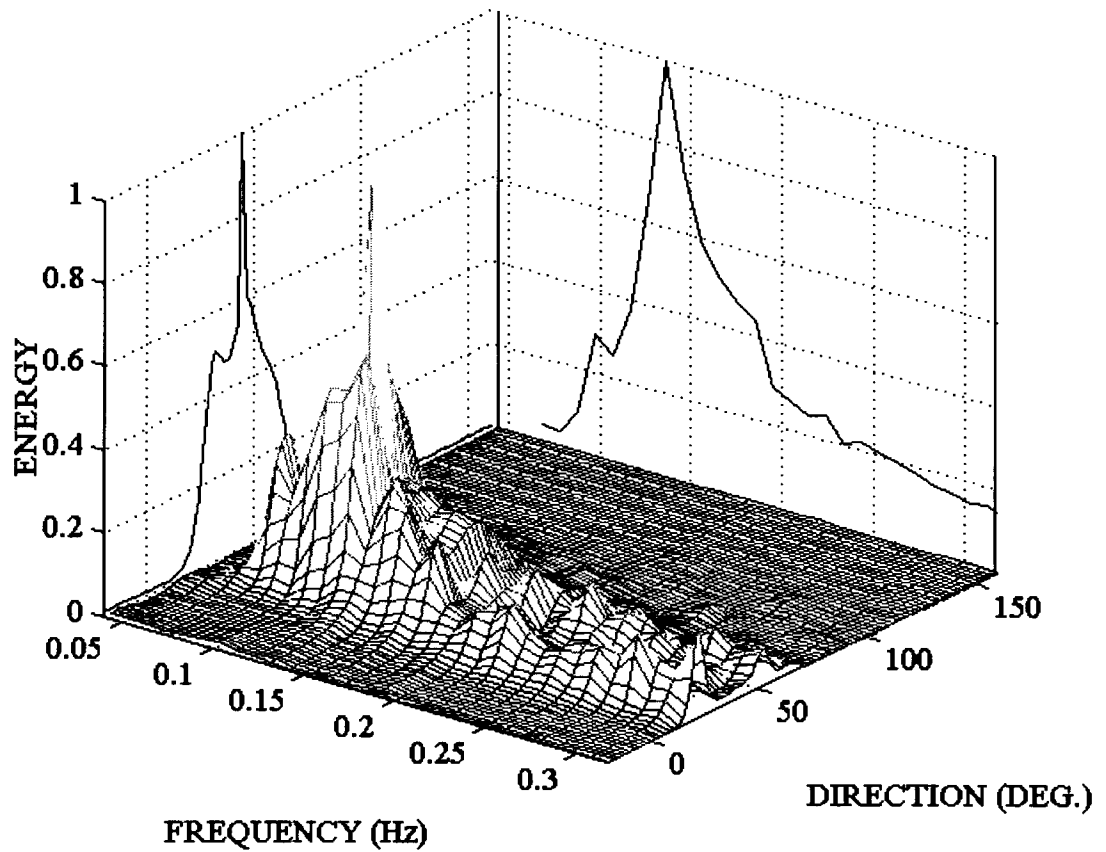


Figure 2.4: Input directional wave spectra used to force SWAN (shown normalized) for the three simulations (a) 1994, (b) 1996 and (c) 1998.

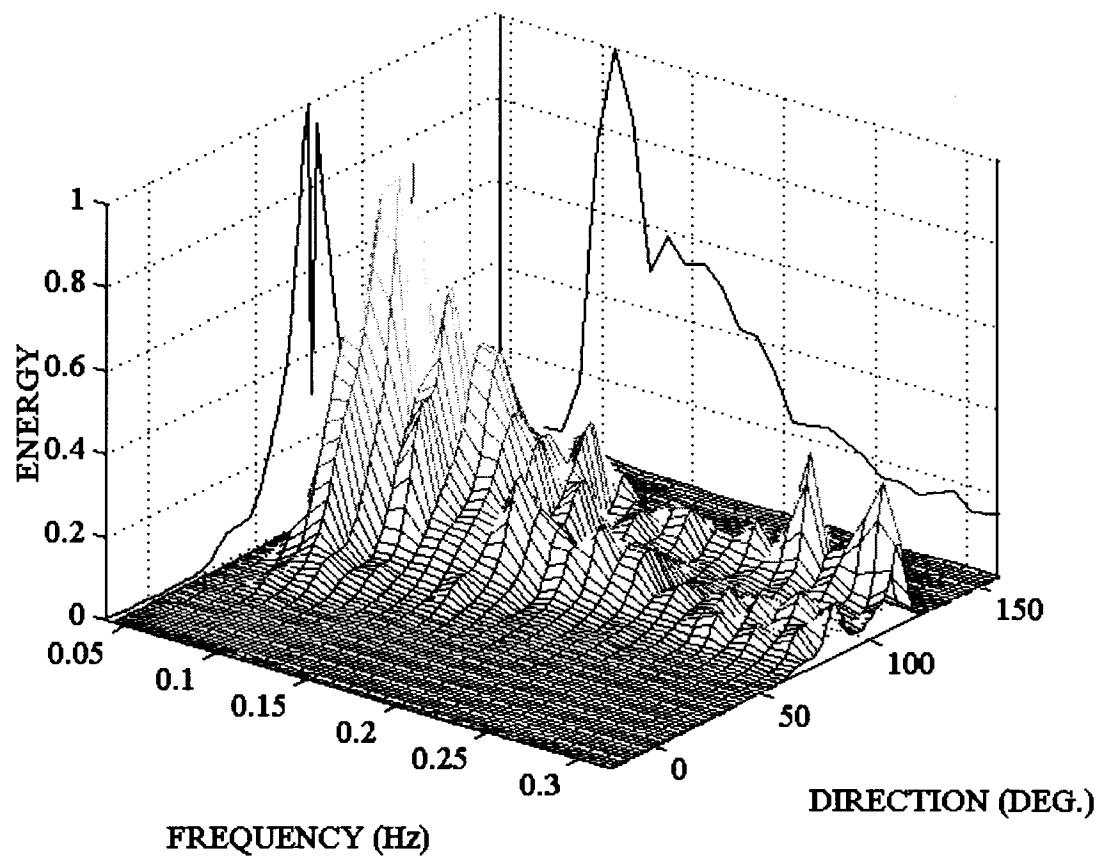
- a. Input directional wave spectrum used to force SWAN 1994 simulation. Left wall, normalized 1-d directional spectrum for peak frequency; facing wall, normalized 1-d frequency spectrum.

(b) SEPTEMBER 6th, 1996 ; 01:00 - 03:16



- b. Input directional wave spectrum used to force SWAN 1996 simulation. Left wall, normalized 1-d directional spectrum for peak frequency; facing wall, normalized 1-d frequency spectrum.

(c) MAY 13th, 1998 ; 13:00 - 15:16



- c. Input directional wave spectrum used to force SWAN 1998 simulation. Left wall, normalized 1-d directional spectrum for peak frequency; facing wall, normalized 1-d frequency spectrum.

The SWAN model runs were made using a personal computer equipped with an AMD Athlon 700 MHz processor and 256 megabytes of RAM. On average a SWAN run takes about 1 hour. Spectral CGWAVE runs were made using a highly parallelized version of the code (described by Bova et al. 2000) on the US Army Corps of Engineers' supercomputer. For non-breaking runs, a typical simulation for 400 spectral components using 50 processors takes about 3 minutes. However, when breaking is specified as a function of all spectral components (i.e. the significant wave height), the effect of the parallelization is diminished and a typical simulation requires about 20 hours.

2.4 Results and Discussion

The model results are presented and discussed in the following order. After a preliminary quality control examination of model performance, we describe quantitative and then qualitative aspects of the results based on the simulation of the three storm events. Then we provide a quantitative-qualitative study of the effect of the piles of FRF research pier on the waves.

Before the three storm events were simulated, the performance of the two numerical models was preliminary examined in a qualitative sense. This was done by simulating several cases with different monochromatic incident wave conditions. While this is not a problem with CGWAVE, SWAN does not really run in a monochromatic mode; a narrow-peaked spectrum was therefore provided as input. Fig. 2.5 shows the results obtained for the 1996 bathymetry for an incident wave of height = 1 m, period =

10.6 seconds, and angle of approach = 30 degrees to the right of the pier. The phase diagram (showing cosine of the phase) obtained from the CGWAVE simulation, Fig. 2.5 (top panel), shows the expected bending of the phase lines due to refraction across the bathymetry and the expected decrease in the wavelength in the shoreward direction. No spurious oscillations encountered in earlier models of this category (e.g. Thompson et al. 1996) are seen. Peak wave directions obtained with SWAN, shown in Fig. 2.5 (bottom panel), also appear to be reasonable and orthogonal to the phase diagram shown in Fig. 2.5 (top panel). These and other tests indicated satisfactory performance. (Note that in these and other figures, the offshore extent of the two domains is different; even though this dimension is smaller for the CGWAVE domain, as noted earlier, the input waves are specified at the same location for both models (Fig. 2.3) by using the two 1-D sections to account for the effect beyond the offshore end of the semi-circular domain.)

2.4.1 Quantitative Model Performance

All simulations with SWAN have been made with the default formulations for wind generation, wave refraction, wave breaking, bottom friction, wave-wave interactions, and white-capping (Booij et al. 1999). Initially, SWAN runs were made with all the physical mechanisms turned on ("all-on runs") for all 3 conditions. An example of the significant wave heights computed with SWAN is shown in Fig. 2.6 (top panel) for the 1998 simulation. The results at the gauge locations are given in Table 2.2 and Fig. 2.7 (top panel) for all three conditions. It may be seen that SWAN simulates the observed changes in the significant wave heights very well for the three storm events.

a.

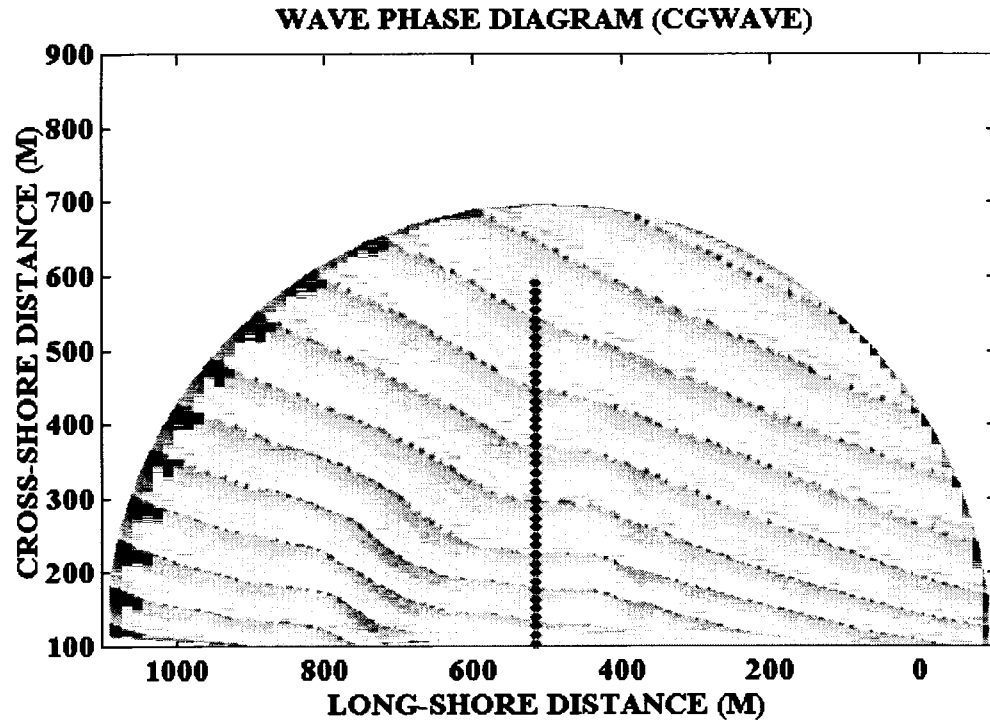
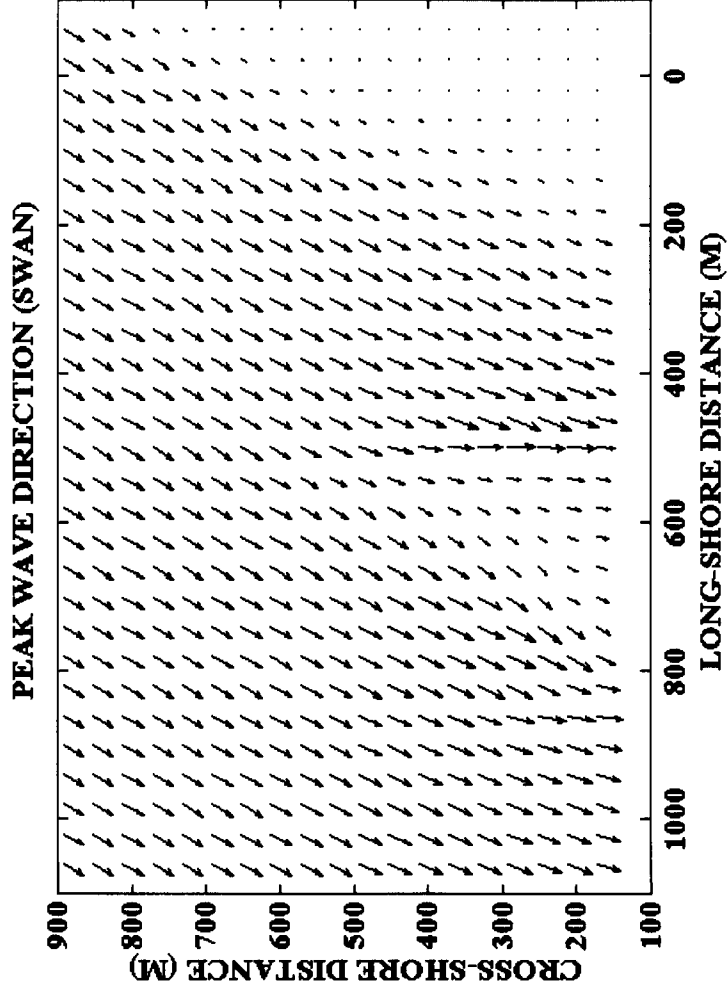


Figure 2.5: Phase diagram (a) produced by CGWAVE and peak wave directions (b) produced by SWAN for a monochromatic wave.

- a. Phase diagram produced by CGWAVE for a monochromatic wave incident from 30 degrees to the right of the research pier with height = 1 m and peak period = 10.6 sec.

b.



b. Peak wave directions produced by SWAN for a monochromatic wave incident from 30 degrees to the right of the research pier with height = 1 m and peak period = 10.6 sec.

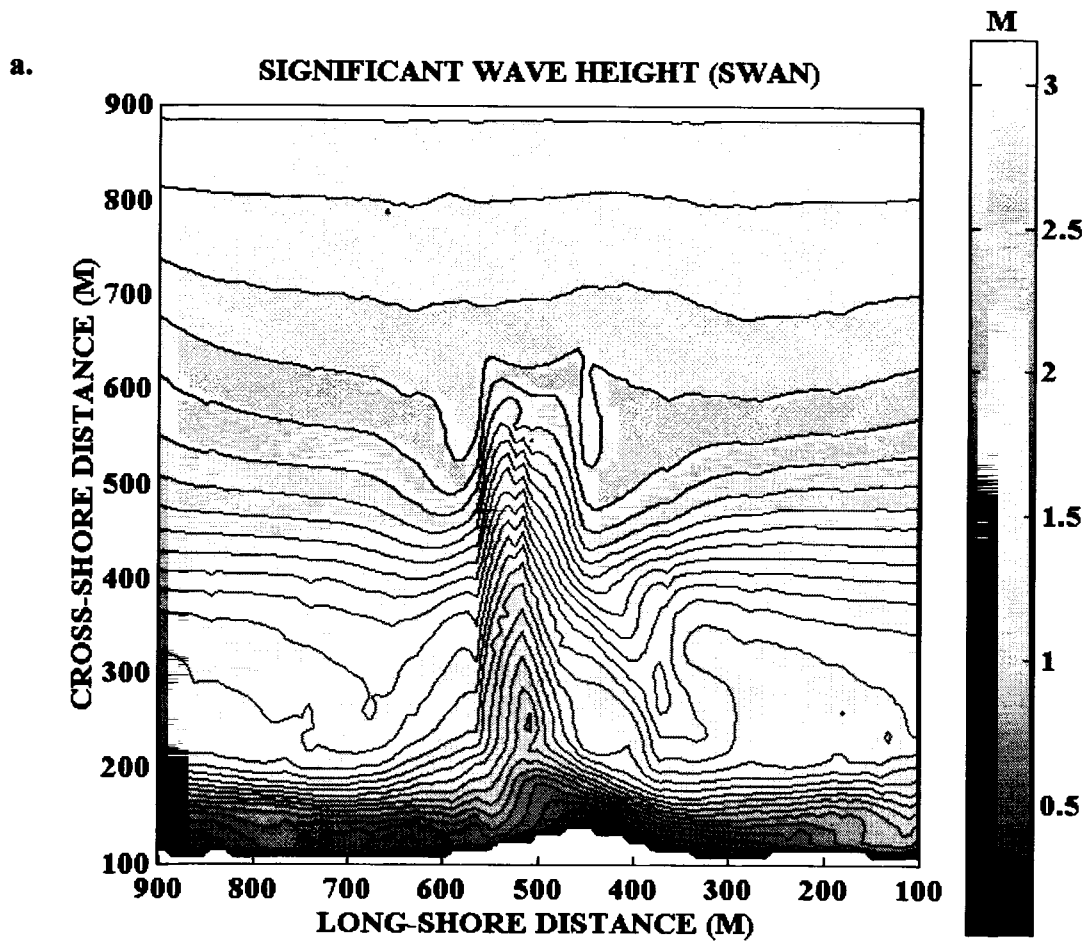
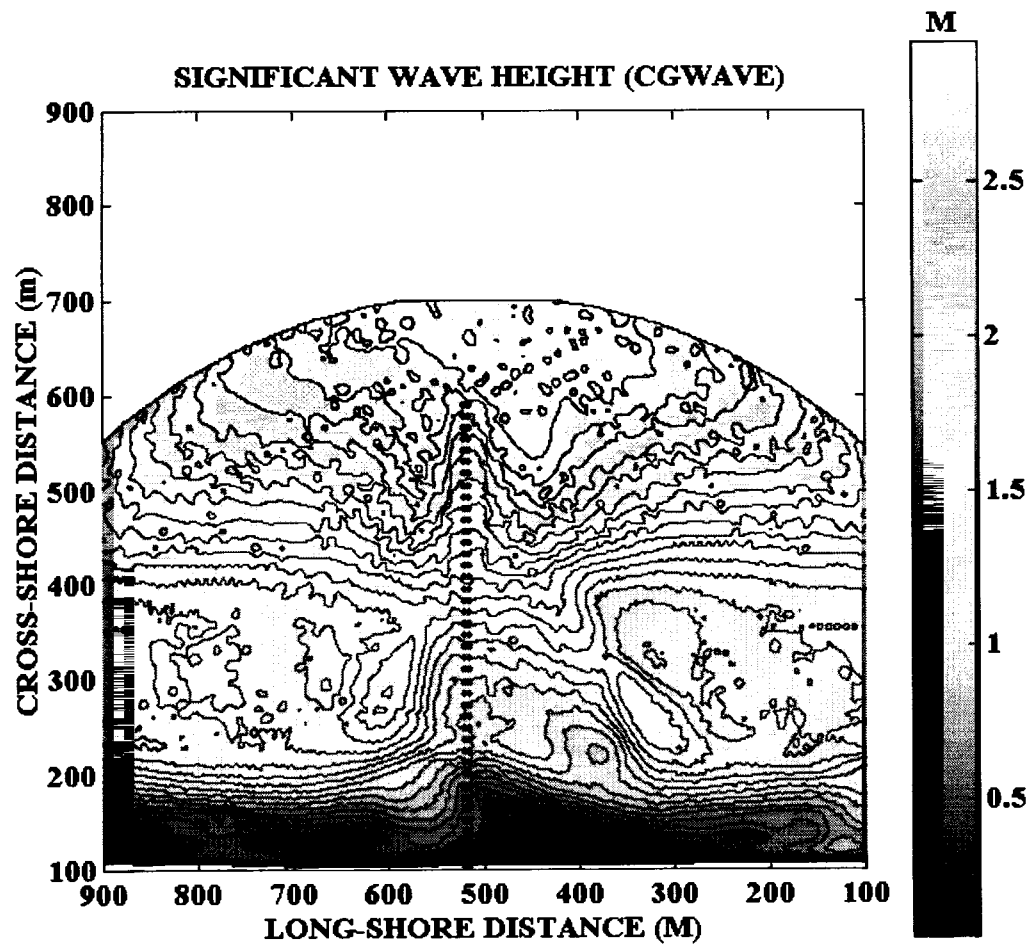


Figure 2.6: Significant wave heights computed by (a) SWAN and (b) CGWAVE for the May 1998 simulations.

a. Significant wave heights computed by SWAN for the May 1998 simulation.

b.



b. Significant wave heights computed by CGWAVE for the May 1998 simulation.

		Date : Nov. 18,1994		Sep. 06,1996		May 13, 1998	
		Time : 04:00 - 06:16		01:00 - 03:16		13:00 - 15:16	
Physics	Gage #	Hs (m)	Tp (sec)	Hs (m)	Tp (sec)	Hs (m)	Tp (sec)
All On	625	3.143	13.529	2.717	8.536	2.692	12.530
	641	1.446	13.529	1.629	8.536	1.081	12.530
Wind Off	625	3.194	13.529	2.792	8.536	2.625	12.530
	641	1.414	13.529	1.597	8.536	1.034	12.530
Refrc. Off	625	3.338	13.529	2.820	8.536	2.790	12.530
	641	2.336	13.529	2.000	9.217	2.090	12.530
Break. Off	625	4.685	13.529	3.013	8.536	2.944	11.604
	641	3.077	13.529	2.635	8.536	1.958	11.604
Frict. Off	625	3.170	13.529	2.740	8.536	2.715	12.530
	641	1.463	13.529	1.656	8.536	1.095	12.530
Triad Off	625	3.179	13.529	2.851	8.536	2.649	11.604
	641	1.381	13.529	1.538	8.536	1.006	11.604
Wtcap. Off	625	3.145	13.529	2.723	8.536	2.694	12.530
	641	1.448	13.529	1.630	8.536	1.082	12.530

Table 2.2: SWAN-computed significant wave heights (Hs) and peak wave periods (Tp) for three storm events with different physics incorporated.

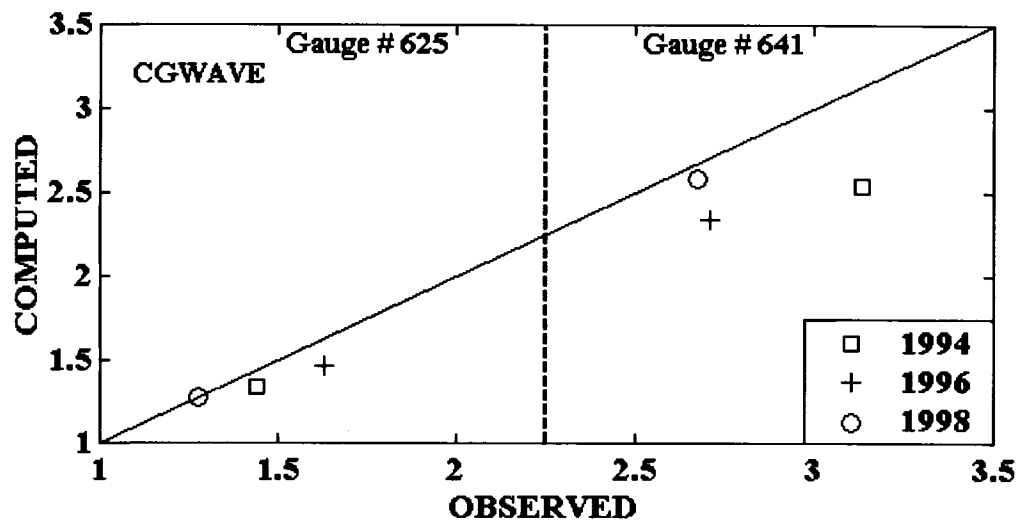
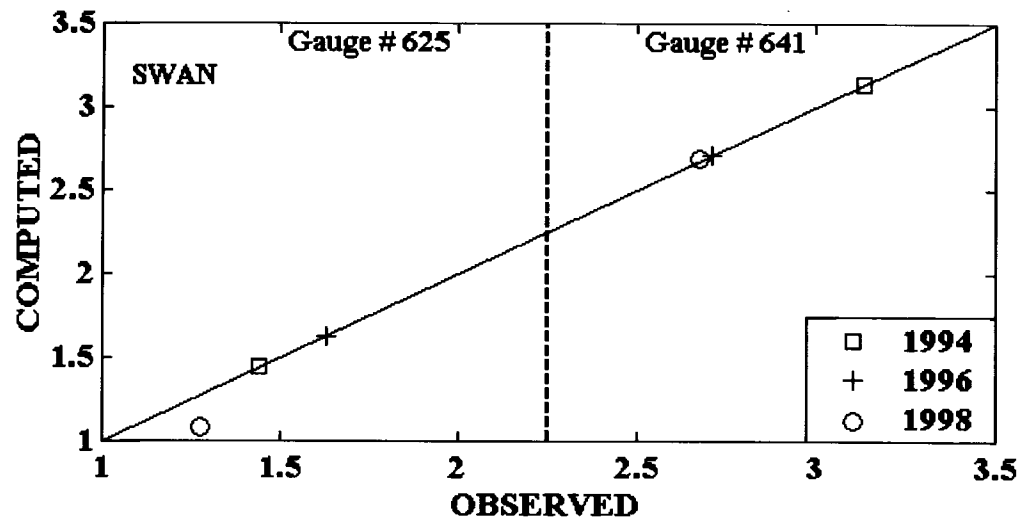


Figure 2.7: Significant wave height comparisons for SWAN (top panel) and CGWAVE (bottom panel) for the three storm events.

In addition to the “all-on” SWAN runs; six additional SWAN runs were made for each storm event, by turning off the physical mechanisms one at a time. This allows one to determine the significance of each mechanism on the wave transformation near FRF. Of these runs, the computed significant wave heights and mean wave periods (Table 2.2) deviate from the “all-on” runs and from the observations when refraction and bottom-induced breaking are turned off, indicating that these are the two most significant mechanisms affecting wave propagation. The other physical mechanisms, viz. wind, bottom friction, white-capping, and triad wave-wave interaction showed little significance. This validates, to a large extent, the suitability of CGWAVE, in which the effects of wind, white-capping, and wave-wave interactions are absent, for simulating these cases.

Fig. 2.6 (bottom panel) shows a contour plot of the significant wave heights computed with CGWAVE for the 1998 storm event. From Table 2.3 and Fig. 2.7 (bottom panel), it can be seen that at gauge G625, CGWAVE results are, on average, smaller than the observations (and the SWAN results); the discrepancy is much less at gauge G641. Additional CGWAVE runs were made with the breaking turned off to quantify the significance of the breaking mechanism. The results (Table 2.3) showed that the bottom-induced breaking is indeed significant. While it is not possible to turn off refraction in CGWAVE (since it is inherent in the “combined refraction-diffraction” equation), the example in Fig. 2.5 (top panel) clearly shows its importance. Thus the results of the two models are compatible insofar as the identification of the dominant mechanisms for these simulations is concerned.

		Date :	Nov. 18,1994	Sep. 06,1996	May 13, 1998
		Time :	04:00 - 06:16	01:00 - 03:16	13:00 - 15:16
Physics	Gage #		Hs (m)	Hs (m)	Hs (m)
With Breaking	625		2.540	2.340	2.580
	641		1.388	1.468	1.276
W/O Breaking	625		4.080	2.440	3.020
	641		2.640	2.580	1.834

Table 2.3: CGWAVE-computed significant wave height (Hs) for three storm events, with and without breaking.

For comparing the performance of the two models, instead of relying only on the two gauge locations, we also examined the significant wave heights obtained by the two models along three cross-shore sections (Fig. 2.8). The sections were taken along the pier line and to the right and left of the pier at cross-shore coordinates (shown in Fig. 2.1) equal to 275m (Right Section) and 775m (Left Section). Fig. 2.8 shows that for the 1994 and 1996 events, significant wave heights computed by CGWAVE were always less than those computed by SWAN along all three sections. For the 1998 storm event, CGWAVE results along the pier line were closer to SWAN results but along the two other sections, the significant wave heights obtained with CGWAVE were again smaller. Despite the fact that CGWAVE results were quantitatively lower, the two models show qualitatively similar behavior along the three sections for the three events. The two models also behaved in the same way when the breaking was turned off for the three storms, as can be seen in Fig. 2.9. For both models, the onset of breaking is found to occur far offshore and not only in shallow waters.

In addition to the numerics (relatively coarse finite difference grids versus high-resolution finite element grids), the differences in the model results noted in the above paragraph may be attributed to the input conditions and the wave physics modeled. To examine the effect of the former (i.e. the number of spectral components), the reduced spectra were used (as done for CGWAVE) to force SWAN for the three storm events. For both 1998 and 1996 storm events there were insignificant changes in the results. The 1994 case showed a slight change in the significant wave height (of the order of about 0.3 m at the "G625" and "G641" wave gauges). There were no changes in the SWAN-

computed peak wave periods. Turning to wave physics, refraction was seen to be properly modeled (Fig. 2.5) by both models. (In any case it is not possible to “turn off” refraction in CGWAVE). The similarity of the overall results and the discussion provided earlier preclude the absence of pier-induced diffraction in SWAN and the absence of wind generation in CGWAVE as possible sources of discrepancy. The good performance shown by SWAN for the three storm events and also the consistency in the results of CGWAVE and SWAN along the research pier line indicate that bathymetric and structural (piling-induced) diffraction (which is absent in SWAN) is not particularly significant for the wave periods investigated. The discrepancies may hence be attributed to wave breaking and nonlinear interactions.

Wave breaking is simulated in the two models in different ways. CGWAVE uses the Dally et al. (1985) formulation without tuning the stable wave factor and wave decay factor used therein, while SWAN uses the Battjes and Janssen (1978) formulation. For examining the effect of these formulations, wave propagation over the bar-trough bathymetry (Fig. 2.10) used by Booij et al. (1999) was modeled with a simple, one-dimensional version of CGWAVE. The results (Fig. 2.10) and other tests described by Zhao et al. (2001) suggest that the Dally et al. (1985) breaking formulation (denoted by DDD in Fig. 10) underestimates the observed wave heights somewhat, compared with the laboratory data and the Battjes and Janssen (1978) formulation (denoted by BJ). (Of course, the values for the two parameters (stable wave factor and wave decay factor) may be adjusted according to the bottom slope, but that is difficult for field applications. Clearly, the treatment of breaking is a dominant factor influencing the discrepancy

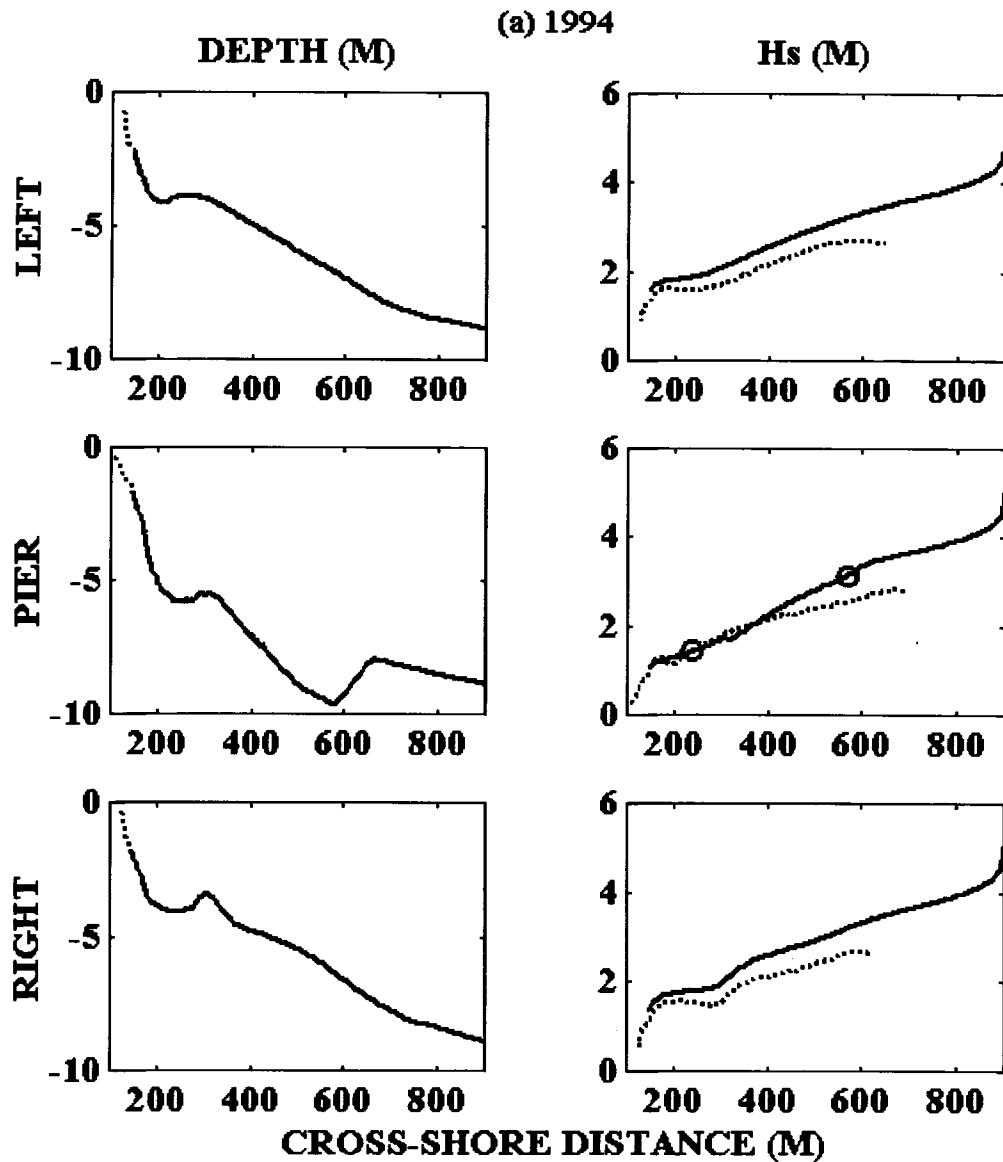
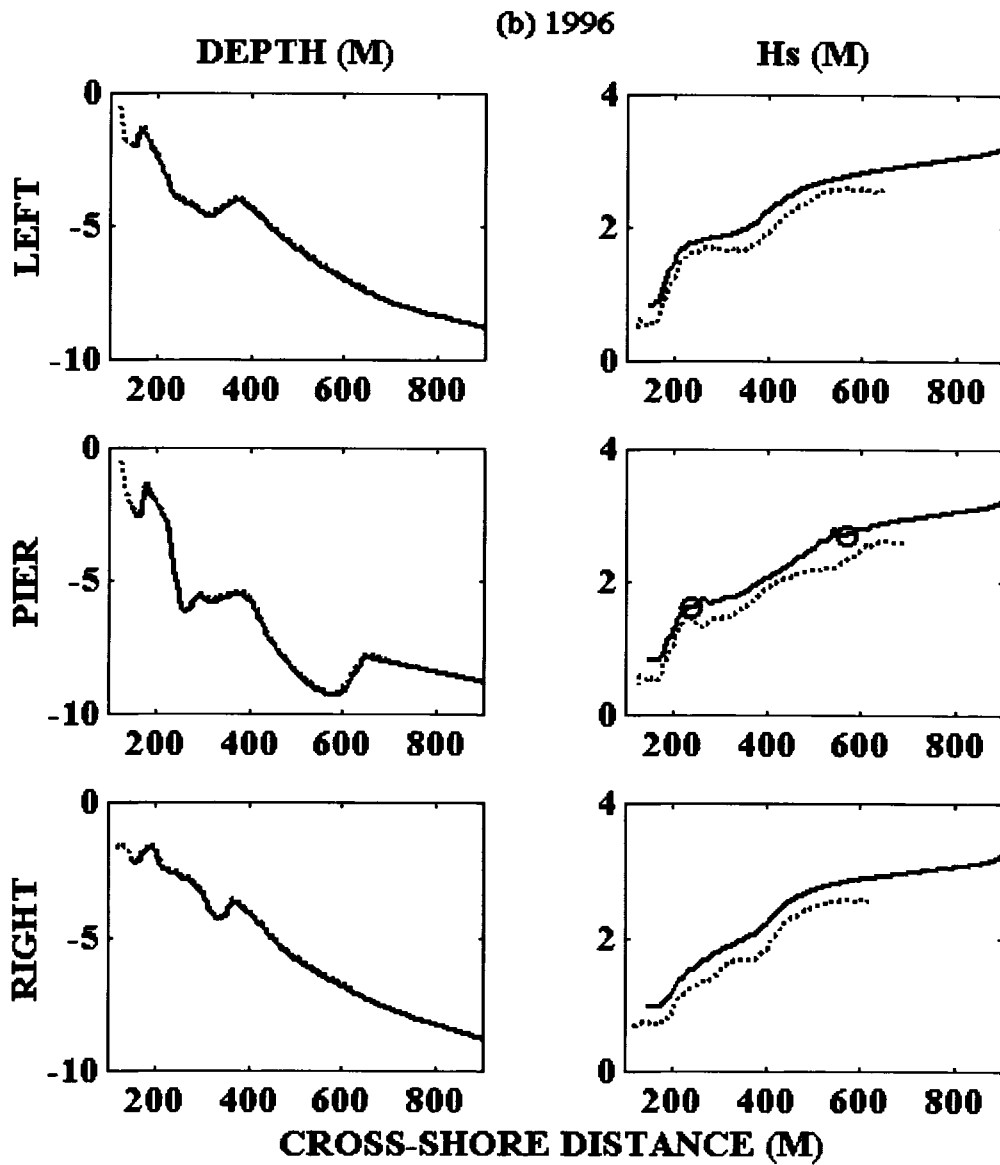
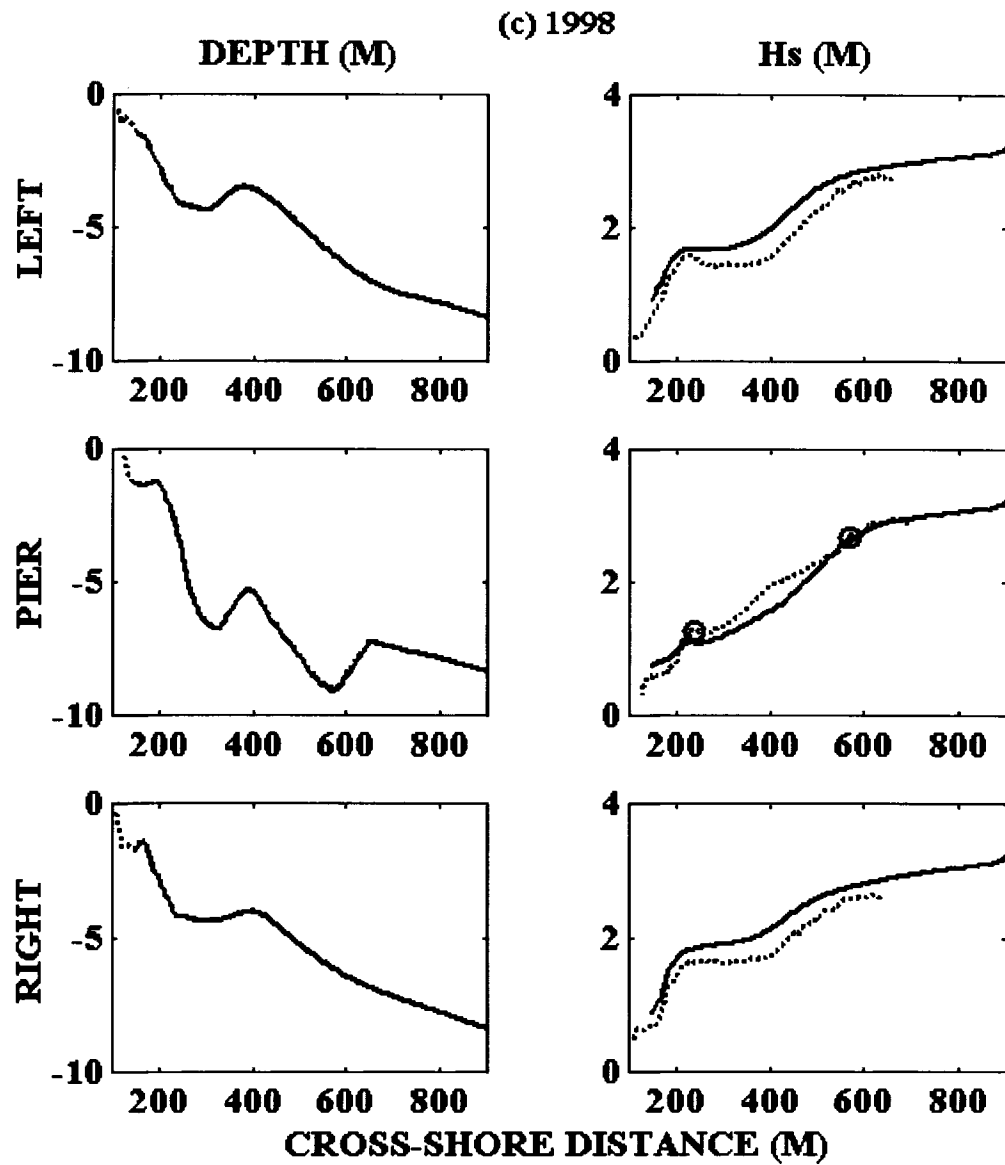


Figure 2.8: Water depth profiles and significant wave heights (H_s) obtained with SWAN and CGWAVE along three different cross-shore sections for the (a) 1994, (b) 1996, and (c) 1998 simulations.

- a. Water depth profiles and significant wave heights (H_s) obtained with SWAN (solid lines) and CGWAVE (dashed lines) along three different cross-shore sections for the 1994 simulation. Circles (o) represent observed significant wave heights at two gauge locations.



b. Water depth profiles and significant wave heights (H_s) obtained with SWAN (solid lines) and CGWAVE (dashed lines) along three different cross-shore sections for the 1996 simulation. Circles (o) represent observed significant wave heights at two gauge locations.



c. Water depth profiles and significant wave heights (H_s) obtained with SWAN (solid lines) and CGWAVE (dashed lines) along three different cross-shore sections for the 1998 simulation. Circles (o) represent observed significant wave heights at two gauge locations.

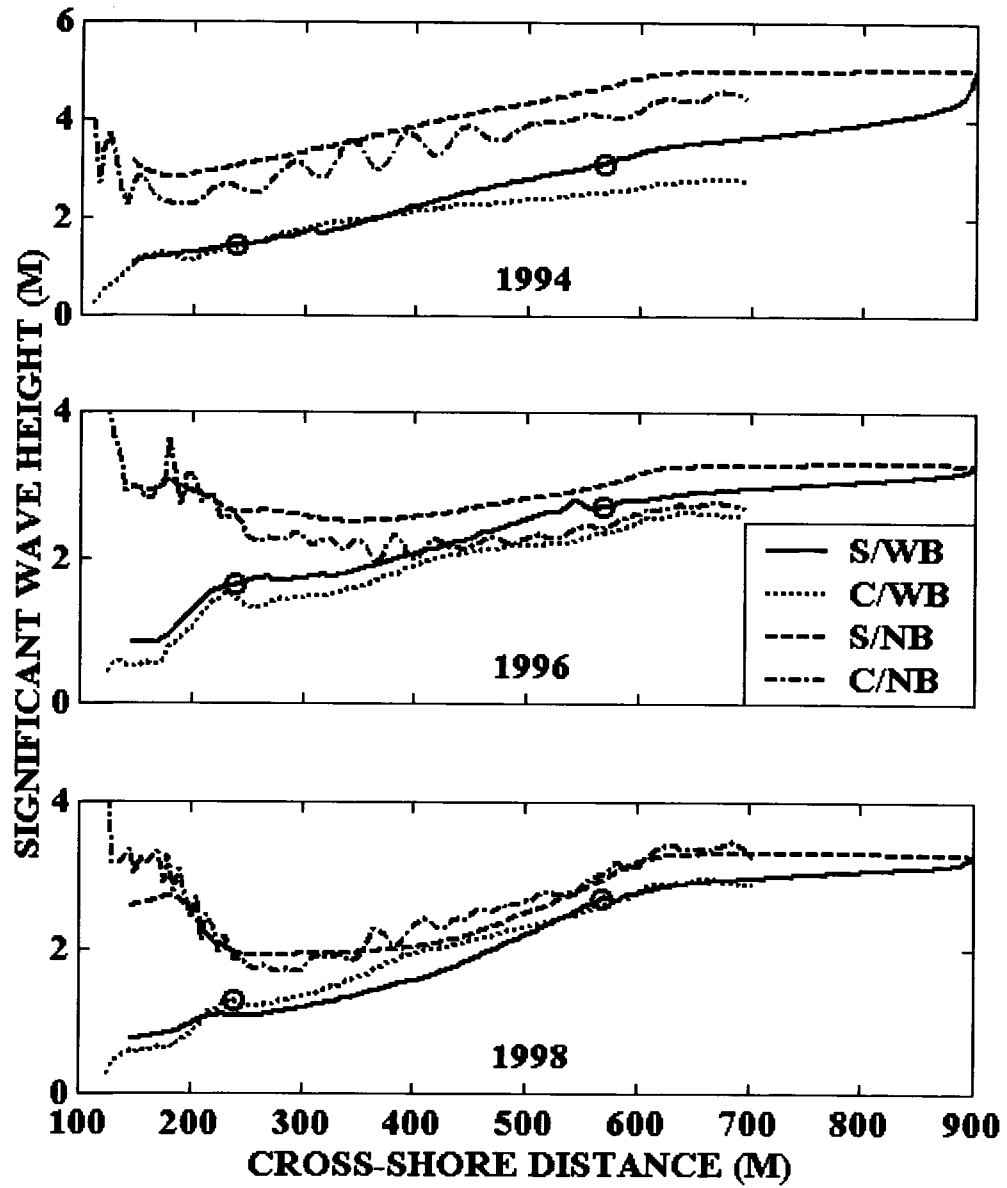


Figure 2.9: SWAN (S) and CGWAVE (C) computed significant wave height, with and without breaking (WB and NB), along the pier line section for the three storm events. Circles (o) represent observed significant wave heights at two gauge locations.

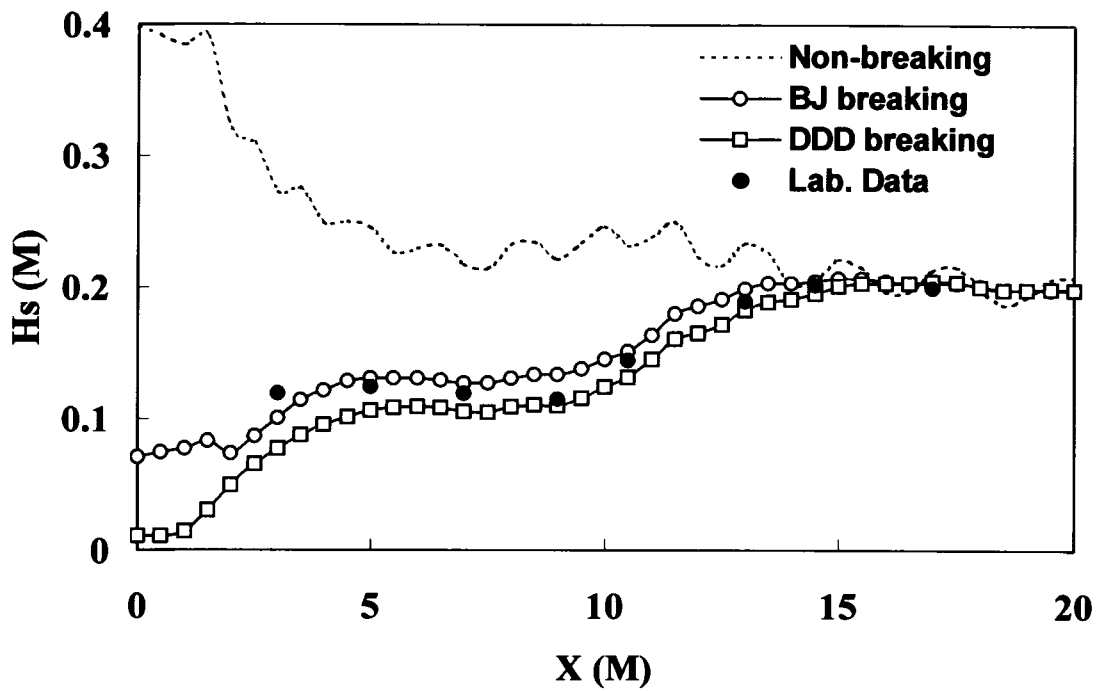
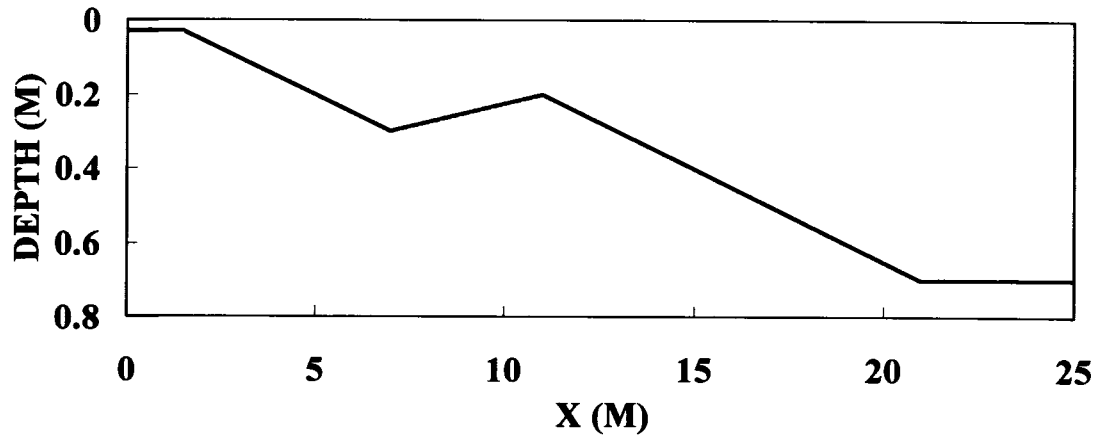


Fig.2.10: Water depth profile (top panel) and CGWAVE-computed significant wave height comparison (bottom panel).

between the models. However, as described in Sec. 2.4.2, breaking is linked to wave-wave interactions as well.

2.4.2 Qualitative Model Performance

Chen et al. (1997), Elgar et al. (1997), and Herbers et al. (2000) suggested that nonlinear interactions in the FRF surf zone transfer energy to higher frequencies from where it is rapidly dissipated by bottom-induced breaking. At the two wave gauge locations, however, we have noted that the effect of the wave-wave interactions was insignificant (Table 2.2). In light of the suggestions by Chen et al. (1997), Elgar et al. (1997), and Herbers et al. (2000), the effect of wave-wave interactions over the entire domain was investigated. Fig. 2.11 shows the values obtained by subtracting the significant wave heights of the “all-on” run from the significant wave heights of the “triad-off” run for the 1998 simulation. Maximum positive values are found to occur along the surf zone that extends in the cross-shore direction to a distance of about 100 m offshore. In these areas, the “triad-off” wave heights are larger than the “all-on” wave heights, suggesting that breaking has less of an effect when the interactions are absent. This is confirmed by examining the spectral characters for the “all-on” and the “triad-off” runs for these areas; see Figure 2.12. For each simulation, the triad interactions are seen to transfer energy from the low frequency part of the spectrum to the high frequency part. Thus a greater amount of energy is available for dissipation in the high frequency waves (which are more susceptible to breaking), leading to smaller wave heights. These numerical results are consistent with the suggestions of Chen et al. (1997), Elgar et al. (1997) and Herbers et al. (2000).

While the effect of wave-wave interactions on the overall SWAN results is somewhat small at the gauges, as seen earlier, we have just seen that it influences wave breaking in shallow areas. Due to the difference in the breaking formulation, the discrepancy between the results of the two models as one approaches the nearshore areas could be expected to increase. However the differences diminish (Fig. 2.8), because of the role of wave-wave interactions in this area, which is to enhance the effect of breaking in SWAN. In a sense, the combination of wave-wave interactions and breaking with the Battjes and Janssen (1978) formulation (in SWAN) has the same effect as breaking with the untuned Dally et al. (1985) formulation (in CGWAVE) in shallow areas. Further offshore, the larger wave heights seen along the transects in Fig. 2.8 for SWAN may be attributed to the effect of wave-wave interactions: in this area, the effect of wave-wave interactions is to create an energy distribution such that breaking effects are smaller, hence enhancing the wave heights (based on Fig. 2.11).

By examining the field data from FRF, Herbers et al. (1999) suggested that wave breaking over the sand bar causes significant scattering of wave energy and enhanced directional spreading. Their estimates of directional spreading along FRF cross-shore transects are shown in Fig. 2.13; these results are based on data collected when the nearshore bar was present. Since the location of the nearshore bar frequently changes (Gallagher et al. (1998) and Fig. 2.14) and the periods associated with our model simulations and the field measurement program of Herbers et al. (1999) are different, we may view Fig. 2.13 in a representative sense and use it only for an approximate comparison. Fig. 2.14 shows the directional spreading calculated by SWAN along cross-

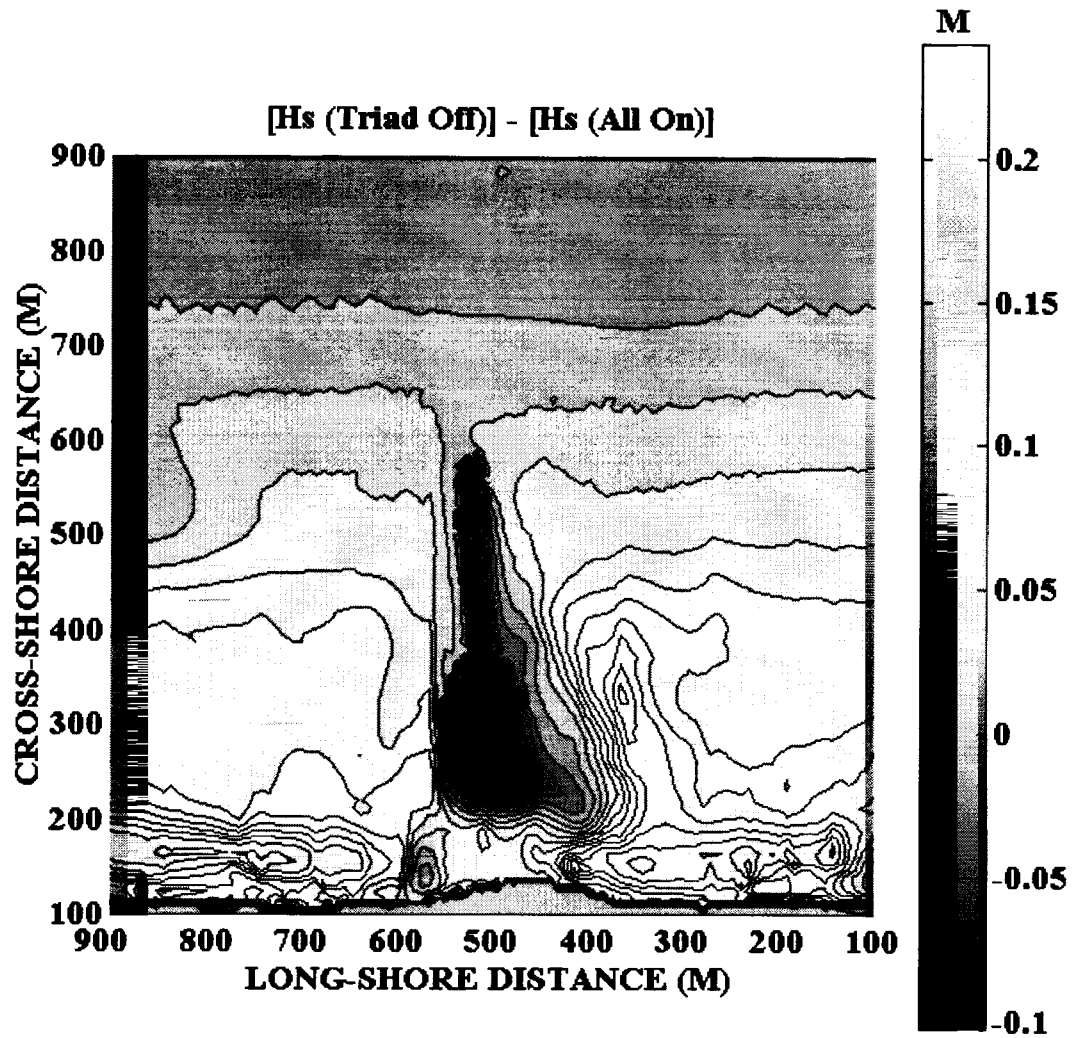


Figure 2.11: Difference between “all on” significant wave heights and “triad off” significant wave heights obtained from SWAN for the May 1998 simulation.

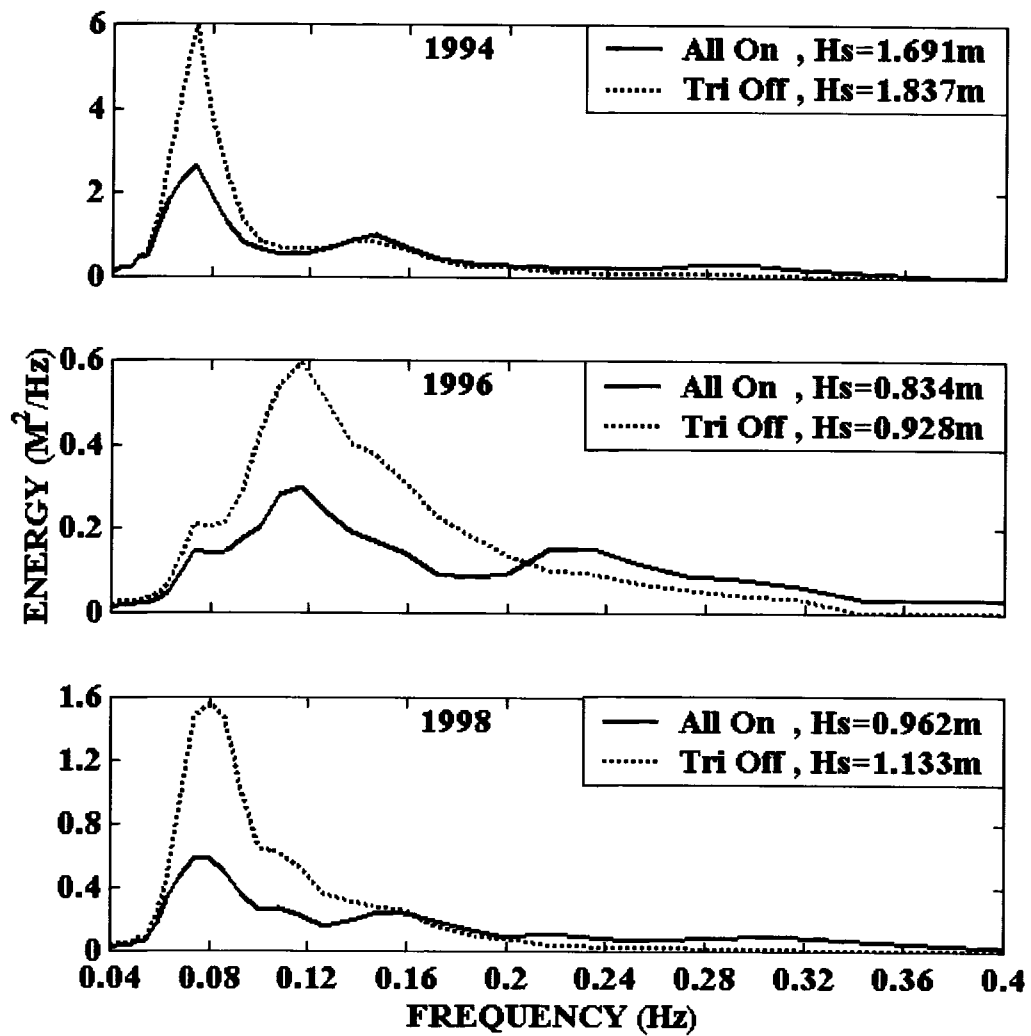


Figure 2.12: Spectra and significant wave heights (H_s) obtained using SWAN with all physical mechanisms turned on (All On) and with the triad wave-wave interaction turned off (Tri Off) at nearshore locations.

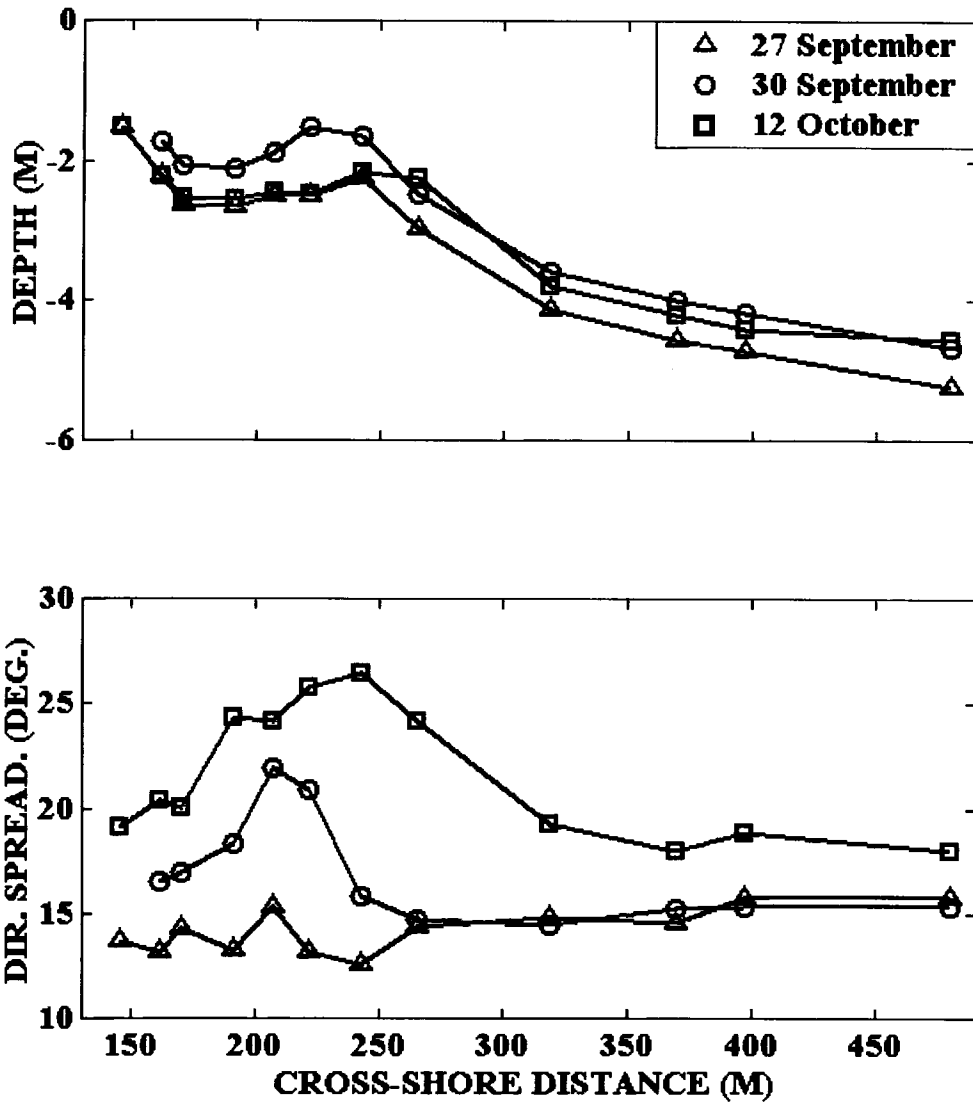


Figure 2.13: Water depth profiles (top panel) and the wave directional spreading (bottom panel) observed along cross-shore transects for three storm events in 1994 (after Herbers et al. 1999).

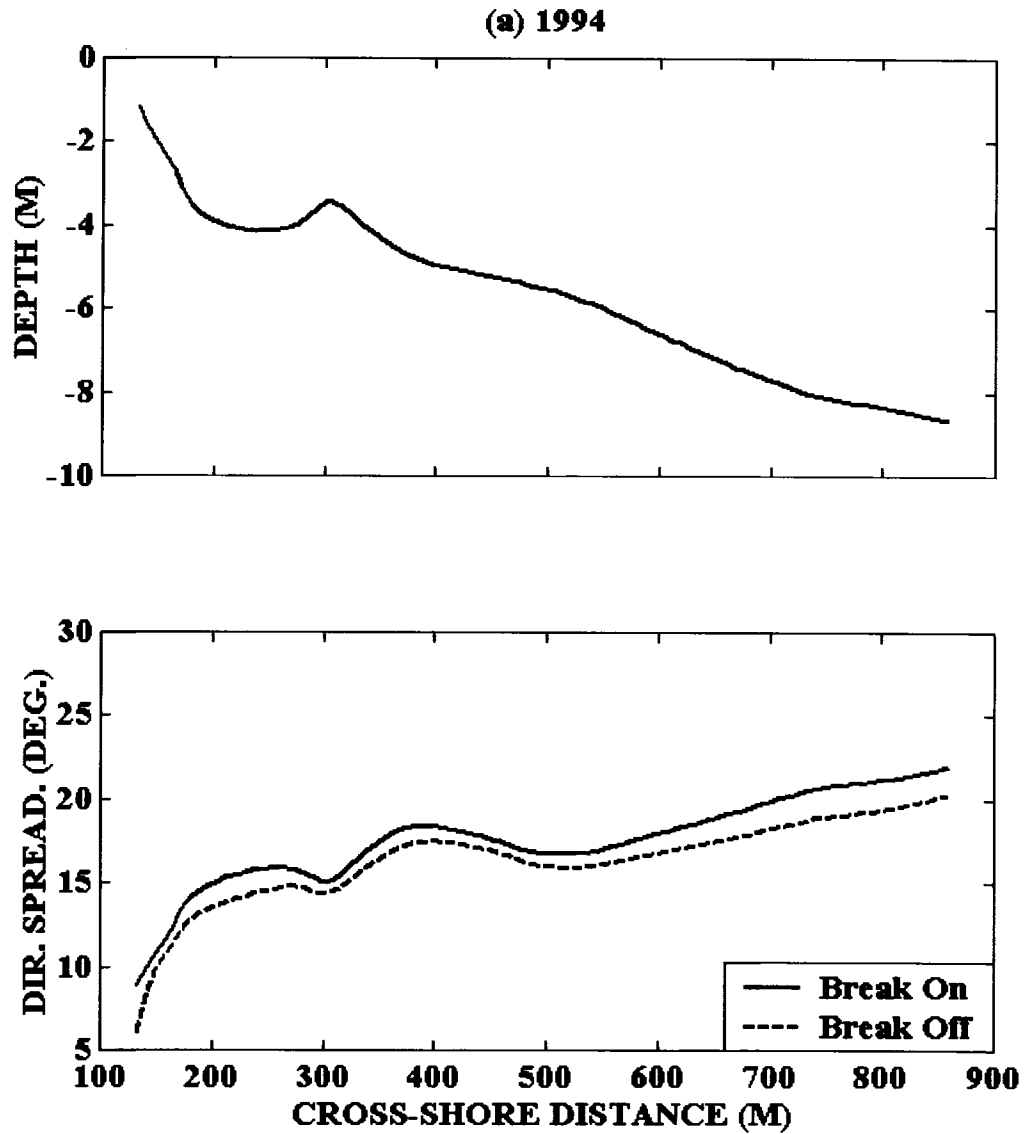
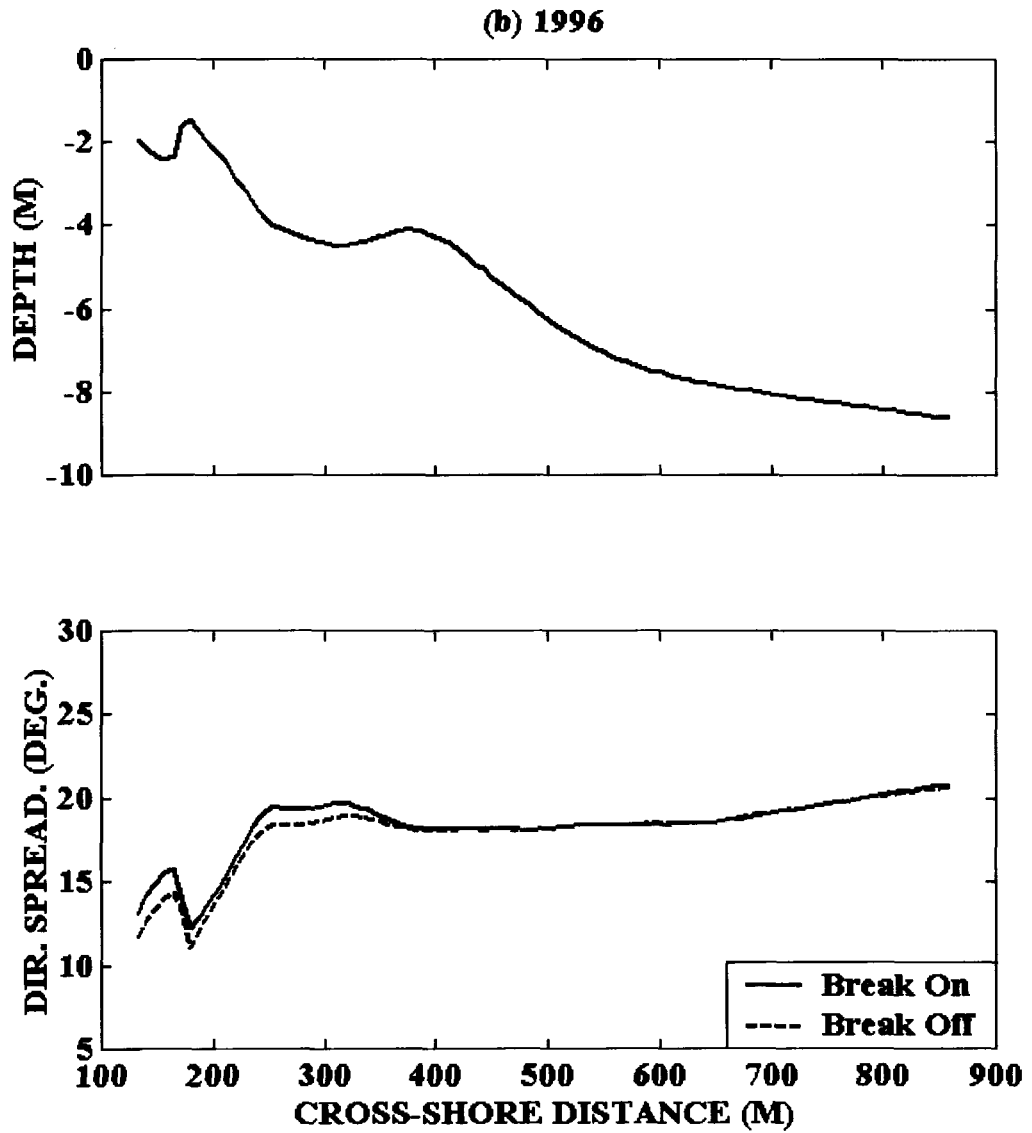
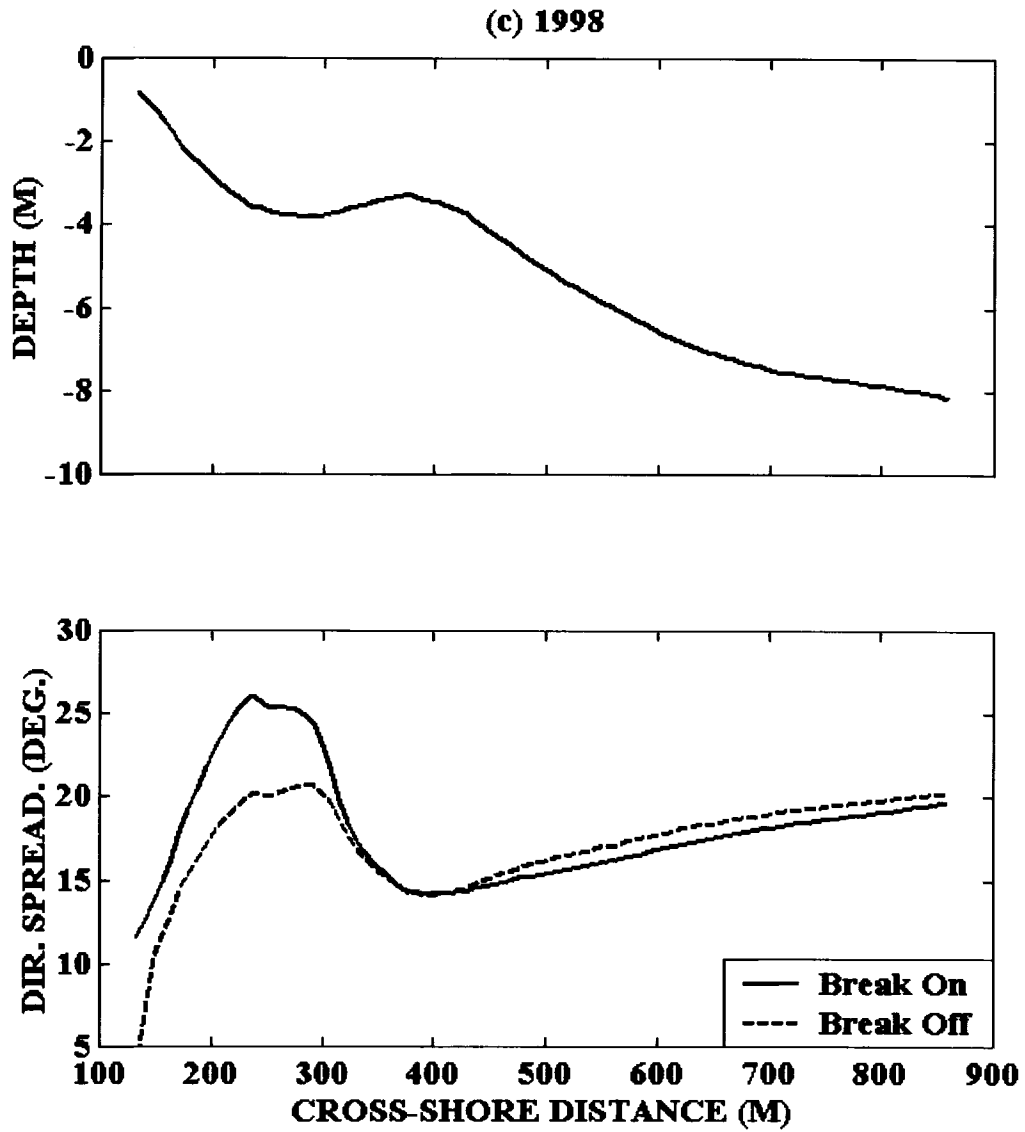


Figure 2.14: Water depth profiles (top panel) and the wave directional spreading (bottom panel) with breaking (Break On) and with no breaking (Break Off), along a cross-shore transect for the (a) 1994, (b) 1996, and (c) 1998 simulations.

- a. Water depth profiles (top panel) and the wave directional spreading (bottom panel) with breaking (Break On) and with no breaking (Break Off), along a cross-shore transect for 1994 simulation.



b. Water depth profiles (top panel) and the wave directional spreading (bottom panel) with breaking (Break On) and with no breaking (Break Off), along a cross-shore transect for 1996 simulation.



c. Water depth profiles (top panel) and the wave directional spreading (bottom panel) with breaking (Break On) and with no breaking (Break Off), along a cross-shore transect for 1998 simulation.

shore transects for the three events. In general, the model results are similar to the estimates of Herbers et al. (1999); the similarity is pronounced when the bathymetry is similar (compare Fig. 2.14c with data for 12 October in Fig. 2.13).

In Fig. 2.14 we also show directional spreading calculated by SWAN with wave breaking turned off. Breaking is seen to enhance the directional spreading in the nearshore areas, which agrees with the suggestion of Herbers et al. (1999). Again the greatest enhancement is seen for the 1998 case. For the other two cases, however, the effect appears to be somewhat minimal. This is probably because the breaking mechanism in SWAN is not strongly dependent on wave direction (and also of course, because the bathymetries are different). Overall, the results from SWAN tend to confirm the observations of Herbers et al. (1999).

Miller et al. (1983) investigated the effect on the waves of the deep bathymetric trough near the offshore end of FRF research pier. Their statistical comparison of measurements at two locations (gauge G625 at the end of the pier and another gauge (GM83) located about 300 m to the northeast from it) showed that during normal wave conditions, the wave parameters were identical at the two locations; however, during storm conditions, the high waves were usually about 10 to 15 percent lower at gauge G625. CGWAVE and SWAN results were investigated at these two locations for the three storm events (Table 2.4). The comparisons showed that the modeled waves were lower at wave gauge G625 by approximately 10 % (on average). Thus, the modeled results are consistent with the observations of Miller et al. (1983).

2.4.3 Effect of the Pilings

The present modeling study also enables one to address the issue of the pier legs on measurements made at the highly-used Field Research Facility. In a recent paper, Elgar et al. (2001) presented some data obtained from the north of the pier in the region bounded approximately between $x \approx 700$ m and $x \approx 900$ m (long-shore coordinates, see Fig. 2.1) and $y \approx 150$ m and $y \approx 500$ m (cross-shore coordinates). Data for two cross-shore transects are shown in Fig. 2.15 for waves approaching the pier from the southeast during a low-wave event in 1997. Using a simple refraction model, Elgar et al. (2001) attributed the observed reduction in the wave heights in the cross-shore direction in the immediate shadow of the piers (e.g. $x = 703$ m) to a 30-50% “wave blocking” effect induced by the pier legs. Further away from the pier (e.g. $x = 905$ m), there is no such reduction because wave reaching this area do not traverse through the pier legs. CGWAVE can explicitly include internal boundaries in a non-empirical manner. It solves the governing equations as boundary value problem with an assigned reflection coefficient for the piles. Therefore, it was used to perform two dissipation-less simulations with and without the pier legs being accommodated in the model domain. Although, the pier legs are not accommodated in SWAN, a simulation using SWAN has been also made with wind, nonlinear wave-wave interactions and all dissipation mechanism turned off. For grid generation and input conditions for the two models, we followed the same modeling schemes presented earlier (section 2.3) for the three storm events (i.e. grid generation, spectral discretization, etc.). It must be noted here that our model domains are completely different in size from the domain used by Elgar et al.

<u>Date</u>	<u>SWAN</u>			<u>CGWAVE</u>		
	<u>G625</u>	<u>GM83</u>	<u>%</u>	<u>G625</u>	<u>GM83</u>	<u>%</u>
Nov. 18, 1994	3.143	3.593	12.52	2.541	2.754	07.73
Sep. 06, 1996	2.717	2.972	08.60	2.340	2.621	10.72
May 13, 1998	2.692	2.958	09.00	2.580	2.880	10.42
<u>Average</u>			10.04			09.63

Table 2.4: Significant wave height comparison between wave gauge G625 and near the location of the wave gauge (GM83) used by Miller et al. (1983).

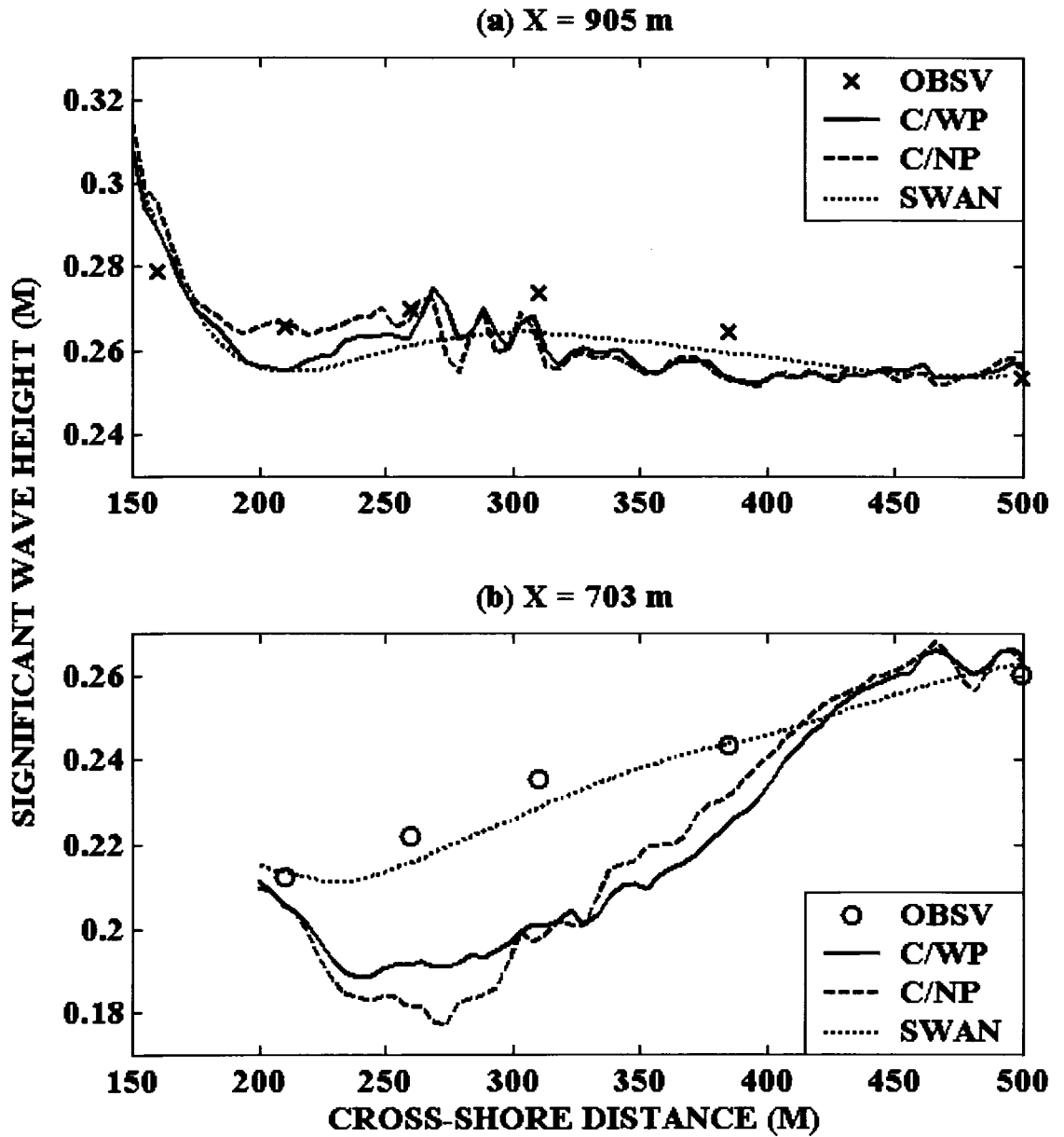


Figure 2.15: Observations (OBSV) of Elgar et al. (2001) and modeled significant wave height along (a) $x = 905$ m and (b) $x = 703$ m for the 1997 case. CGWAVE results with pilings (CWP) and with no pilings (CNP); and SWAN results (SWAN).

(2001) and so are the locations where the input conditions are provided to the model. To obtain input conditions, Elgar et al. (2001) performed back-refraction of the frequency-directional spectra observed at the 5 m water depth to estimate input wave conditions at 6.5 m depth. For the sake of consistency in the inter-model comparisons, the energy contained in the input spectrum from the 8 m array (8.5 m water depth) was adjusted in order to reproduce the farthest observations of Elgar et al. (2001) (i.e. at $y = 500$ m).

In Fig. 2.15 the significant wave heights obtained using CGWAVE with and without the pier legs (denoted by CWP and CNP) along the two cross-shore transects ($x = 703$ m and $x = 905$ m) are shown. (The oscillations in the wave heights produced by CGWAVE are due to diffractive effects, typically seen near areas of complex bathymetry such as shoals and trenches (e.g. Bondzie and Panchang 1993).) Although CGWAVE results show some underestimation in comparison with the observations (along the $x = 703$ m transect), the observed increasing and decreasing trends are still obtained. The reasonable agreement between the results with and without the pilings suggests that the effect of the pilings is very minimal and cannot account for the 30-50% blocking suggested by Elgar et al. (2001). This suggests that the observed reduction in the wave heights is probably an effect of the deep bathymetric trench that is located under the pier. One way to confirm this suggestion is by using SWAN (which does not accommodate the pilings) to simulate this case. Fig 2.15 shows the significant wave heights obtained using SWAN for this case. The comparison between SWAN results and the observations along the two cross-shore sections showed good agreement. Furthermore, the comparison between SWAN computed and observed spectra at three different gauge locations, Fig.

2.16, showed reasonable agreement. This indicates that the pier legs (not included in SWAN domain) have an insignificant effect on the waves for the investigated conditions. However, this may not be always the case, since the wave blocking and diffraction/reflection by circular objects (e.g. pier legs) are in fact functions of the wave conditions. The apparent wave height reduction in the immediate shadow of the pier for the case presented here is hence attributable to the deep bathymetric trench located under the pier.

2.5 Concluding Remarks

It is often necessary to implement wave models on coastal domains where there are insufficient data for validation. Results may have to be accepted at face value (without tuning.) This is difficult from the user's viewpoint; for example, see Thieler et al. (2000) who suggest that several models may demonstrate poor performance in the field. It is therefore important to demonstrate that the models provide reasonable predictions using whatever data are available.

In this paper we have demonstrated that CGWAVE and SWAN provide fairly accurate simulations of three events modeled at the FRF, Duck (North Carolina). Although the two models are intended for different types of applications as a consequence of differing physics, turning various physical mechanisms on and off allowed an inter-comparison. It was demonstrated that the underestimation of wave heights by CGWAVE was possibly due to the absence of wave-wave interactions and the

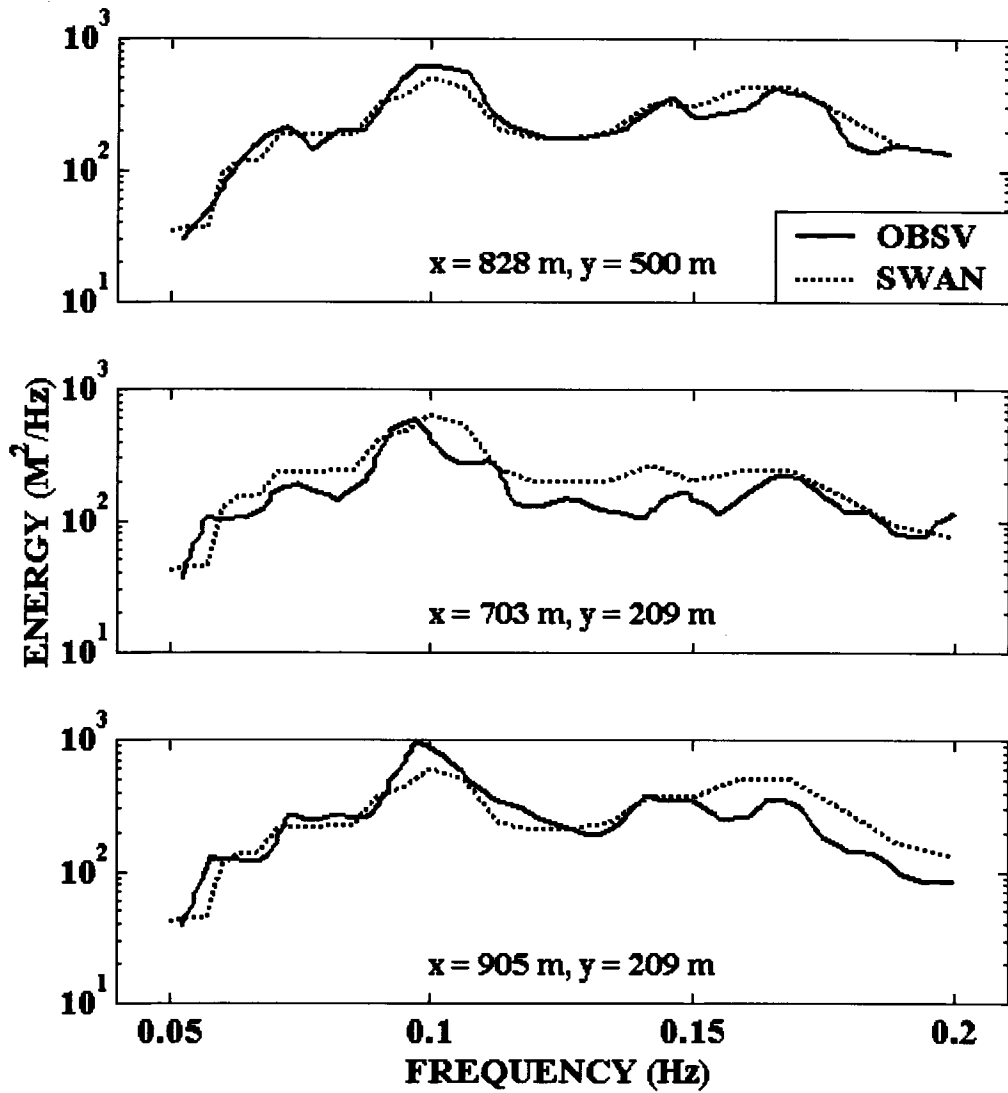


Figure 2.16: Elgar et al. (2001) observed (OBSV) and SWAN-computed (SWAN) wave energy spectra at three gauge locations for the 1997 case.

use of Dally et al. (1985) breaking formulation with unadjusted wave decay factors. Inclusion of wind generation on length scale of about 1 km (the approximate size of the domains modeled) has little effect. SWAN was able to qualitatively confirm observational findings of other researchers regarding wave breaking, triad wave-wave interactions, and wave directional spreading at this site. In a recent study, Elgar et al. (2001) have suggested including the effects of the pier legs through an empirical wave blocking mechanism. Here we have used CGWAVE, which includes structural and bathymetric diffraction, to show that the pier legs have little effect for the case examined. Further, the trends observed by Elgar et al. (2001) in the shadow of the pier and further away from it were replicated by CGWAVE and also by SWAN, which does not accommodate the pier legs. While the similarity of the results of SWAN and CGWAVE indicated that bathymetric and structural diffraction effects were not significant in the dissipative simulations, there is no guarantee that this will always be the case for all incident wave conditions; e.g. differences can certainly be expected for narrow peaked spectra or swell conditions (Bondzie and Panchang, 1993). Here too, variability in the wave field is found to be enhanced for non-breaking waves (e.g. Fig. 2.9 and Fig. 2.15). The effects of diffraction and reflection cannot be easily estimated *a priori*, and if the domains are small enough to ignore wind generation, it may be best to use combined refraction-diffraction models. The analysis and results presented here show that when the modeled physics are commensurate with what is occurring in the field, both models provide fairly reasonable and compatible predictions.

Chapter Three

OPERATIONAL WAVE PREDICTION AND WAVE DATA ASSIMILATION AT THE GULF OF MAINE

3.1 Introduction

The Gulf of Maine is a region of a very energetic wave climate compared to most of the United States Atlantic coastal regions, yet it is a region extremely lacking in wave information. Most of the energetic wave conditions that occur in this region are due to the extra-tropical storm systems "Northeasters" that typically reach their maximum strength as they pass through the region. The high seas generated from such systems represent a permanent threat not only to navigation but also to coastal areas. Wave observations from buoys and ships are limited in their spatial and temporal coverage. Although Satellite-derived wave measurements provide more coverage, these are not reliable near the coastal areas where measurements are most needed. Furthermore, satellite observations regardless of their coverage, do not provide near future wave predictions (forecast) that are essential for both economic and safety reasons. Analysis of long records of wave measurements can only provide statistical estimations of chances of occurrence for certain wave conditions in a given year at a specific location.

Numerical wave modeling, therefore, constitutes the only efficient and cost-effective approach to provide the required wave information in the Gulf of Maine over a large spatial domain at different times. Numerical wave models like WAM (Komen et al. 1994) and WAVEWATCH (Tolman 1989); are now routinely operational and produce ongoing forecasts for much of the global oceans. However, the resolutions used in such operations are too coarse for obtaining reliable wave information in coastal regions and the models themselves are intended to handle neither the finite depth effects nor the complex geometric features and the resulting wave-scattering effects that may be important in the near-shore areas. In these contexts, the Gulf of Maine region is not an exception. The National Center for Environmental Prediction (NCEP) runs WAVEWATCH III (hereinafter referred to as WW3) operationally to produce wave predictions for the Western North Atlantic region (including the Gulf of Maine region) with a grid size of 0.25 degrees. Operational wave predictions produced for the Gulf of Maine region by the Naval Oceanographic Office (NAVO) using WAM have a resolution of 0.20 degrees. Such coarse resolution range is insufficient to obtain required wave information at coastal and near-shore regions in the Gulf of Maine. Furthermore, even if the resolution was sufficient the wave information is still unreliable because these models do not account for the physical mechanisms affecting the wave evolution in the near-shore region.

The only possible approach to over come such limitations is through the local use of specialized models in the intermediate region between the grid points of the outer-ocean WAM or WW3 operations and the very near-shore areas. The off-shore extension

of the intermediate domain has to be sufficiently large in order to minimize the possible differences in the predicted wave conditions between two neighboring grid points of the coarse grid model. Such extension is also necessary to avoid any possible shallow water effects which are not fully accounted for in the coarse grid models. The intermediate domain, which in this case may be in the order of tens to few hundreds kilometers, will therefore experience local wave growth due to wind and calls for the use of phase-averaging models.

Traditionally, numerical wave models were run without the use of actual wave observations to improve the overall quality of the model results. The limited numbers of wave buoy observations were only useful for model validation/verification studies since, for many cases, these buoys are too localized for their measurements to provide a proper representation of the complete wave scattering problem. The significant increase in both spatial and temporal coverage of wave observations, which occurred over the last two decades, is mainly attributed to the wave measurements made available by satellite mounted instruments such as the Synthetic Aperture Radar (SAR) and Wave Altimeter. This dramatic increase in wave observations was utilized for improving the quality of wave model predictions via data assimilation techniques. Studies like those presented in Komen et al. (1994) have demonstrated that a considerable improvement in the quality of WAM model predictions can be achieved by data assimilation. Similar improvement have been also shown in studies by Janssen et al. (1989), Bauer et al. (1992), Lionello et al. (1992), Houlthuijsen et al. (1996), Breivik et al. (1998) and Dunlap et al. (1998). The increasing number of wave buoys in many marginal and shelf seas also provided wave

measurements that can be used in data assimilation schemes to improve wave prediction in marginal and shelf seas. The study by Voorrips et al. (1996) concluded that the assimilation of these "high quality" buoy measurements in addition to the "low quality" satellite measurements will lead to more improvement in model predictions compared with the use of the satellite measurements alone.

The principal motivation of the research presented in this chapter is to develop a high resolution operational wave forecasting system for the Gulf of Maine. The system is based on the numerical wave model SWAN (Holthuijsen et al. 2000); a state-of-the-art phase averaging model that accounts for the physical mechanisms associated with the wave generation and propagation in both deep and shallow waters. The major goal of this research is to examine the impact of assimilating wave buoy measurements on the quality of SWAN model predictions for the Gulf of Maine. The research mainly investigates the extent to which wave buoy data can be cross validated and assimilated using the model SWAN.

The research attempts to answer two major questions, relevant to the future of high resolution wave forecasting in the Gulf of Maine. The questions are: (1) How significant is the impact of the wave data assimilation technique used on the quality of SWAN model predictions?, and (2) Is the assimilation of the observed wave height data sufficient or is the assimilation of other types of observation (e.g. spectral data), which requires higher level of sophistication, needed?.

The layout of this chapter is as follows. A general description of the wave climate in the Gulf of Maine is given in section 3.2, along with some details about the events simulated in this study. A brief description of SWAN model is given in section 3.3, followed by a detailed description of the modeling schemes used in this study. Results are presented and discussed in section 3.4. Summary and concluding remarks are given in section 3.5

3.2 Wind and Wave Climates in the Gulf of Maine

3.2.1 General Background

The Gulf of Maine (Figure 3.1) is a semi-enclosed sea that is bounded to the south and the east by the Western North Atlantic Ocean. The northern and western boundaries for the Gulf of Maine are formed by the coastlines of Massachusetts, New Hampshire, Maine and Nova Scotia. Due to its location, the Gulf of Maine is rarely hit by hurricanes (unlike the U.S. east coast south of Cape Cod). The extreme wind and wave conditions in the Gulf of Maine occur primarily due to the extra-tropical storms "Northeasters", which (as the name implies) generate the most violent northeast winds in the region. The term "Northeaster" refers to a cyclonic (counter-clockwise) storm associated with an intense low pressure system that develops off the east coast. After such storm system develops it typically progresses northward or northeastward till it reaches its maximum intensity as it passes New England and then start declining. While the center of the storm is still to south of the coast, the local winds will be blowing from the east or the north east

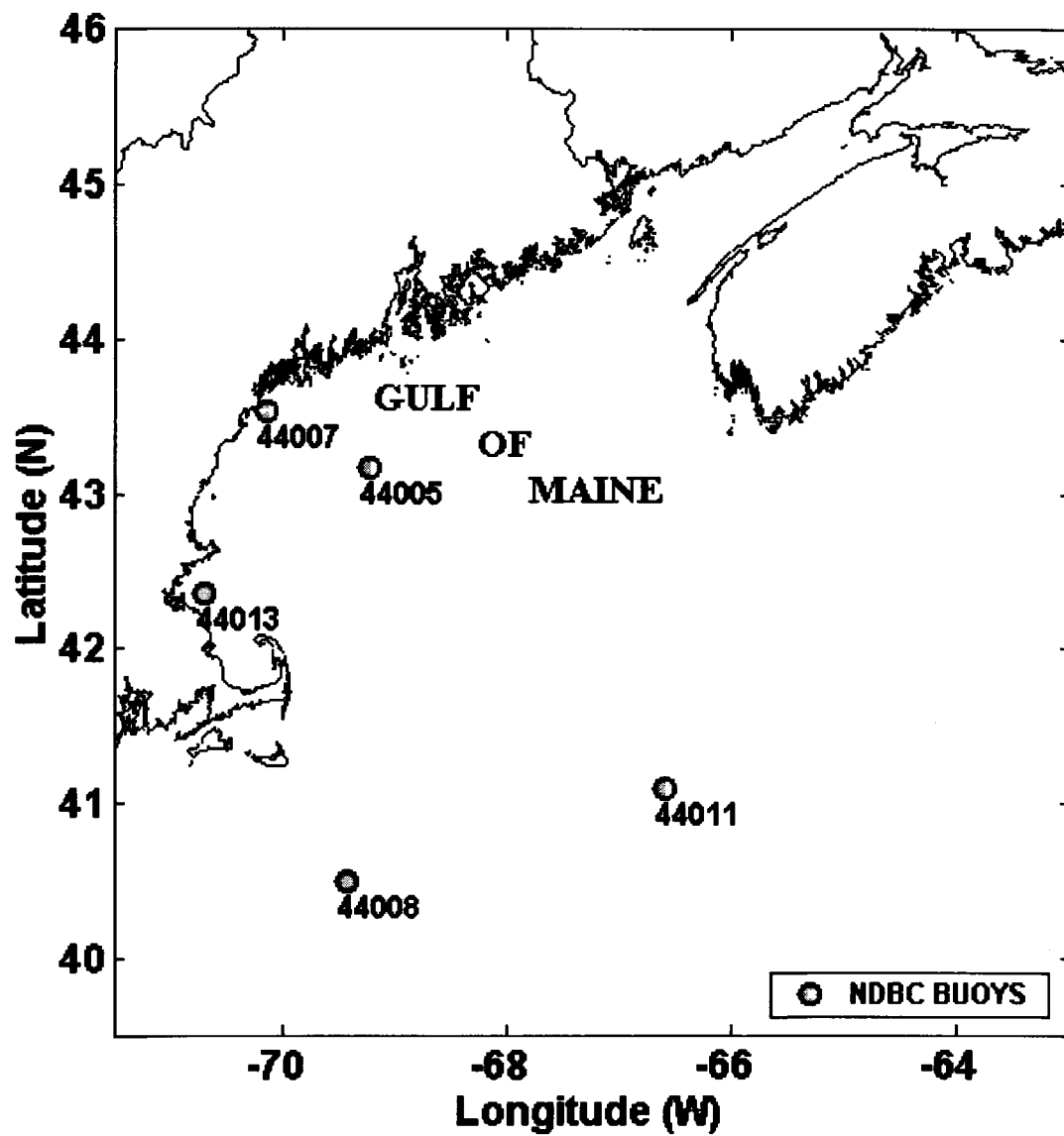


Figure 3.1: The model region with NDBC buoy locations used in this study indicated.

and as the center progresses northward or northeastward the local winds will shift to blow from north, northwest and west directions. Although Northeasters can typically occur any time during the year, these storms are most violent during the period from September to April.

The three buoys located inside the Gulf of Maine (Figure 3.1) are among the Western North Atlantic buoys that are operated and maintained by the U.S. National Data Buoy Center (NDBC). Since the early 1980's most of these buoys started continuously collecting wind and wave observation along with measurements of other atmospheric and oceanographic parameters. The relatively long records of wave measurements obtained from these buoys have been used in producing long term statistical estimates of wave heights at the buoy locations. The monthly mean wave heights, calculated by Gaillhousen et al. (1990), for Portland Buoy (44007) showed a low of 0.6 m in July and August and a high of 1.2 m in January, indicating strong seasonality of wave characteristics. According to their statistics, waves with significant wave height of 5m or larger have 0.4% chance of occurrence at buoy 44007 (Portland) in a given year, which is equivalent to about 35 hours per year. Dickson (1999) used the archived NDBC buoy data to compute the maximum wave heights for each month over a 14 years period. His computations showed that the largest wave height at Portland buoy (44007) was 7.3 m and was recorded in both February and November and the lowest wave height (2.6 m) was recorded in July. The compiled monthly maximum wave heights did not only show strong seasonality but also showed large inter-annual variabilities suggesting that the

long-term averages can be quite different from what might be expected in a given year (Dickson, 1999).

Another approach to produce long term wave height statistics for the Gulf of Maine is to use long term historical wind records (> 20 years) to hind-cast wave conditions. Using this approach, Jensen (1983) calculated the significant wave height at 10 m depth contour along Maine coastline. His estimates suggested that the annual maximum and minimum wave heights occur in December and July respectively indicating strong seasonality. Panchang et al. (1990) computed extreme wave statistics for the Gulf of Maine by numerically hindcasting wave conditions associated with 22 winter Northeasters that occurred over a 34 year period. For each Northeaster, the recorded storm characteristics were first fed to a model to generate the wind field, which then was used to force a hybrid, parametric type wave model. The wave model results for the 22 storm events were then analyzed to produce wave height statistics at each grid point of the model domain. The resulting statistics, which agreed very well with estimates based on shipboard observations, suggested that the maximum 100-year and 50-year significant wave heights are in the order of 13 m and 11 m respectively. This indicated that a wave with 13 m significant wave height has 1% chance of occurrence and a wave with 11 m significant wave height has 2% chance of occurrence in a given year.

3.2.2 Description of Storms

The wave conditions simulated in the present study represent the seasonal maximum wave conditions that occurred in the year 2001. These maximum wave conditions were associated with Northeaster systems that passed over the region in early February, late April, early September and late November. The February and November Northeasters generated the strongest wind conditions, hence, the largest wave heights. These observations are in agreement with the computations of monthly maximum wave heights compiled by Dickson (1999) for Portland buoy. Each seasonal maximum conditions are contained into an 8 days period which represent the model simulation period (Table 3.1). For each storm event, the description of the observed conditions at one of the NDBC buoys is provided below as a representation of the general characteristics of storms in the Gulf of Maine.

Storm 1: An intense extra-tropical low pressure passed over the region in the period between February 5th and 8th (Figure 3.2a). Typically, the wind started blowing from the northeast when the storm reached Portland buoy (44007) around noon time on the 5th. Less than 24 hours later the winds were blowing from the north before shifting and started coming from the northwest until they slackened. This typical winter Northeaster lasted for about 36 hours (Figure 3.2a). The maximum wind speed and significant wave height recorded at Portland buoy during this storm were 18 m/s and 5 m, respectively.

	Simulation Period	Storm Period
Storm 1	February 3 rd – 11 th	February 5 th – 8 th
Storm 2	April 15 th – 23 rd	April 18 th – 20 th
Storm 3	September 10 th – 18 th	September 14 th – 16 th
Storm 4	November 4 th – 12 th	November 6 th – 9 th

Table 3.1: Simulation period and approximate storm period for year 2001 seasonal maximum wave conditions simulated in this study.

Storm 2: The maximum wind and wave conditions recorded at buoy 44005 (Gulf of Maine) between the 18th and the 20th of April were also associated with an intense extra-tropical low pressure (Figure 3.2b). The wind started blowing from the northeast in the early morning hours of the 18th, and by the end of the day, winds were blowing from the northwest before slackening significantly by the noon time of the 19th. The maximum recorded wind and waves at this buoy were 19 m/s and 4 m respectively. Similar to the February storm, this mid spring storm also lasted for about 36 hours (Figure 3.2b).

Storm 3: The wind started to blow from the northeast few hours after the low pressure reached its minimum late in the 13th of September at buoy 44005 (Figure 3.2c). The wind continued from the north from the late morning till the early evening on the 14th before it slightly shifted and started blowing from the northwest. By the end of the day, the wind has completely slackened. At this location, the maximum recorded wind speed and wave height during this event were 10 m/s and 2.8 m respectively. This mild late summer Northeaster lasted only for about 24 hours only (Figure 3.2c).

Storm 4: The northeast wind started to blow at buoy 44005 around the early morning of the 6th of November in association with a very intense low pressure (Figure 3.2d). By the late morning the wind was blowing almost from the north and shifted gradually till it became from the northwest by the early morning of the 7th. The wind continued blowing from the northwest until it slackened in the late hours of the 8th. With typical conditions maintained for almost 48 hours this fall Northeaster was the longest lasting strong

a.

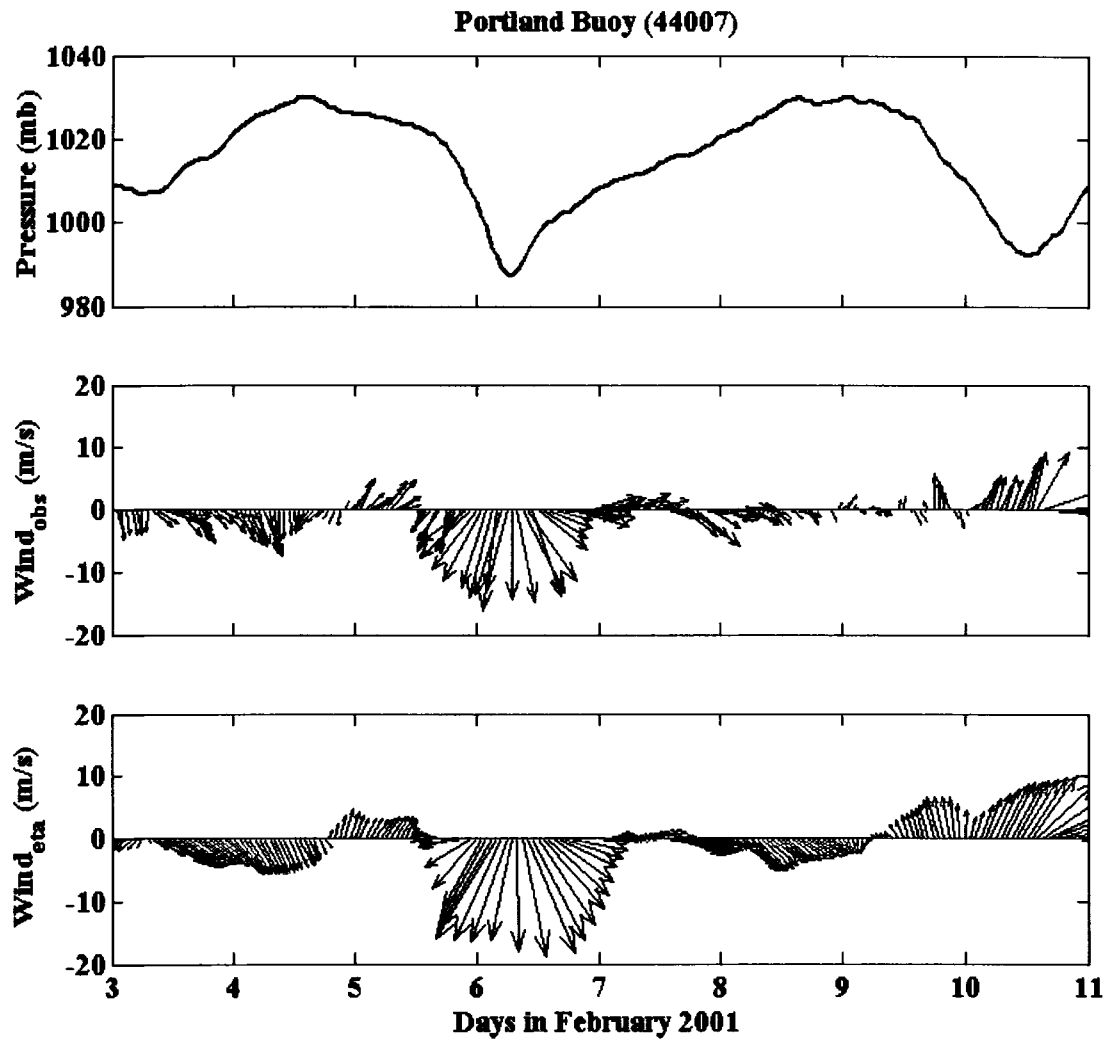
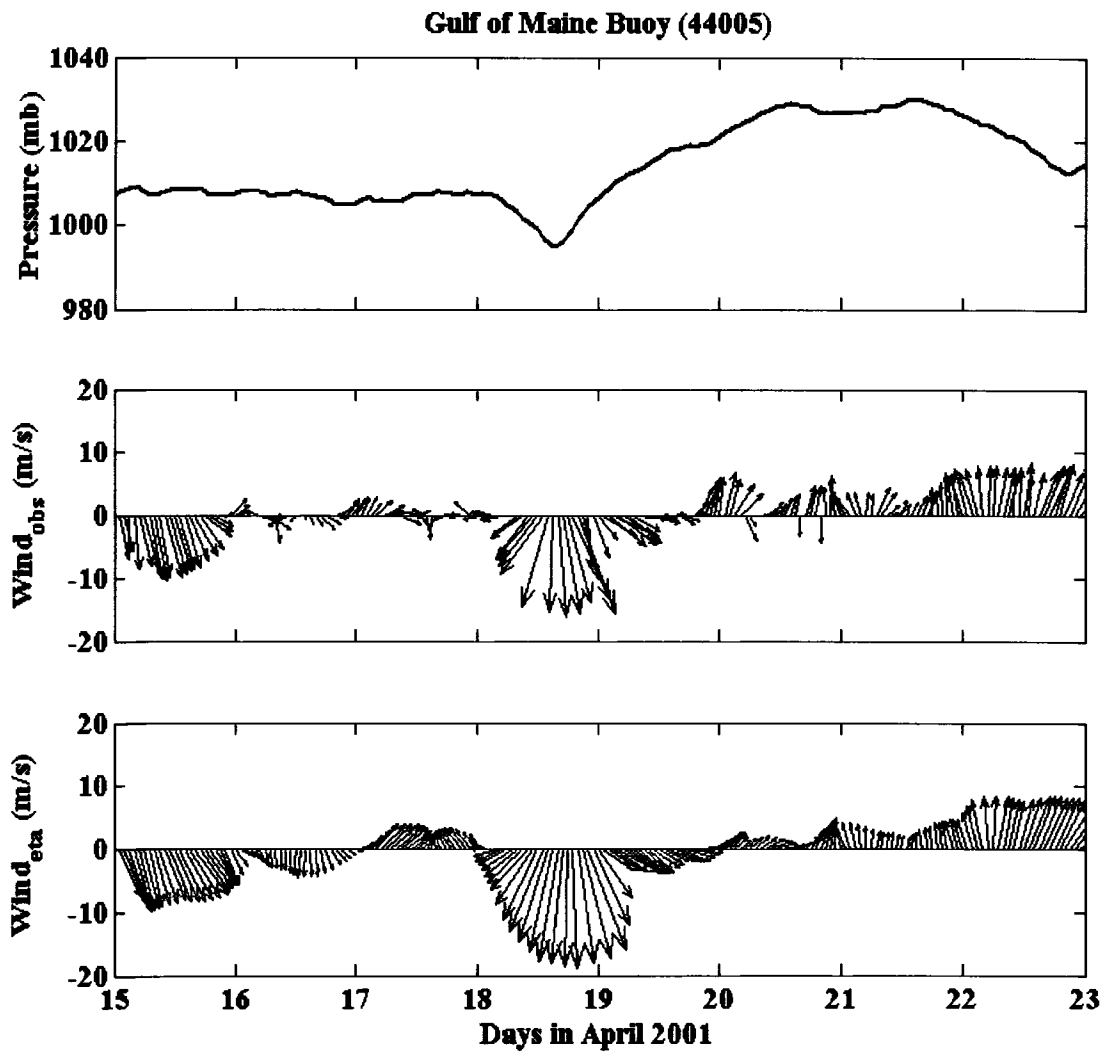


Figure 3.2: Observed and predicted atmospheric parameters at NDBC buoy locations during 8-day periods.

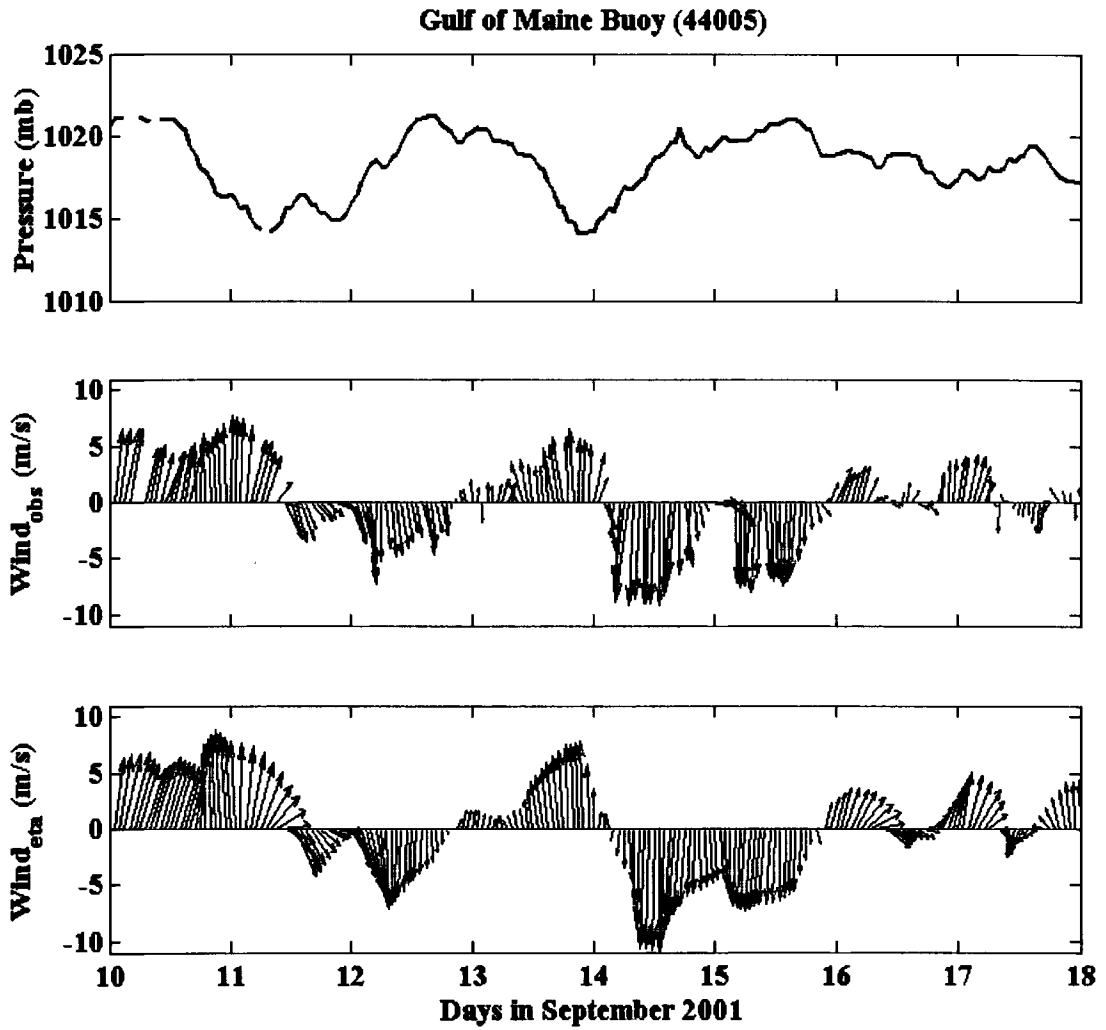
- a. Observed and predicted atmospheric parameters at buoy 44005 during an 8-day period in February 2001. Observed pressure (top panel), observe wind velocity (middle panel) and ETA model predicted wind velocity (bottom panel).

b.



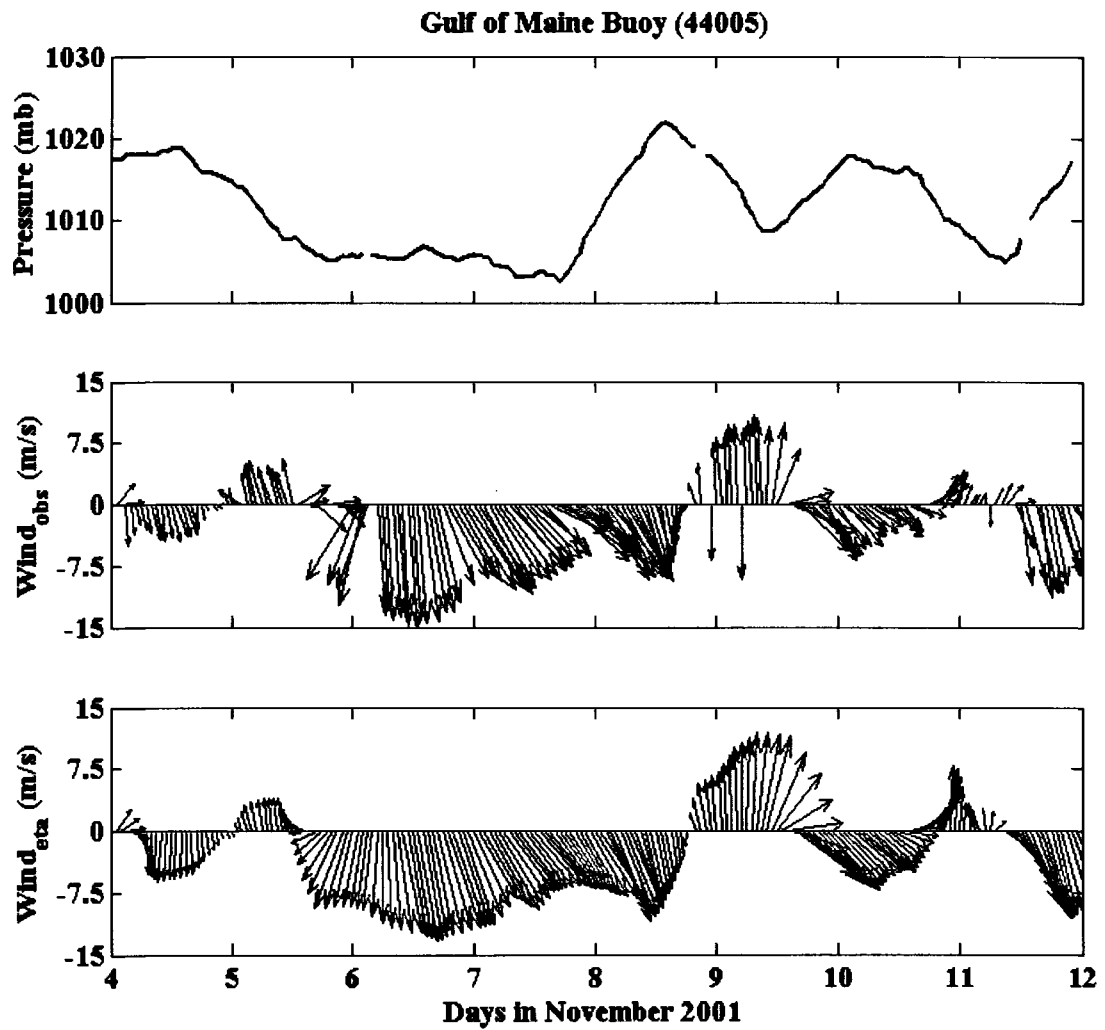
b. Observed and predicted atmospheric parameters at buoy 44005 during an 8-day period in April 2001. Observed pressure (top panel), observe wind velocity (middle panel) and ETA model predicted wind velocity (bottom panel).

c.



- c. Observed and predicted atmospheric parameters at buoy 44005 during an 8-day period in September 2001. Observed pressure (top panel), observe wind velocity (middle panel) and ETA model predicted wind velocity (bottom panel).

d.



d. Observed and predicted atmospheric parameters at buoy 44007 during an 8-day period in November 2001. Observed pressure (top panel), observe wind velocity (middle panel) and ETA model predicted wind velocity (bottom panel).

Northeaster in 2001 (Figure 3.2d). The wind and wave conditions reached their maximum of 15 m/s and 3.8 m, respectively at this location.

3.3 Modeling Details

3.3.1 SWAN Model

The model SWAN (<http://swan.ct.tudelft.nl>) is a third generation numerical wave model developed at the Technical University of Delft in the Netherlands (Booij et al. 1999; Ris et al. 1998; and Ris et al. 1999). The model is based on the following spectral action balance equation:

$$\frac{\partial}{\partial t} N + \frac{\partial}{\partial x} c_x N + \frac{\partial}{\partial y} c_y N + \frac{\partial}{\partial \sigma} c_\sigma N + \frac{\partial}{\partial \theta} c_\theta N = \frac{S}{\sigma} \quad (3.1)$$

where N is the action density (= spectral energy/ σ), σ is the wave frequency, θ is the wave direction, and c_x and c_y are components of the wave propagation velocity. The first term on the left hand side of (3.1) represents the rate of change of action in time. The second and the third terms represent the propagation of action in the (x,y) space. The fourth and fifth terms represent, respectively, the frequency shift and refraction induced by depth and currents. The source/sink term (S) on the right hand side of (3.1) represents the effects of generation, dissipation and nonlinear wave-wave interactions on wave energy; and is given by:

$$S = S_{inp} + S_{brk} + S_{frc} + S_{wcp} + S_{trd} + S_{qud} \quad (3.2)$$

where S_{inp} represents the atmospheric wind input, S_{brk} represents dissipation due to wave breaking, S_{frc} represents the dissipation due to bottom friction, S_{wcp} represents the dissipation due to whitecapping; and S_{trd} and S_{qud} represent the effect of triad and quadruplet non-linear wave-wave interactions respectively.

The SWAN model was originally developed to simulate wave conditions in the very near-shore area (domain sizes of 25 km or less). However, the recent developments to the model allow its application to areas as large as marginal seas. The recent version of SWAN were not, by any mean, intended to replace WW3 or WAM models and therefore, it has not been verified on oceanic scales where it is certain to be less efficient model since it has not been parallized.

3.3.2 Modeling Schemes

Table 3.2 shows the major modeling schemes used in the SWAN-based operational wave prediction system developed for the Gulf of Maine. For comparison purposes Table 3.1 also shows the modeling schemes used by the other two operational wave models (WW3 and WAM) which provide wave predictions for the Gulf of Maine region. Model grid size constitutes one of the major modeling schemes in which SWAN considerably differ from WW3 and WAM models. The smaller grid size used in SWAN

	SWN	WAM	WW3
Domain	GOM	GOM	WNA
ΔX	0.05°	0.2°	0.25°
ΔY	0.05°	0.2°	0.25°
Frequencies	25	25	25
Directions	24°	24°	24°
Wind	ETA	COAMPS	ETA
Hindcast	12 hours	12 hours	12 hours
Forecast	48 hours	48 hours	126 hours
Platform	PC	S. Computer	S. Computer

Table 3.2: Modeling schemes used in three different operational wave prediction systems.

increases the resolution by a factor of 4 to 5 compared to grids of WAM and WW3 models. The model domain of SWAN for the Gulf of Maine is shown in Figure 3.3, along with the model grid mesh. Other major difference in the modeling schemes pertains to the bottom induced wave breaking mechanism included only in the SWAN model.

All three models shown in Table 3.2 use different input boundary conditions and data assimilation procedures. The following two subsections provide details of the schemes used for incorporating the input boundary conditions and wave data assimilation into the SWAN-based system.

3.3.3 Data Assimilation Scheme

Attempts to improve the quality of wave models predictions through data assimilations started early in the last decade, after being motivated by the large spatial and temporal coverage of wave measurements from satellite mounted instruments. Although many studies have demonstrated that data assimilation could considerably improves wave model predictions, most studies have shown that the obtained improvements fade away shortly after turning off the data assimilation scheme. This is mainly due to the fact that waves in the model (and also in the real world) are primarily controlled by the forcing wind field. Correction to the wind field through assimilating wind measurements from satellite scatterometer constitutes one approach to over come

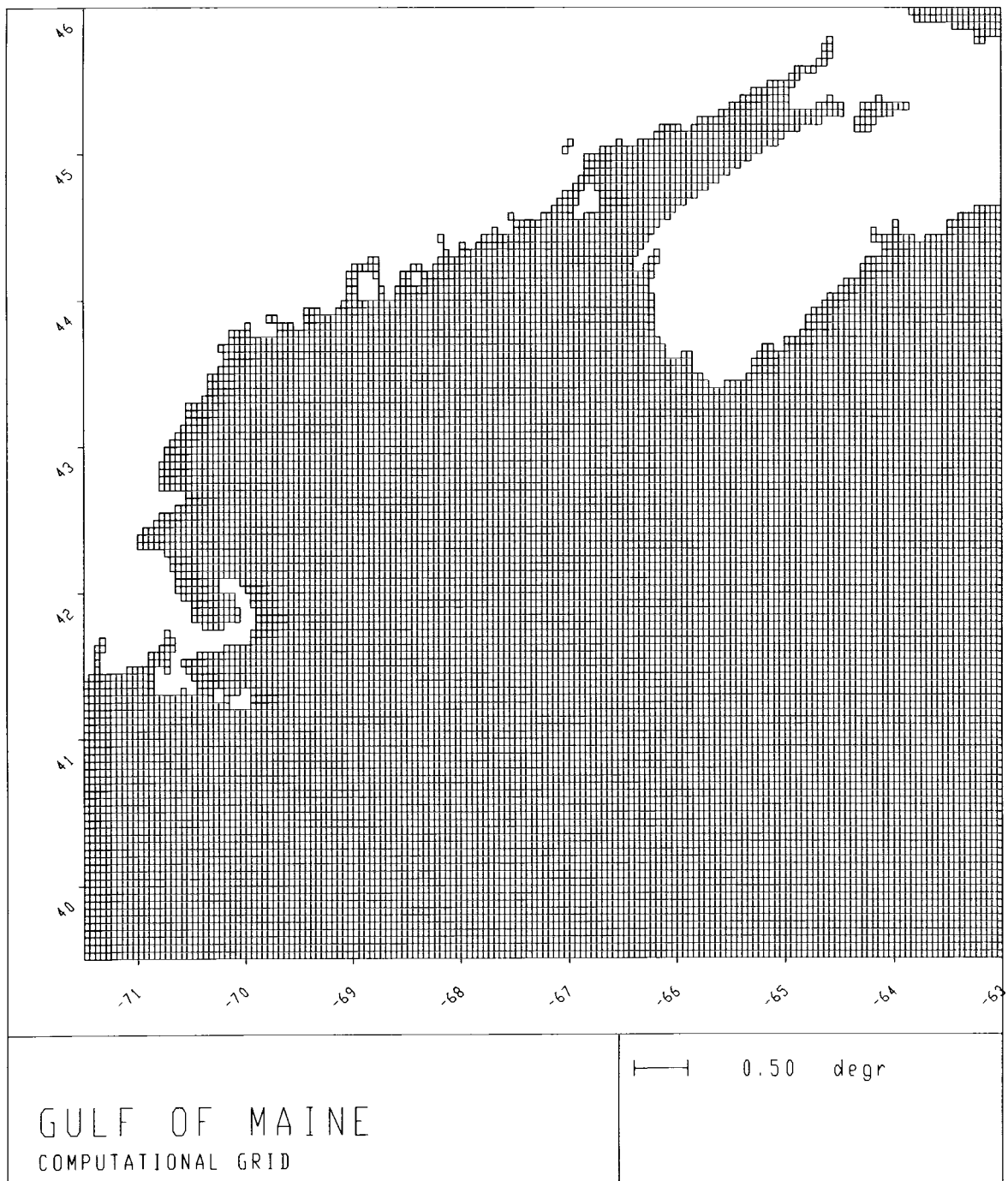


Figure 3.3: SWAN wave model computational domain.

such limitation. The more sophisticated approach involves correcting the atmospheric input source term " S_{inp} " (e.g. Equation 3.2) through inverse modeling procedures after assimilating the wave conditions.

The availability and reliability of wave data are two key limiting factors of the data assimilation. Satellite wave measurements over regional areas might be available only few days apart. These measurements are not reliable in the coastal and nearshore areas (Siddabthula and Panchang, 1996). The measurements from the available wave buoys, most of the times, are too localized to provide a proper representation of the complete wave scattering problem, and therefore are of less benefit for data assimilation.

Data assimilation schemes used in wave modeling vary considerably in their levels of sophistication. In general, the assimilation of wave height data obtained from satellite altimeter or non-directional buoys requires a lower level of sophistication than assimilating the two dimensional wave spectra inverted from satellite SAR measurements or obtained from directional wave buoys. Schemes that involve the assimilation of integrated wave parameters (wave height and waves period) are referred to as Optimal Interpolation of Integrated wave parameters (OI-I) schemes. In these schemes the modeled wave spectrum is corrected based on the analysis of the observed and modeled wave height and period. In operational wave forecasting systems the most used schemes are those based on the assimilation of significant wave height since it is the most operationally available wave data. Wave height observations; however, are not enough to correct the model predicted two-dimensional wave spectrum. More sophisticated

schemes are based on the assimilation of the full 2D wave spectrum. These schemes involve partitioning the observed and modeled wave spectra into several segments that represent a distinct wave type (i.e. windsea or swell). The interpolation of the mean parameters from the cross-examined observed and modeled partitions provide the necessary information to update each segment spectrum. Such schemes are referred to as Optimal Interpolation of Partitions (OI-P) schemes.

In this study the (OI-I) data assimilation scheme used by Bauer et al. (1992) is implemented in the SWAN-based system to assimilate the wave height measurements obtained from wave buoys located in the Western North Atlantic (including the Gulf of Maine). The comprehensive study by Bauer et al. (1992) has shown that significant improvements could be achieved in WAM model predictions by using this scheme. Particularly in regions dominated by swell conditions, relaxation times after the data assimilation procedure was switched off were as long as 5 days (Bauer et al. 1992). This simple and straight forward assimilation scheme was selected for three important reasons:

- (1) Computational Resources: The simulations in this study as well as the experimental operational wave prediction system had to run on personal computers and therefore a less computationally demanding technique was favored.
- (2) Available Data: All the buoys located inside the model domain are non-directional; however they provide 1D spectra which without any directional

information can not be converted in a reliable way to the 2D spectra for assimilation purposes.

- (3) Systematic Order: The present research, to the best of the author's knowledge, represents one of the earliest studies involving wave data assimilation using SWAN model. Therefore, it was necessary to employ a simple scheme that has shown to work, i.e. less risk is involved.

In this scheme, the SWAN-generated 2D wave spectrum at every grid point (i,j) inside a specified range of influence (L_x, L_y) is corrected by a factor $C_{i,j}$ that relates the new spectrum $E_{new}(\sigma, \theta)$ to the spectrum $E_{swan}(\sigma, \theta)$ predicted by SWAN model. Thus, we have

$$E_{new}(\sigma, \theta)_{i,j} = C_{i,j} \times E_{swan}(\sigma, \theta)_{i,j} \quad (3.3)$$

The correction factor $C_{i,j}$ is defined as

$$C_{i,j} = \left(1 + w_{i,j} \times \frac{H_s(obs)_{ii,jj} - H_s(swam)_{ii,jj}}{H_s(swam)_{ii,jj}} \right)^2 \quad (3.4)$$

where $H_s(obs)$ and $H_s(swam)$ represent the buoy observed and SWAN computed significant wave heights at the nearby buoy location (ii,jj), respectively. The weighting function $w_{i,j}$ is selected as

$$w_{i,j} = \begin{cases} 1-R & ; R \leq 1 \\ 0 & ; R > 1 \end{cases} \quad (3.5)$$

where R is given by

$$R = \left\{ 0.5 \times \left[\left(\frac{X(i) - X(ii)}{L_x} \right)^2 + \left(\frac{Y(j) - Y(jj)}{L_y} \right)^2 \right] \right\}^{\frac{1}{2}} \quad (3.6)$$

where the terms $[X(i)-X(ii)]$ and $[Y(j)-Y(jj)]$ represent the longitudinal and latitudinal distances of the model grid point from the observation point respectively. These distances are normalized by the corresponding scales L_x and L_y on either side of the measurement point.

In the present study, the selection of the range of influence for each buoy was mainly controlled by how close the buoy of interest is to the nearest buoy. Ranges of influence for closely located buoys are small while they are larger for buoys that are relatively far away from the other buoys. Several assimilation experiments with different ranges of influence were carried out before those shown in Table 3.3 were finally selected to be used in this study. Experiments showed considerable variabilities in the results obtained with different ranges of influence. In particular, small differences in the latitudinal ranges of influence produced significant variabilities in the model results. In general, the most acceptable model results were obtained when assigned ranges of influence for the buoys did not overlap.

Buoys	L_x	L_y
44005	0.54°	0.18°
44007	0.65°	0.04°
44008	1.40°	0.10°
44011	1.60°	0.10°
44013	0.20°	0.36°

Table 3.3: Longitudinal (L_x) and Latitudinal (L_y) ranges of influence used in the assimilation of wave data from 5 NDBC buoys into the model simulations.

3.3.4 Boundary Conditions Schemes

The use of input boundary conditions is a way to account for the swell conditions generated by storms that occur outside the model domain. Storm generated swells propagate shoreward for a long distance before their energies start to dissipate. Such swell conditions are commonly observed in the Gulf of Maine especially during the summer season when the sea-state is relatively calm. Two different boundary conditions schemes had to be used in this study. Detailed descriptions of the two boundary conditions schemes used are provided below.

- **Boundary Condition Scheme 1:** Running SWAN in an operational basis to provide wave predictions for the Gulf of Maine requires that predicted boundary conditions along SWAN open boundaries should be provided to the model on an operational basis. The only possible source for the required boundary conditions would be the wave predictions obtained by one of the coarse grid wave models. The WW3 predictions for the Western North Atlantic are routinely provided on the public domain every 12 hours. However, these wave predictions are only provided in parametric format (i.e., significant wave height, peak wave period and peak wave direction) in 3-hours interval. Two dimensional (2D) wave spectra predictions are provided only at the locations of two NDBC buoys (44008 and 44011), inside the model domain of the present study.

Wave conditions along the open boundaries of SWAN model domain (Figure 3.3) vary significantly, and therefore waves at the open boundaries of the model cannot be assumed constant. For such a case, waves along the open boundaries of SWAN has to be specified in a nested format which consists of 2D wave spectra at points along the boundary, that do not have to precisely coincide with SWAN grid points. The boundary conditions scheme that was developed for this purpose uses the WW3 parametric wave predictions and generates 2D wave spectra at WW3 grid points along SWAN open boundaries for the prediction period. In order to improve the quality of the generated spectra they are weighted by the WW3 predicted spectra at the location of buoys 44008 and 44011. The generated 2D JONSWAP spectra (at each grid point over time) are then written to a file in a format that is recognizable by SWAN as nested boundary conditions (as if it was generated by a previous coarser grid SWAN simulation).

- **Boundary Condition Scheme 2:** For SWAN model simulations that correspond to the seasonal maximum conditions the boundary condition scheme 1 (described above) could not be used. This is mainly due to the fact that WW3 wave predictions for the Western North Atlantic are only archived for a period of 48 hours. Since SWAN simulation, in this case, are made in hindcast mode, it is possible to use the observed data at the two NDBC buoys located outside the Gulf of Maine (i.e. 44008 and 44011) as replacement for the unavailable boundary conditions. Therefore, a second boundary conditions scheme had to be developed specifically for the seasonal maximum conditions simulations. This boundary conditions scheme (2) is based on the continuous assimilation of observed wave

heights at the two buoy locations using the data assimilation scheme described earlier in subsection (3.3.3). This continuous assimilation is carried out along the whole simulation period at an interval of 3 hours which is similar to the interval at which the WW3 predictions would be provided if they were available. This interval is also similar to that at which the NCEP predicted wind fields (using ETA model) are generated. Before this boundary conditions scheme is used it is first tested in subsection 3.4.2 below.

3.4 Results and Discussion

The results are presented and discussed in the following order. First in the sample case presented in subsection 3.4.1, the operation of the developed wave prediction system is replicated with the boundary condition scheme 1 and the data assimilation scheme implemented. WW3 predictions, available for this case only, are used to provide the boundary conditions for SWAN simulation. In the test case presented in subsection 3.4.2; the developed boundary condition scheme 2 is examined. This is achieved by comparing the results obtained using boundary conditions scheme 2 with results obtained using boundary conditions scheme 1. In subsection 3.4.3, the four seasonal maximum wave conditions are simulated with the model forced only by the boundary conditions and input wind. Attempts are then made to improve the quality of the model results through the assimilation of wave buoys data. The effect of data assimilation technique on model results is evaluated by switching off the data assimilation scheme after certain time periods allows for examining the impact of the used assimilation technique on the model

results. The spatial effect of the data assimilation during and after the assimilation period is examined in subsection 3.4.4.

3.4.1 Sample Case

The sample case presented in this subsection experimentally replicates the operation of the above described system over a period of 2.5 days. For this specific time period, the available WW3 wave predictions were used to provide boundary condition for the SWAN simulation. Figure 3.4 shows the observed and predicted wind and wave conditions during the simulation period. Model results obtained with atmospheric wind inputs and WW3-based boundary conditions show significant underprediction in terms of wave heights at buoy location 44005 between the 11th and the 13th of February. Such underprediction might not be attributed to the wind effect since the predicted forcing winds are overpredicted at this location during that period. Similar underprediction in the mean wave period also occurs at this location. With few exceptions, most of the other under- and over- predictions in the wave heights at all three buoy might be attributed to the under- and over- predictions in the forcing wind fields.

The data assimilation scheme has been implemented in an operational wave prediction system for the Gulf of Maine which runs every 12 hours. The system started at February 9th (00 hour) by running the model first in a hindcast mode to simulate the wave conditions in the previous 12 hours. For this hindcast simulation, the observed wave heights at five NDBC buoys (Figure 3.1) are assimilated in an hourly basis into the

wave model run. The results obtained at the end of the 12 hours hindcast mode provide the initial wave conditions for the subsequent forecast mode simulation. This hindcast mode results are also used as initial wave condition for the following hindcast run 12 hours later. By the time the system has been running operationally for 2.5 days (i.e. by 12 hour on the 11th of February) it has actually completed a total of 6 hindcast mode runs subsequently. The results obtained from the last hindcast run provide the hotstart for the forecast mode in which the model then ran for a 4.5 day period between the 12 hour on the 11th and the 00 hour on the 16th.

The model predictions obtained at the end of each hour during the 2.5 days of data assimilations (Figure 3.4) show improvements in the model predicted wave heights in comparison with those obtained without assimilation at buoys 44005 and 44013. In particular, the underprediction in the wave heights obtained at buoy 44013 without assimilation between noontimes of the 9th and the 10th have significantly improved (Figure 3.4c). By the end of the assimilation period the predicted wave heights at the three buoy locations are in good agreement with the observed wave conditions. During the first 36 hours of the forecast mode significant improvements have been obtained at buoy location 44005 (Figure 3.4a) in terms of predicted wave heights and periods. Beyond the first 36 hours forecast, the model predictions with and without assimilation show reasonable agreements with the observed wave conditions at this buoy location. At buoy location 44013, there are no improvements in the model predictions for the first 24 hours of the forecast. Beyond that, minor improvements in the predictions occur for about 48 hours, however, the wave heights are slightly overpredicted on the 13th due to

a.

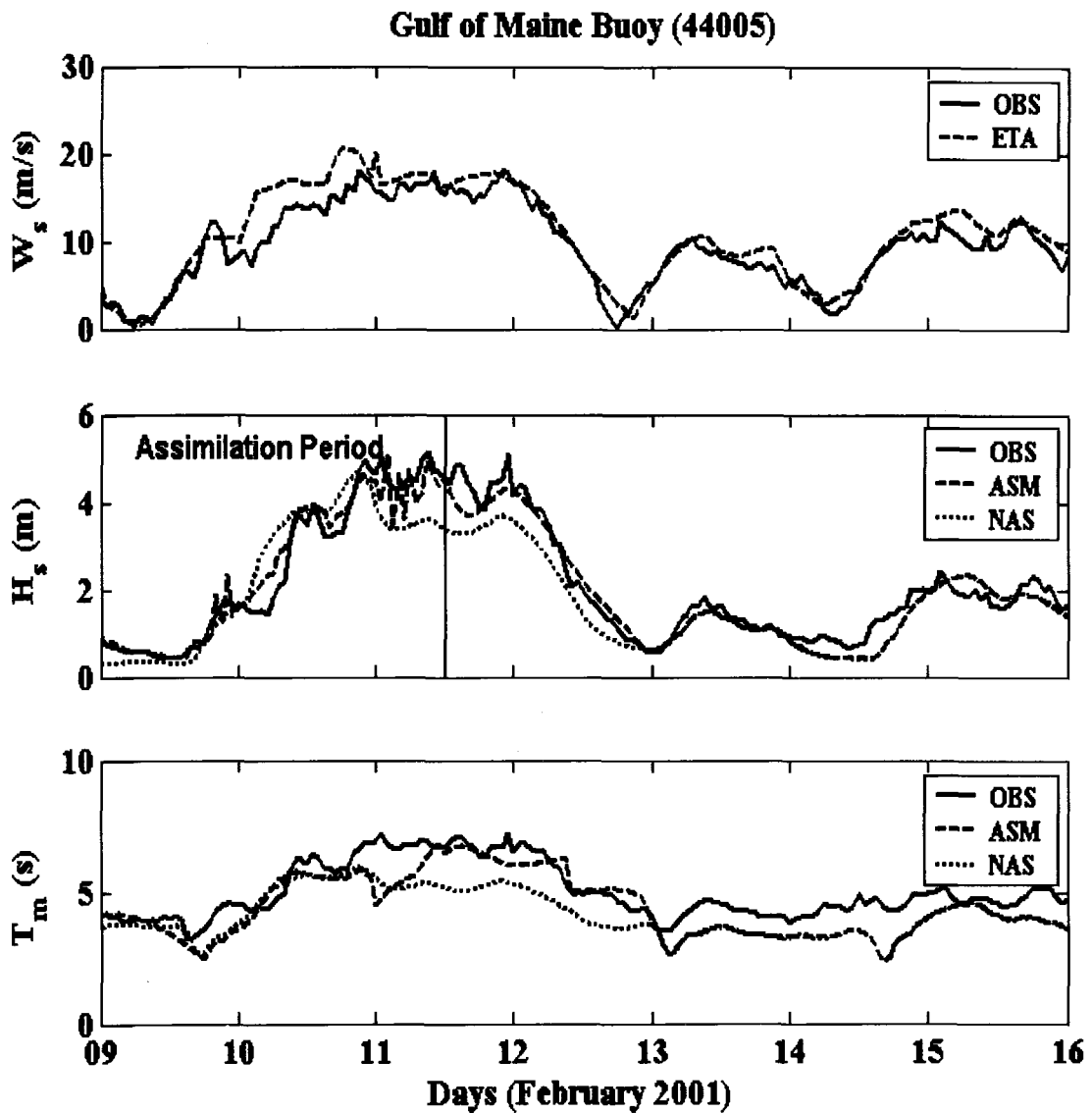
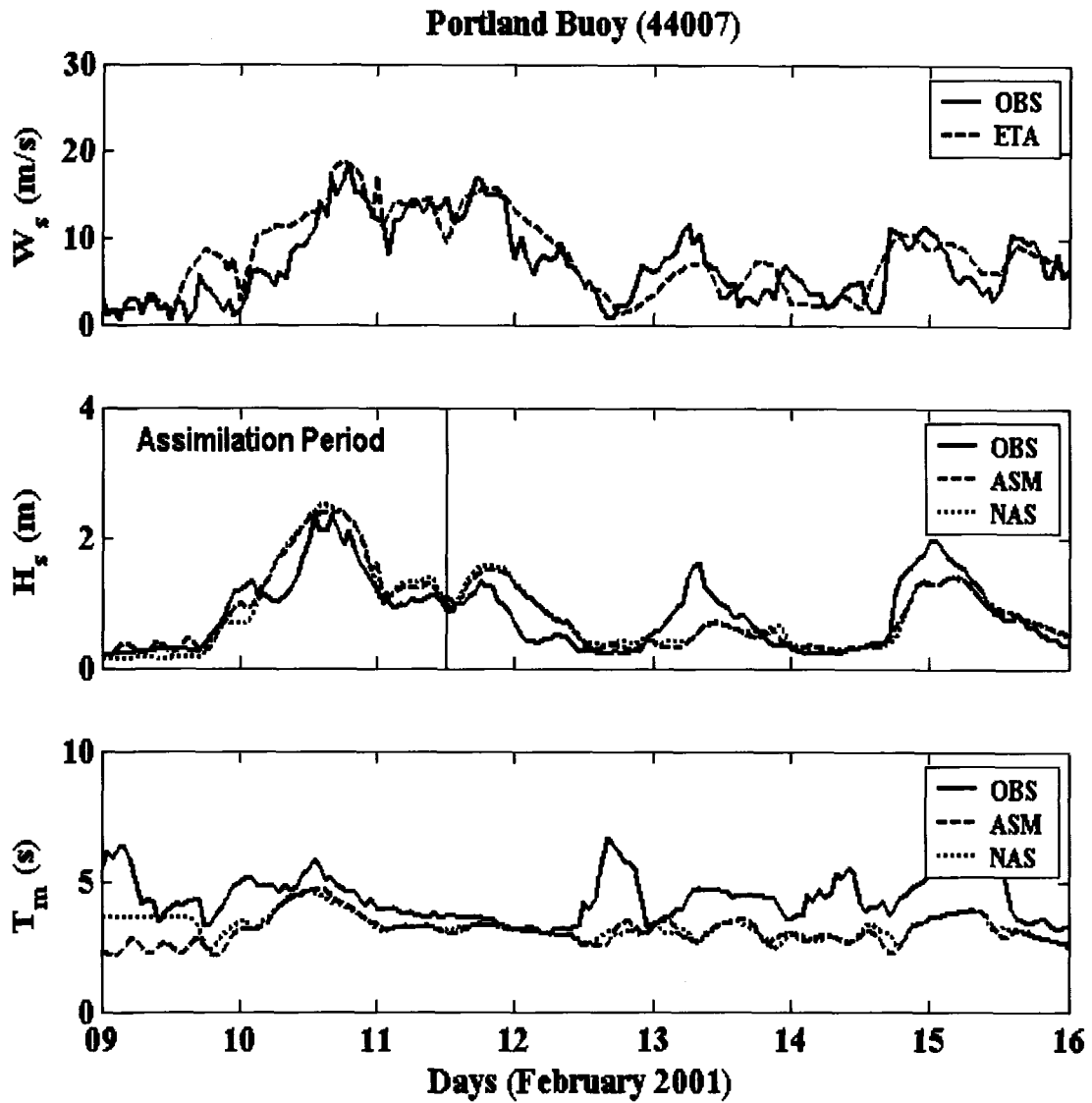


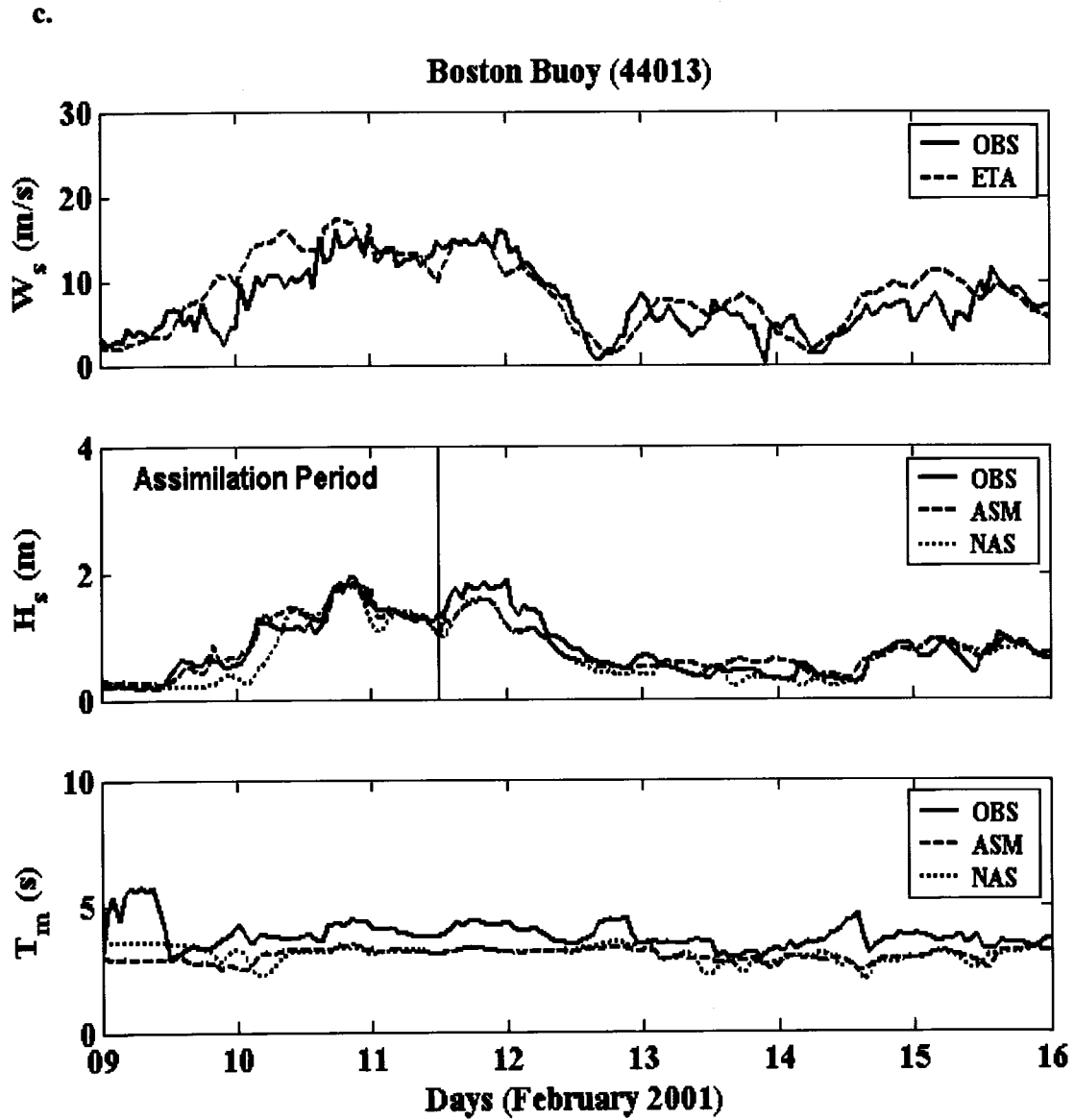
Figure 3.4: Observed (OBS) and predicted wind speed (top panel), significant wave height (middle panel) and mean wave period (bottom panel) for a 7-day period in February 2001 at three buoy locations.

- a. Observed (OBS) and predicted wind speed (top panel), significant wave height (middle panel) and mean wave period (bottom panel) for a 7-day period in February 2001 at buoy 44005. ETA represents ETA model predicted wind speed; ASM and NAS represent SWAN results with and without data assimilation, respectively.

b.



b. Observed (OBS) and predicted wind speed (top panel), significant wave height (middle panel) and mean wave period (bottom panel) for a 7-day period in February 2001 at buoy 44007. ETA represents ETA model predicted wind speed; ASM and NAS represent SWAN results with and without data assimilation, respectively.



c. Observed (OBS) and predicted wind speed (top panel), significant wave height (middle panel) and mean wave period (bottom panel) for a 7-day period in February 2001 at buoy 44013. ETA represents ETA model predicted wind speed; ASM and NAS represent SWAN results with and without data assimilation, respectively.

the overprediction in the forcing wind field (Fig 3.4c). The model predicted wave field during both hindcast and forecast modes at buoy 44007 show no improvement especially beyond the 9th (Figure 3.4b). The significant mismatches between the model predictions and the observations can be largely attributed to the apparent mismatches between the observed and predicted wind fields at this location.

Figure 3.5 and Table 3.4 show that, for the first 48 hours of the forecast the data assimilation yields considerably less scattered wave height predictions at the location of buoy 44005. The data assimilation reduced the scatter index at this buoy location by more than 13%. The large scatter index computed for wind speeds at buoy locations 44007 and 44013, in comparison with that computed at 44005 buoy, also indicate that the mismatches between observed and computed wave conditions can be attributed to winds.

3.4.2 Test Case

In this test case, the observed wave conditions presented in the above sample case are simulated. The available WW3 wave predictions, for this specific time period, were used by boundary conditions scheme 1 to provide the boundary conditions for the first SWAN simulation. In a second SWAN simulation, the WW3-based boundary conditions were replaced by assimilated boundary conditions obtained using the boundary conditions scheme 2.

Figure 3.6 shows reasonable agreements between SWAN results obtained with the two different boundary conditions schemes. Such an agreement validates the use of

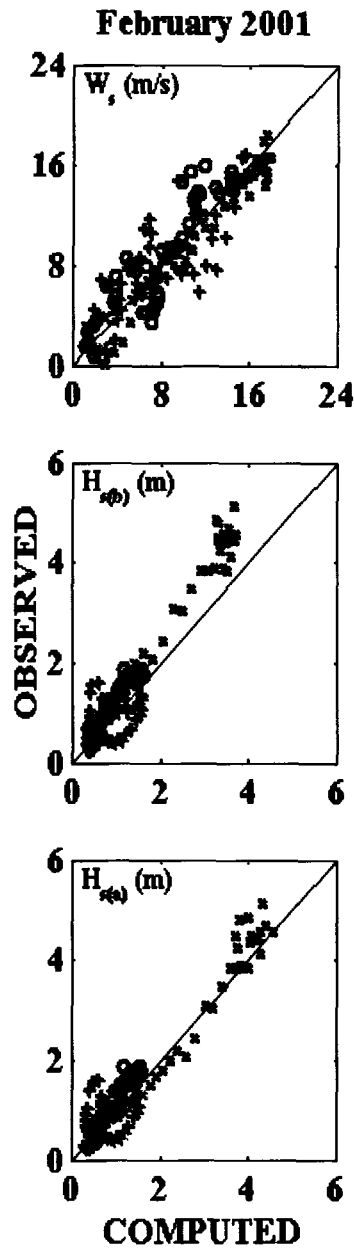


Figure 3.5: February 2001 inter-comparisons of observed and ETA model computed wind speeds (top panel), observed and SWAN computed significant wave heights without buoy data assimilation (middle panel); and observed and SWAN computed significant wave heights with WAVEWATCH predicted boundary conditions for 48 hours after assimilation switched off (bottom panel). (x), (+) and (o) represent buoys 44005, 44007 and 44013, respectively.

Wind Speed				
Gauge #	Bias (m/s)	RMSE (m/s)	SI (%)	Cor. (.)
44005	0.71	1.31	12.69	0.87
44007	-0.26	2.55	30.04	0.70
44013	-0.59	2.11	24.12	0.76

Significant Wave Height (Boundary)				
Gauge #	Bias (m)	RMSE (m)	SI (%)	Cor. (.)
44005	-0.57	0.70	26.67	0.73
44007	0.07	0.43	59.53	0.40
44013	-0.20	0.26	25.38	0.75

Significant Wave Height (Assimilation)				
Gauge #	Bias (m)	RMSE (m)	SI (%)	Cor. (.)
44005	-0.10	0.34	12.93	0.87
44007	0.03	0.43	58.75	0.41
44013	-0.15	0.24	23.58	0.76

Table 3.4: Statistical analysis of computed wind speeds and significant wave heights at three buoy locations for 48 hours forecast in February 2001. SI = Scatter Index, Cor. = Correlation (see Appendix for formulas).

a.

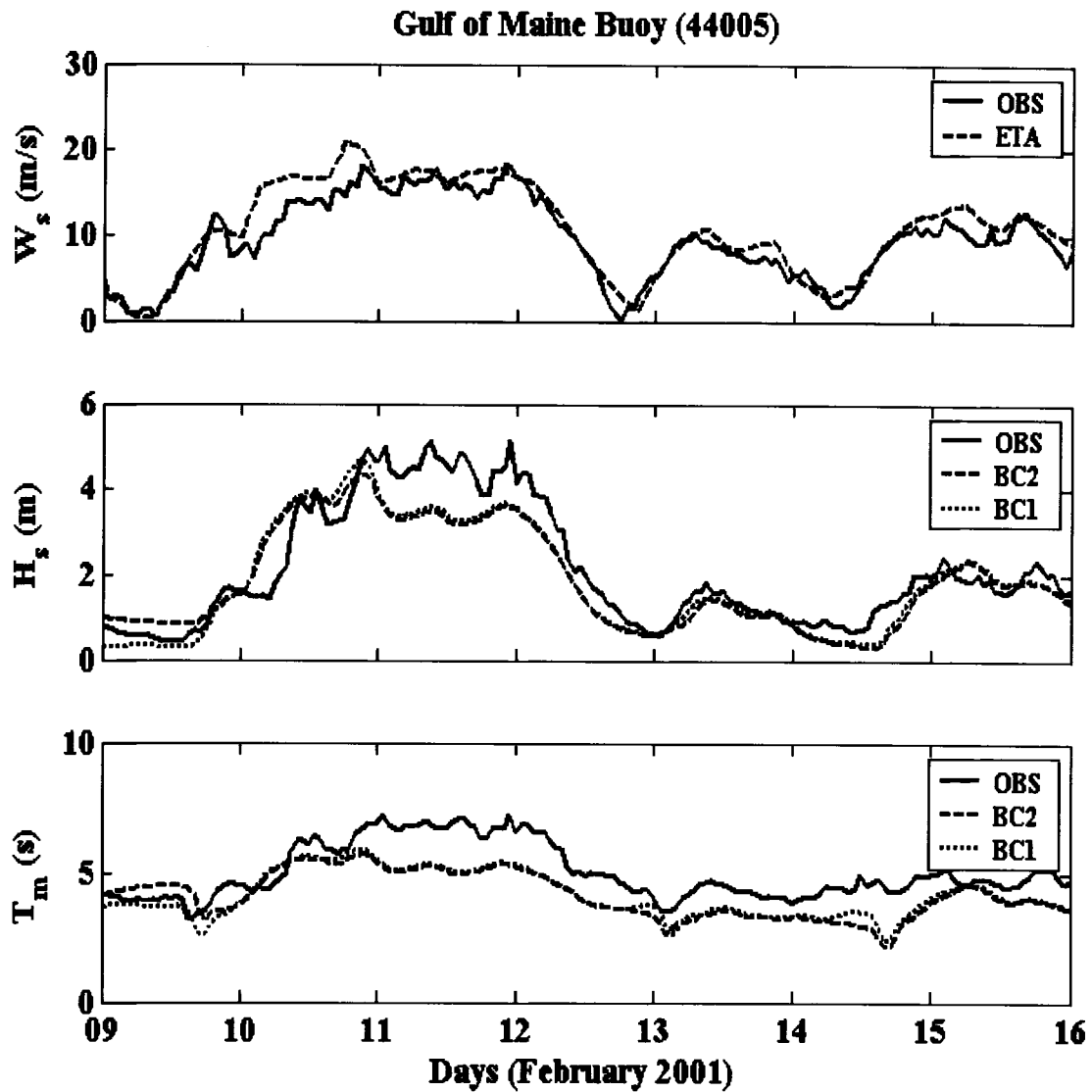
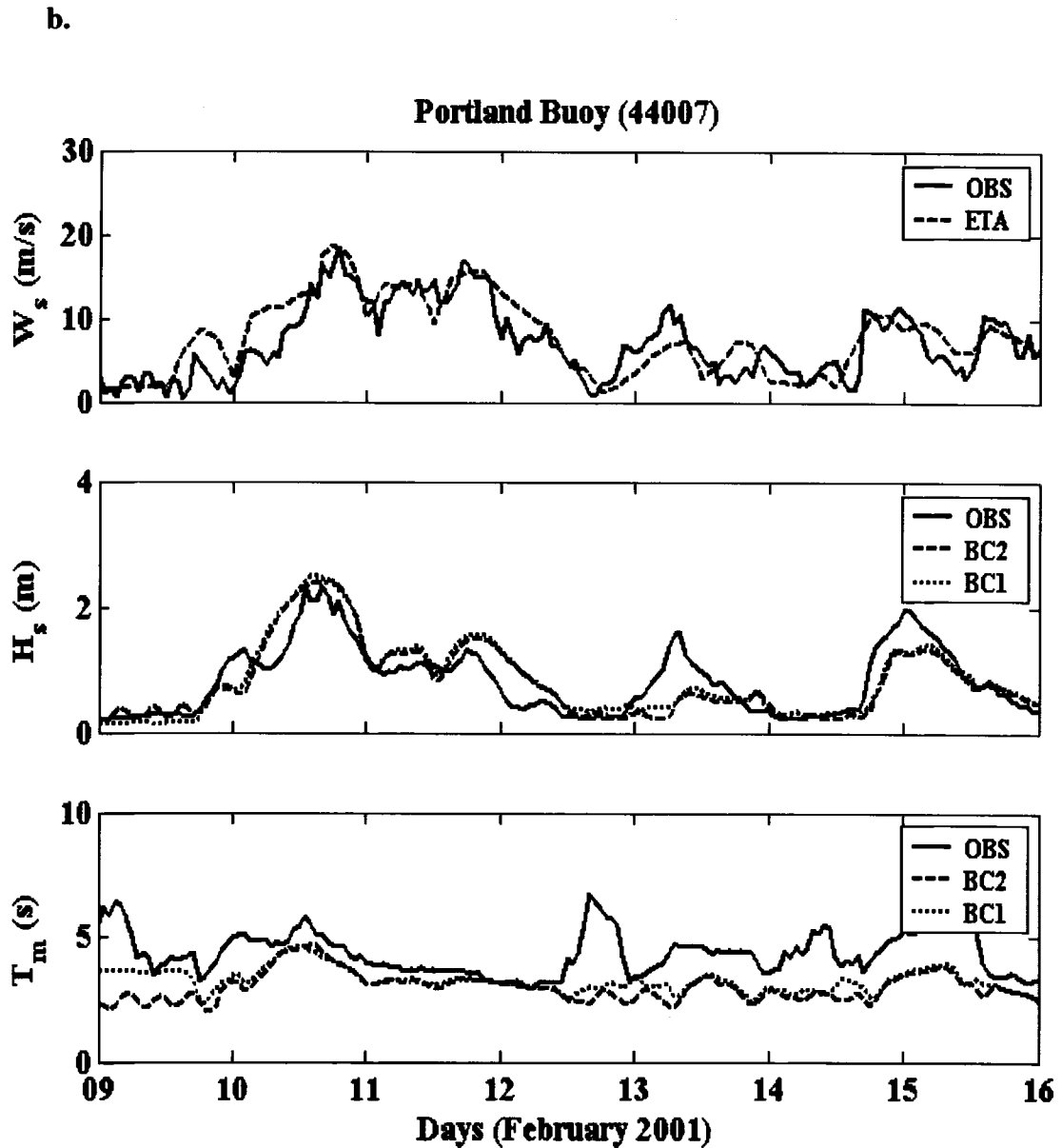


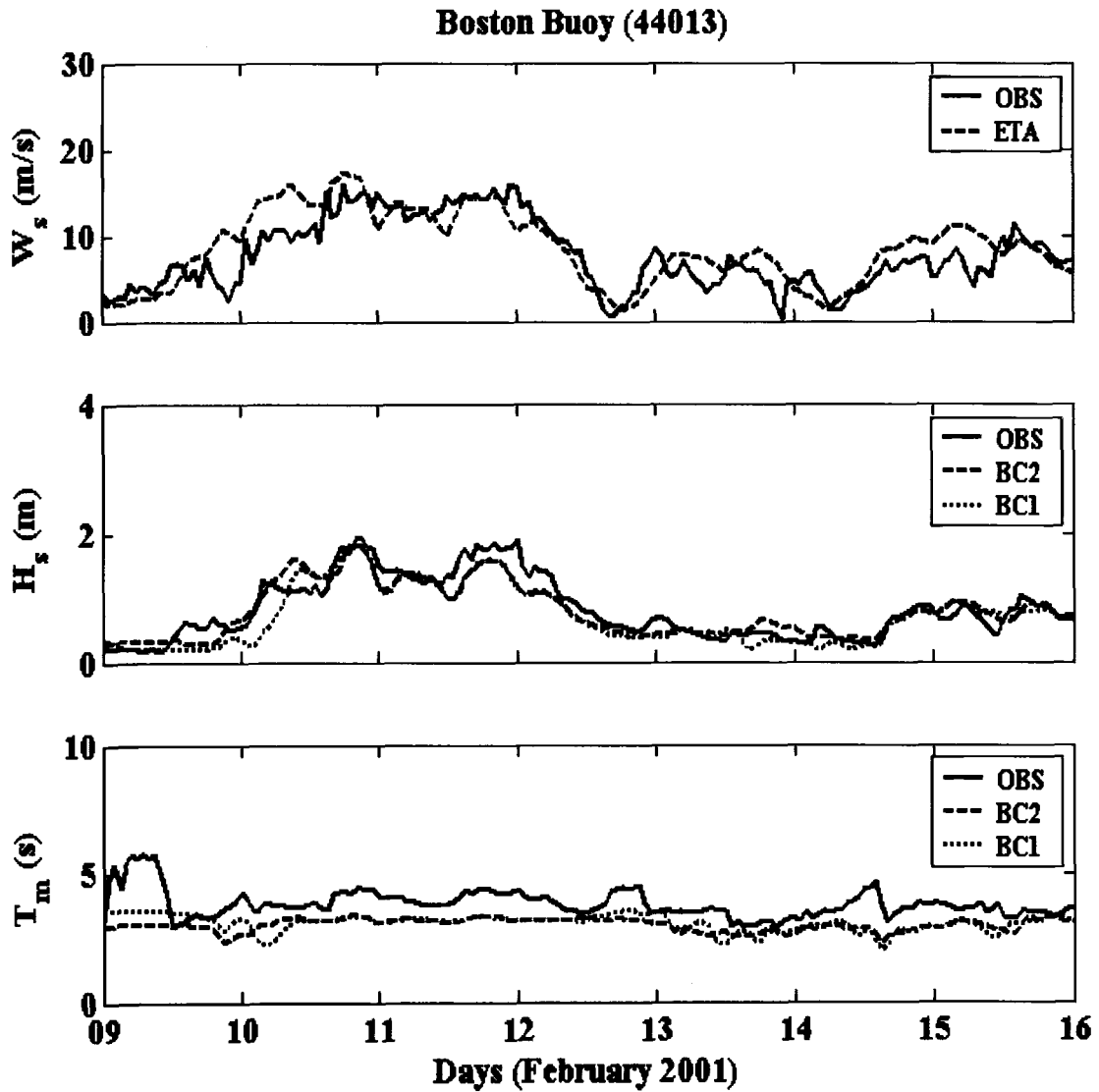
Figure 3.6: Observed (OBS) and predicted wind speed (top panel), significant wave height (middle panel) and mean wave period (bottom panel) for 7 days period in February 2001 at three buoy locations.

- a. Observed (OBS) and predicted wind speed (top panel), significant wave height (middle panel) and mean wave period (bottom panel) for 7 days period in February 2001 at buoy 44005. ETA represents ETA model predicted wind speed; BC1 and BC2 represent SWAN results obtained with boundary conditions schemes 1 and 2, respectively.



b. Observed (OBS) and predicted wind speed (top panel), significant wave height (middle panel) and mean wave period (bottom panel) for 7 days period in February 2001 at buoy 44007. ETA represents ETA model predicted wind speed; BC1 and BC2 represent SWAN results obtained with boundary conditions schemes 1 and 2, respectively.

c.



- c. Observed (OBS) and predicted wind speed (top panel), significant wave height (middle panel) and mean wave period (bottom panel) for 7 days period in February 2001 at buoy 44013. ETA represents ETA model predicted wind speed; BC1 and BC2 represent SWAN results obtained with boundary conditions schemes 1 and 2, respectively.

the continuous assimilation procedure, as a replacement for the unavailable boundary conditions, in the simulations of the seasonal maximum wave conditions presented in following subsection.

3.4.3 Simulations of Year 2001 Seasonal Maximum Wave Conditions

The observed seasonal maximum wave conditions are contained into each one of the 8 day periods simulated in this part of the study. In each case, model runs were initially made with only atmospheric and boundary conditions. In the additional model runs made for three of the four cases attempts were made to improve the quality of the model predictions through the assimilation of the observed significant wave heights at the buoy locations. SWAN results which are obtained during the assimilation periods actually represent the model predictions at the end of each hour (i.e. just before the assimilation scheme is applied at the start of the subsequent hour).

Storm 1: Figure 3.7 shows the observed and model predicted wind and wave conditions at the locations of three Gulf of Maine buoys. While force with atmospheric and boundary conditions the model underpredicted the wave heights at buoy 44005 during the whole simulation period with very few exceptions (Figure 3.7a). Similar underpredictions also occur over most of the first 3.5 days of the simulation at buoy locations 44007 and 44013. The maximum wave conditions are significantly underpredicted at the three buoy location.

a.

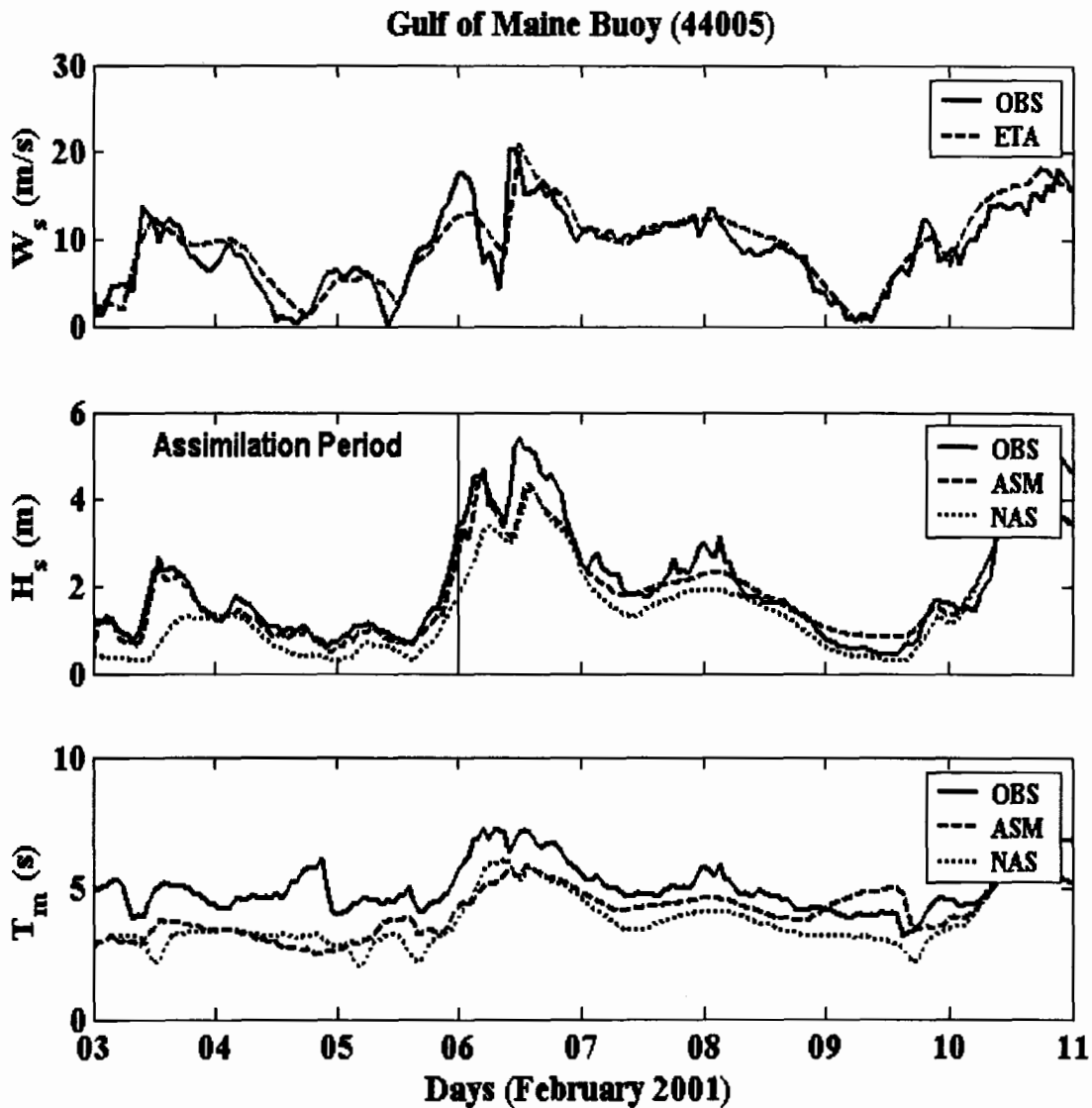
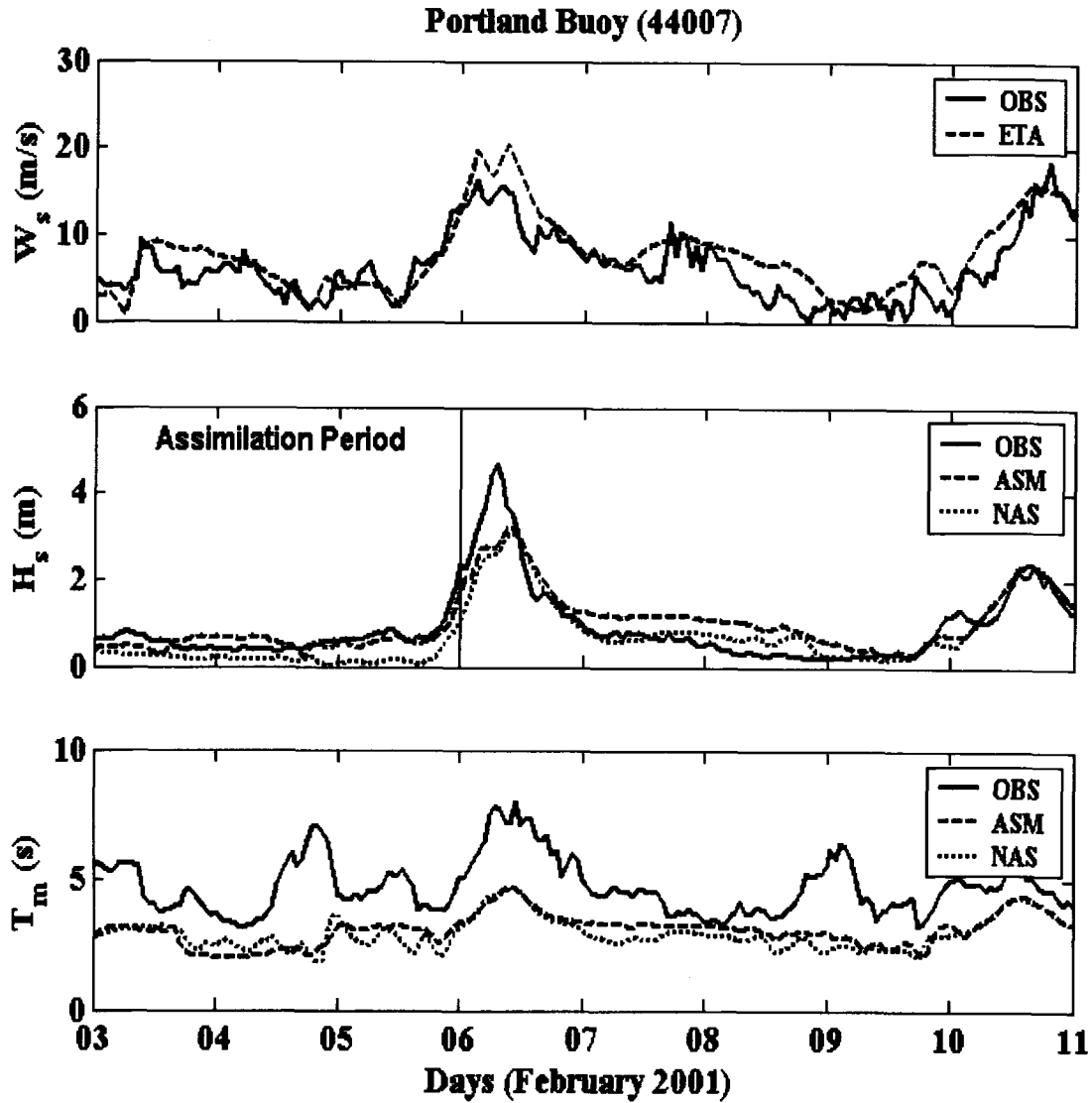


Figure 3.7: Observed (OBS) and predicted wind speed (top panel), significant wave height (middle panel) and mean wave period (bottom panel) for an 8-day period in February 2001 at three buoy locations.

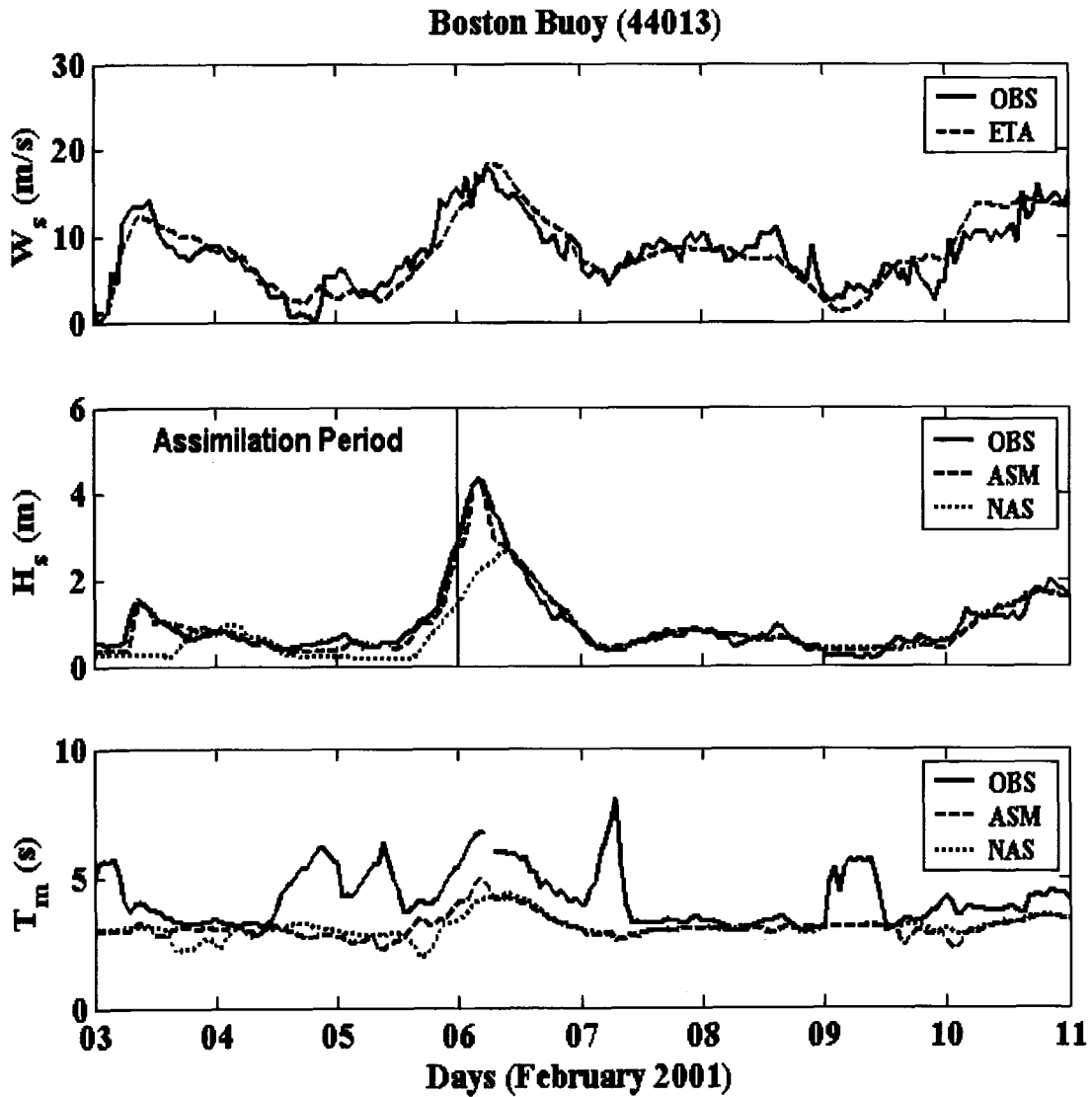
- a. Observed (OBS) and predicted wind speed (top panel), significant wave height (middle panel) and mean wave period (bottom panel) for an 8-day period in February 2001 at buoy 44005. ETA represents ETA model predicted wind speed; ASM and NAS represent SWAN results with and without buoy data assimilation, respectively.

b.



- b. Observed (OBS) and predicted wind speed (top panel), significant wave height (middle panel) and mean wave period (bottom panel) for an 8-day period in February 2001 at buoy 44007. ETA represents ETA model predicted wind speed; ASM and NAS represent SWAN results with and without buoy data assimilation, respectively.

c.



- c. Observed (OBS) and predicted wind speed (top panel), significant wave height (middle panel) and mean wave period (bottom panel) for an 8-day period in February 2001 at buoy 44013. ETA represents ETA model predicted wind speed; ASM and NAS represent SWAN results with and without buoy data assimilation, respectively.

The observed significant wave heights at the five buoy locations were assimilated into the wave model in an hourly basis for a 72 hours period between the 3rd and the 6th of February. During the assimilation period, as Figure 3.7 shows, significant improvements in the model results at the three buoy locations have been achieved. After the assimilation scheme has been switched off at the 00 hour on the 6th the improvements in wave predictions at buoy 44005 lasted for nearly 12 hours (Figure 3.7a). In the following 12 hours, the model largely underpredicts the observed maximum wave height at this location. However, the model predictions at this location started to show some improvements in terms of both wave heights and periods over 72 hours between the 7th and the 10th (Figure 3.7a). At buoy 44013 substantial improvements (in order of 2 m) in the prediction of the maximum wave conditions which occur over the first few hours after the assimilation scheme is switched off. Beyond the first 12 hours of model prediction without assimilation large agreements are found between model predictions (with and without assimilations) and the observed wave conditions at this location. The model result at buoy location 44007 surprisingly did not improve during most of the first 24 hours after the assimilation scheme was switched off (Figure 3.7b). As a result the model did not reproduce the observed maximum wave conditions that occurred during that period. The fact that the forcing wind field at this location is overpredicted during this time period (Figure 3.7b) makes the significant underpredictions in the wave heights even harder to explain. The detailed investigation of the observed and predicted wind fields provided what might be a reasonable justification for this, otherwise, puzzling results. The examination of the observed wind field at buoy 44005 location (Figure 3.8) revealed that wind have switched its direction for a period of more than 3 hours that coincide with

the period at which the observed wave height at buoy 44007 reached its maximum value. Such reversal in the observed wind direction was not captured by the atmospheric model (Figure 3.8) which provides wind predictions every three hours. The observed reversed winds probably have generated waves that propagated at a northwesterly direction (similar to the wind) and reached Portland buoy. The fact that the predicted wind field did not include this reversal might also be the reason for the underestimation of the second wave height peak observed at buoy 44005 around the noontime of February 6th (Figure 3.7a).

The overall improvements in the model results for the first 48 hours after switching off the assimilation scheme at the three buoy locations can be indicated from the inter-comparisons between the computed and the observed conditions shown in Figure 3.9. Both Figure 3.9 and the statistical analysis provided in Table 3.5 show that, for the first 48 hours following the assimilation period, SWAN model results are less scattered compared with the results obtained without data assimilation. The data assimilation appears to have reduced the scatter index of the model computed significant wave height by more than 10% and 35% at the locations of buoys 44005 and 44013 respectively (Table 3.5).

Storm 2: The observed and predicted wind and wave conditions at the locations of three Gulf of Maine buoys are shown in Figure 3.10. The model results obtained with input winds and boundary conditions at the three buoy locations shows that the model has reasonably reproduced the observed changes in the significant wave heights at the three

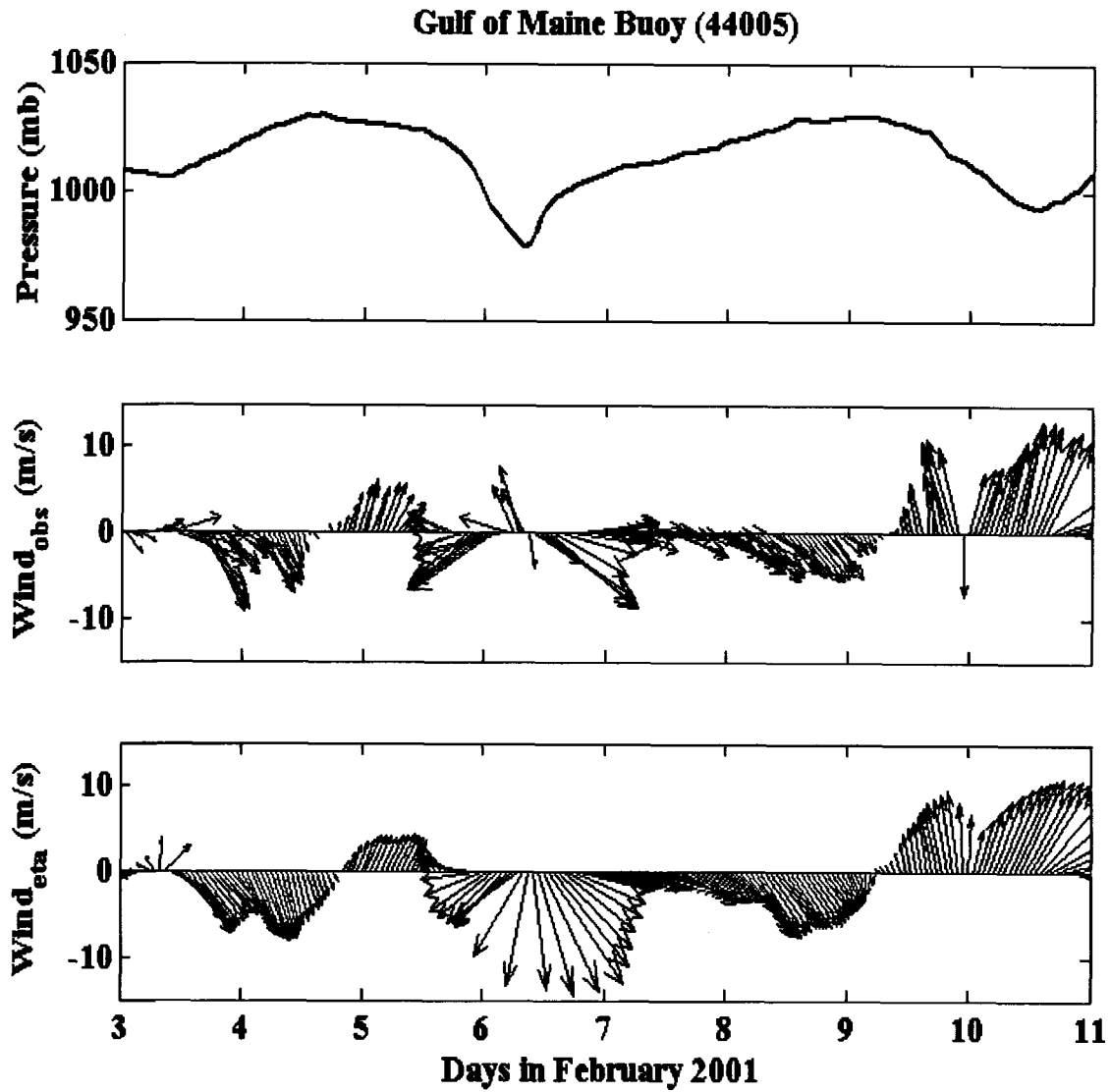


Figure 3.8: Observed and predicted atmospheric parameters at buoy 44005 during an 8-day period in February 2001. Observed pressure (top panel), observe wind velocity (middle panel) and ETA model predicted wind velocity (bottom panel).

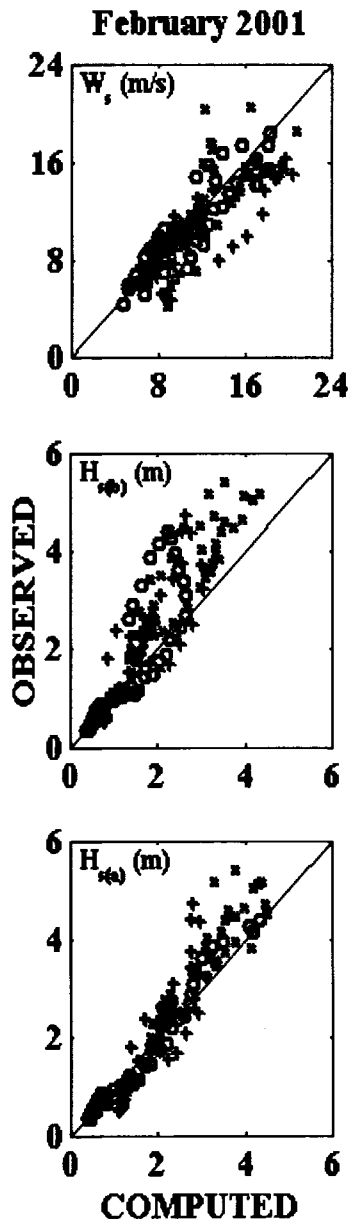


Figure 3.9: February 2001 inter-comparisons of observed and ETA model computed wind speeds (top panel), observed and SWAN computed significant wave heights without buoy data assimilation (middle panel); and observed and SWAN computed significant wave heights wave heights with data assimilation (bottom panel) for 48 hours after assimilation switched off. (x), (+) and (o) represent buoys 44005, 44007 and 44013, respectively.

Wind Speed				
Gauge	Bias	RMSE	SI	Cor.
#	(m/s)	(m/s)	(%)	(.)
44005	0.19	2.44	19.62	0.80
44007	1.93	2.86	29.79	0.70
44013	0.18	1.62	15.41	0.85

Significant Wave Height (Boundary)				
Gauge	Bias	RMSE	SI	Cor.
#	(m)	(m)	(%)	(.)
44005	-0.79	0.92	28.59	0.71
44007	-0.26	0.64	39.74	0.60
44013	-0.29	0.78	49.46	0.51

Significant Wave Height (Assimilation)				
Gauge	Bias	RMSE	SI	Cor.
#	(m)	(m)	(%)	(.)
44005	-0.39	0.58	18.08	0.82
44007	0.09	0.62	38.08	0.62
44013	-0.02	0.23	14.73	0.85

Table 3.5: Statistical analysis of computed wind speeds and significant wave heights at three buoy locations for 48 hours period after assimilation switched off in February 2001. SI = Scatter Index, Cor. = Correlation (see Appendix for formulas).

a.

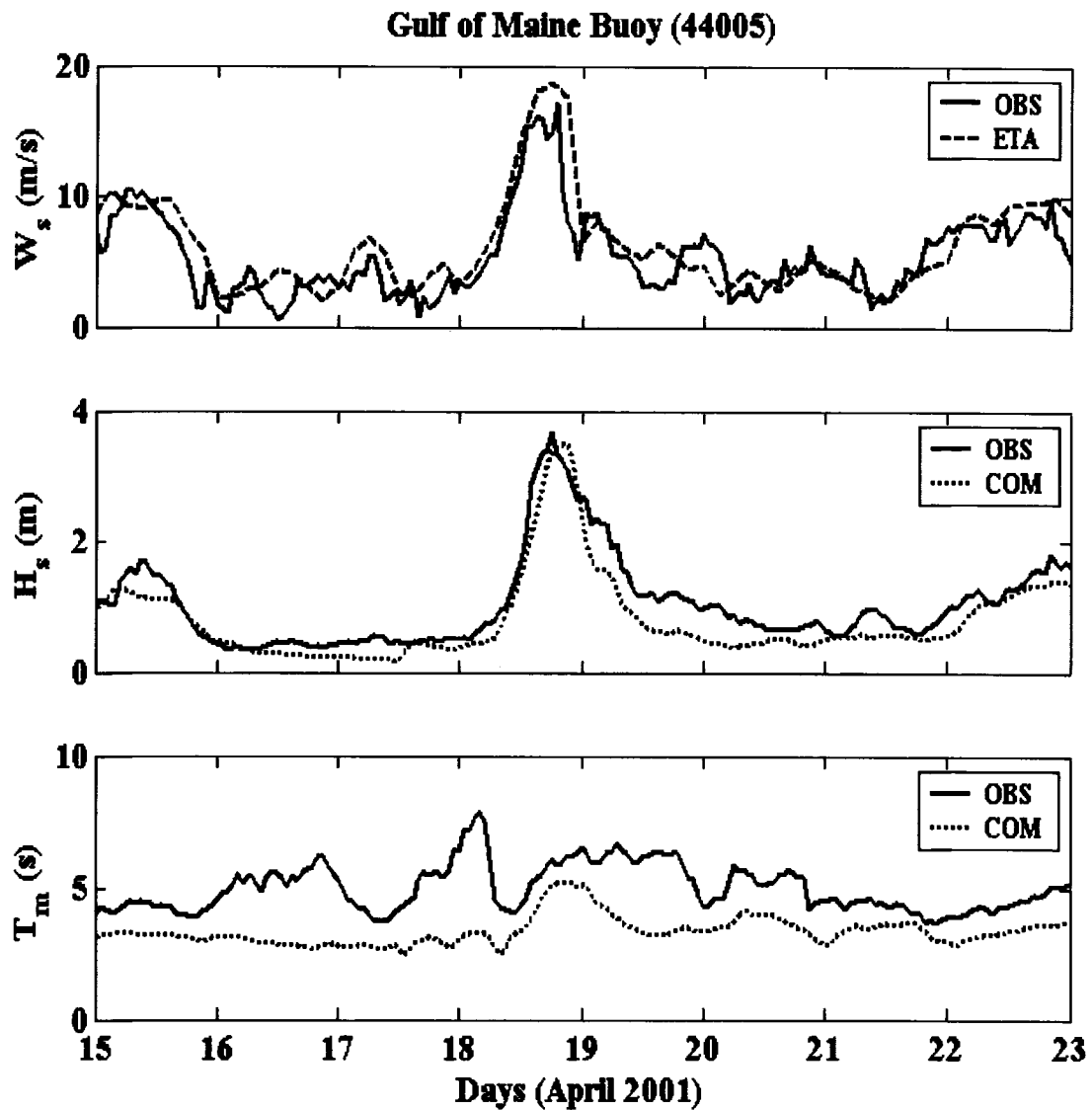
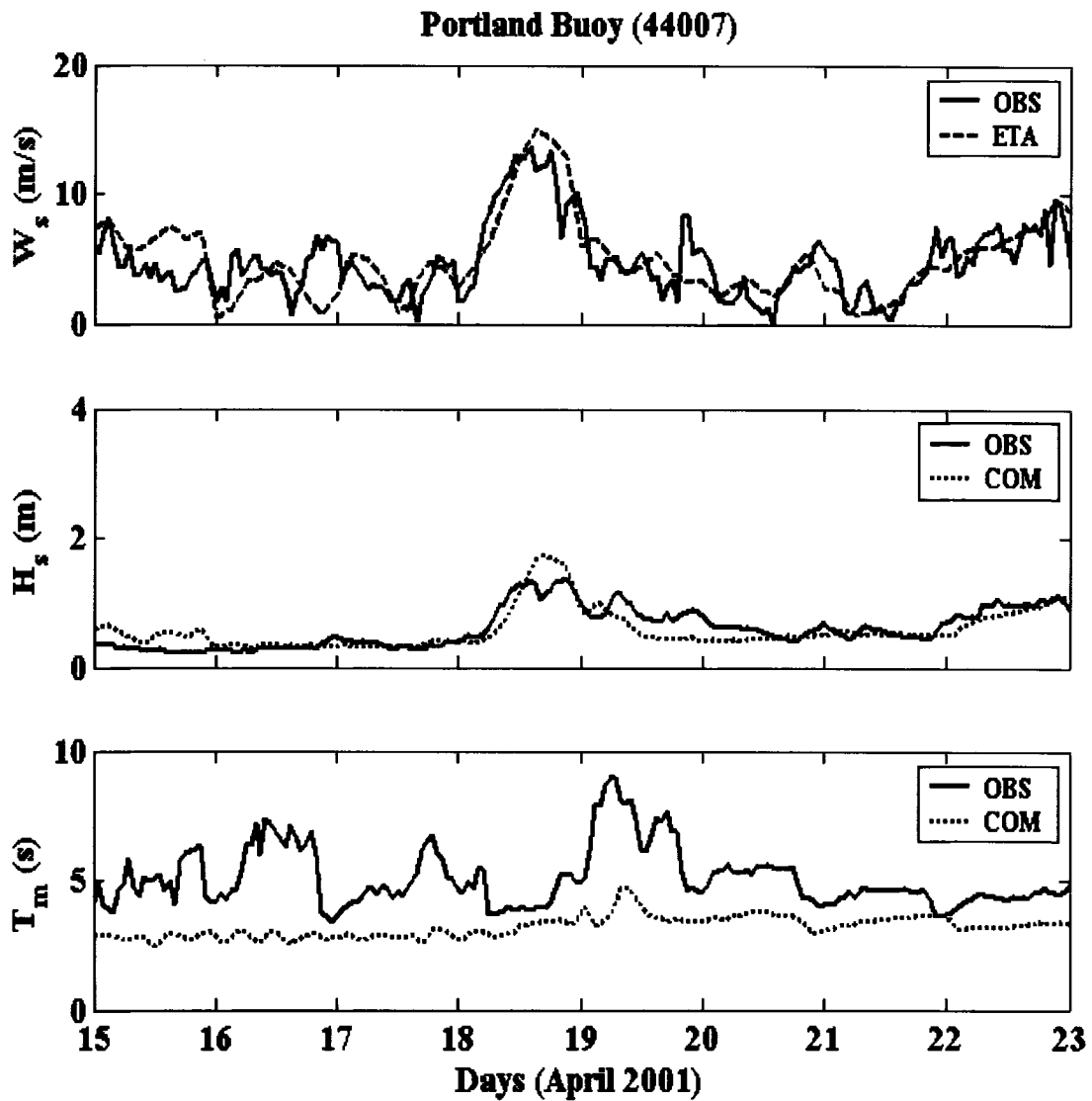


Figure 3.10: Observed (OBS) and predicted wind speed (top panel), significant wave height (middle panel) and mean wave period (bottom panel) for an 8-day period in April 2001 at three buoy locations.

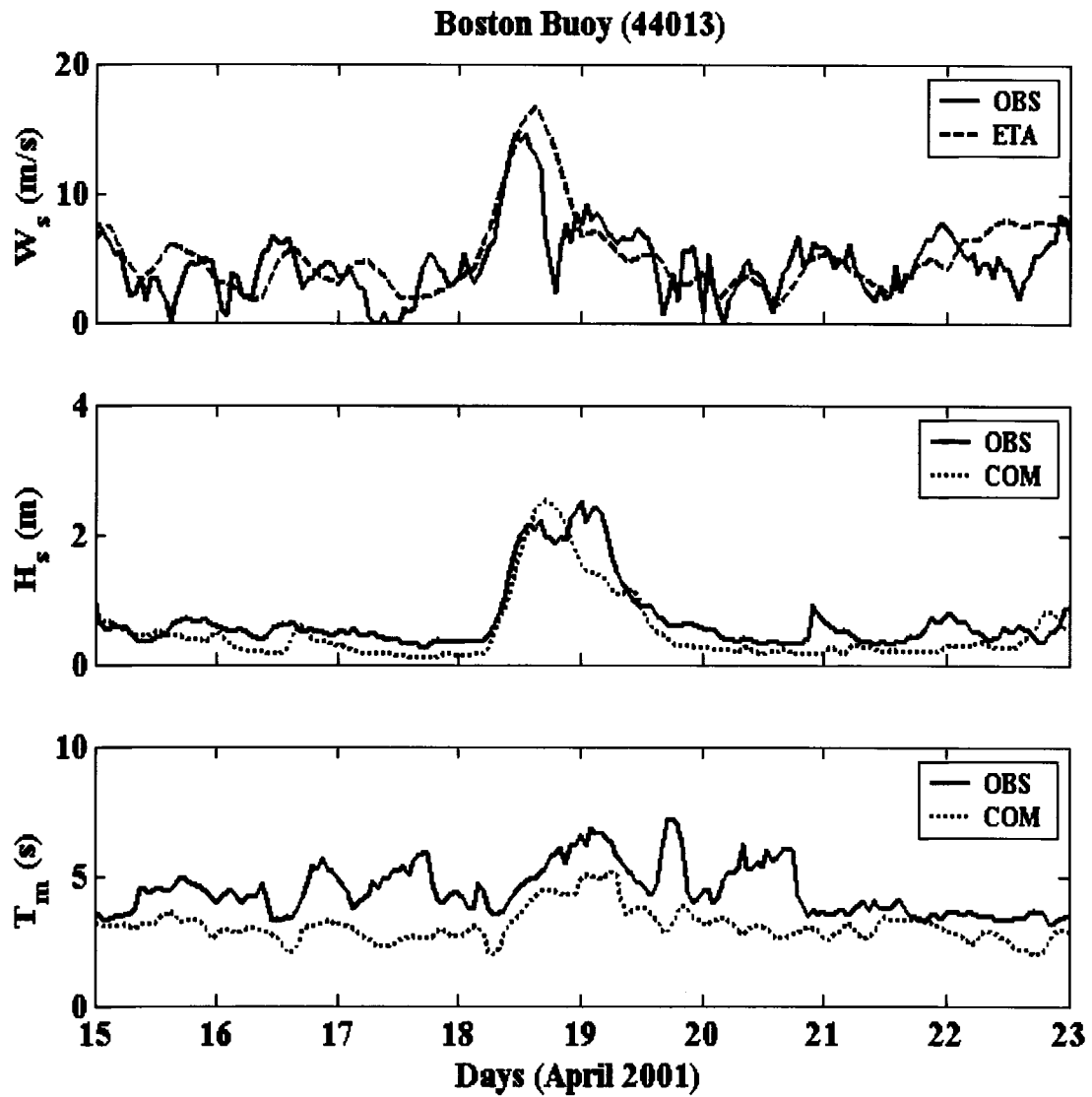
- a. Observed (OBS) and predicted wind speed (top panel), significant wave height (middle panel) and mean wave period (bottom panel) for an 8-day period in April 2001 at buoy 44005. ETA represents ETA model predicted wind speed; (COM) represents SWAN computed results.

b.



- b. Observed (OBS) and predicted wind speed (top panel), significant wave height (middle panel) and mean wave period (bottom panel) for an 8-day period in April 2001 at buoy 44007. ETA represents ETA model predicted wind speed; (COM) represents SWAN computed results.

c.



- c. Observed (OBS) and predicted wind speed (top panel), significant wave height (middle panel) and mean wave period (bottom panel) for an 8-day period in April 2001 at buoy 44013. ETA represents ETA model predicted wind speed; (COM) represents SWAN computed results.

buoy locations for the four days of the simulation. Most of the relatively small mismatches between the observed and predicted wave heights, during the last four days of the simulation, can probably be attributed to the mismatches between the observed and computed wind field at the buoy locations.

For this storm condition, data assimilation procedure was not applied mainly due to two reasons. First, the observed wave conditions during the early hours of the storm event were reasonably well predicted by the model, Figure 3.10, indicating that minor improvements will probably be gained by the buoy data assimilation. Second, most of the mismatches in the wave heights are of small order that is comparable in magnitude to some of the mismatches that occur in other simulations predictions after the data assimilation procedure is switched off.

Storm 3: Figure 3.11 shows the observed and modeled wind and wave conditions at the three buoy locations inside the Gulf of Maine. Observed conditions at buoy 44007 are not available for the first 3.5 days of the record (Figure 3.11b). At the location of buoys 44005 and 44013, the model; forced with boundary and wind conditions; largely underestimated the significant wave heights and the mean wave periods in comparison with the observations during most of the period between the 11th and the 15th of September. The large underestimations in the wave heights cannot be attributed to the forcing wind fields which are actually overpredicted during most of three day period at the two buoy locations. The underestimations can possibly be attributed to the large mismatches in the mean wave periods which probably resulted from inadequate boundary

conditions. In particular, the mean wave periods are significantly underpredicted between the 11th and the 13th at the two buoy locations as shown in Figure 3.11. The observed long period waves at the two buoy locations indicate that these waves have been generated far away before and propagated to the buoy locations. Such waves will experience much less dissipation compared to the short period waves generated by the model.

Wave buoy data were assimilated into the wave model in an hourly basis for the first 72 hours of the 8 days simulation period. Obviously, no data from buoy 44007 were available for assimilation during this period. Model results obtained at the end of each hour at buoy locations 44005 and 44013, Figure 3.11, indicate significant improvements in the model computed wave heights during the assimilation period. Near the end of the assimilation period some improvements in the model predicted mean wave periods has been also achieved at the two buoy locations (Figure 3.11). Reasonable improvements in the model predicted wave heights and period at the two buoy locations were obtained during the first 24 hours after the assimilation scheme has been switched off. During the second day, after switching off the assimilation scheme, the wave heights predictions at three Gulf of Maine buoy locations have improved significantly (Figure 3.11). This is the period during which the wave heights reached their seasonal maximums at the three buoy locations. Despite the fact that no data assimilation has been made at the location of buoy 44007 the effect of the assimilation procedure carried out at the other buoy location is still evident at this buoy location. Figure 3.11 shows that significant increases in the predicted mean periods occurred during the morning hours of September 14th at the three

a.

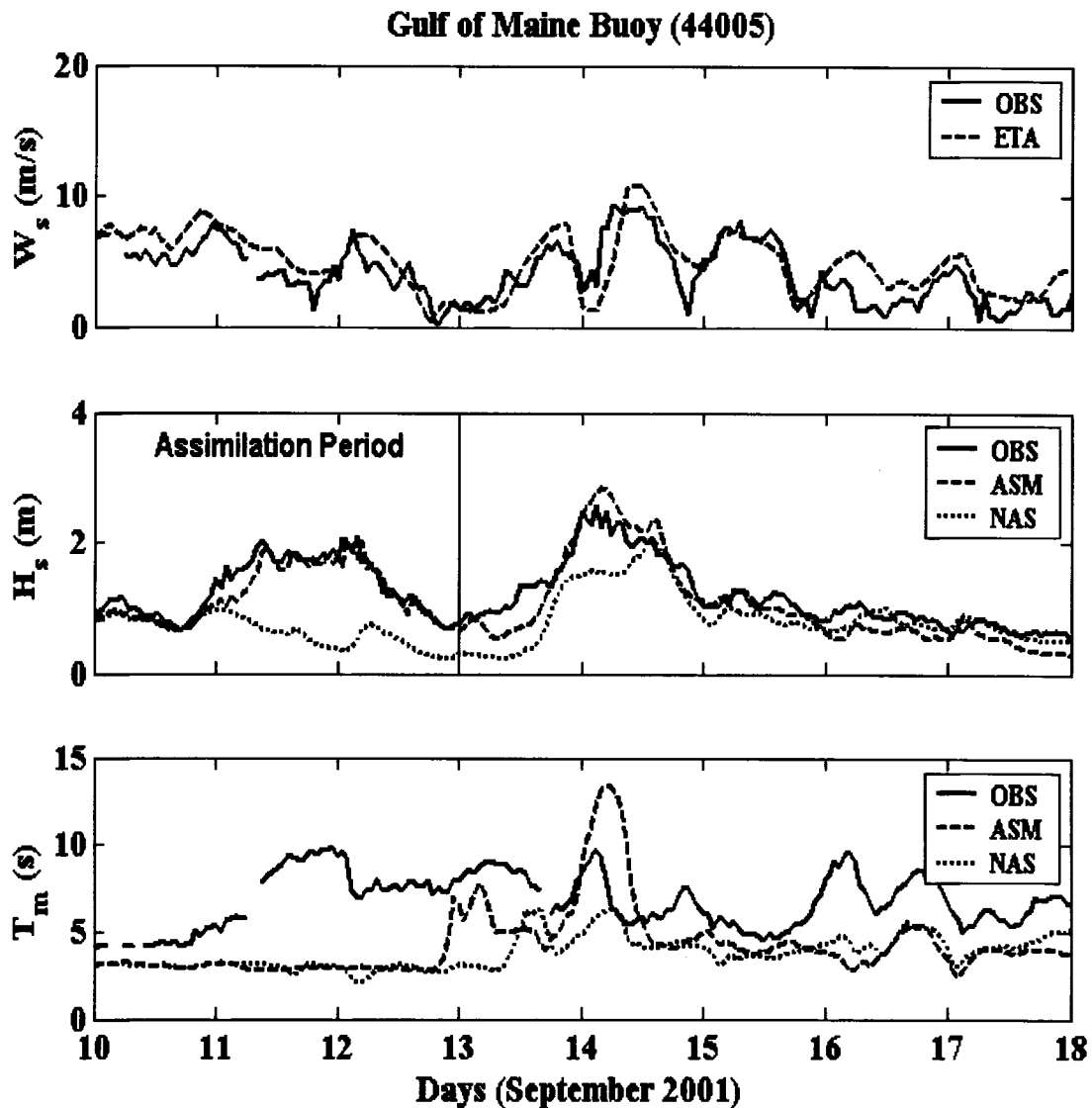
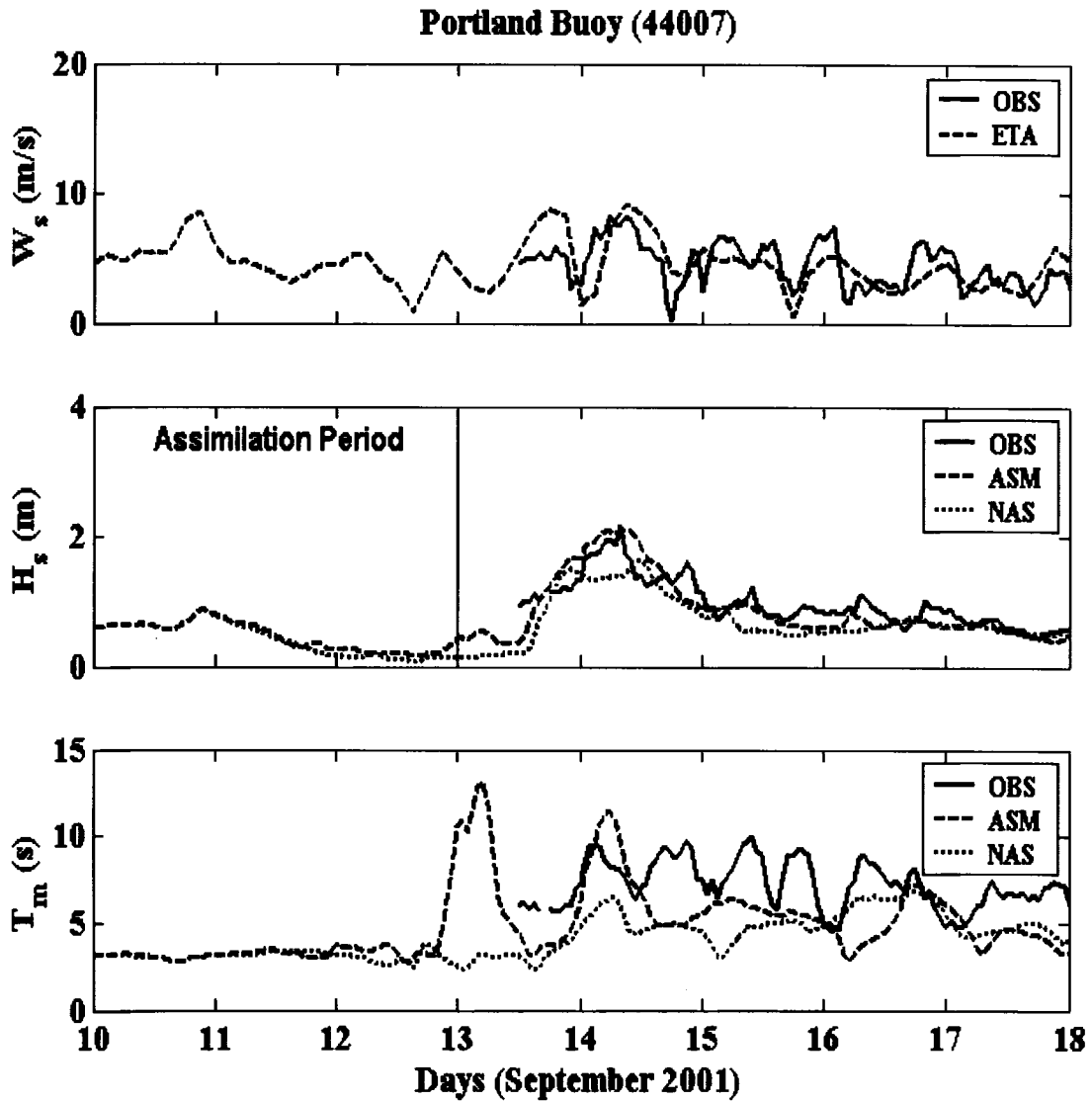


Figure 3.11: Observed (OBS) and predicted wind speed (top panel), significant wave height (middle panel) and mean wave period (bottom panel) for an 8-day period in September 2001 at three buoy locations.

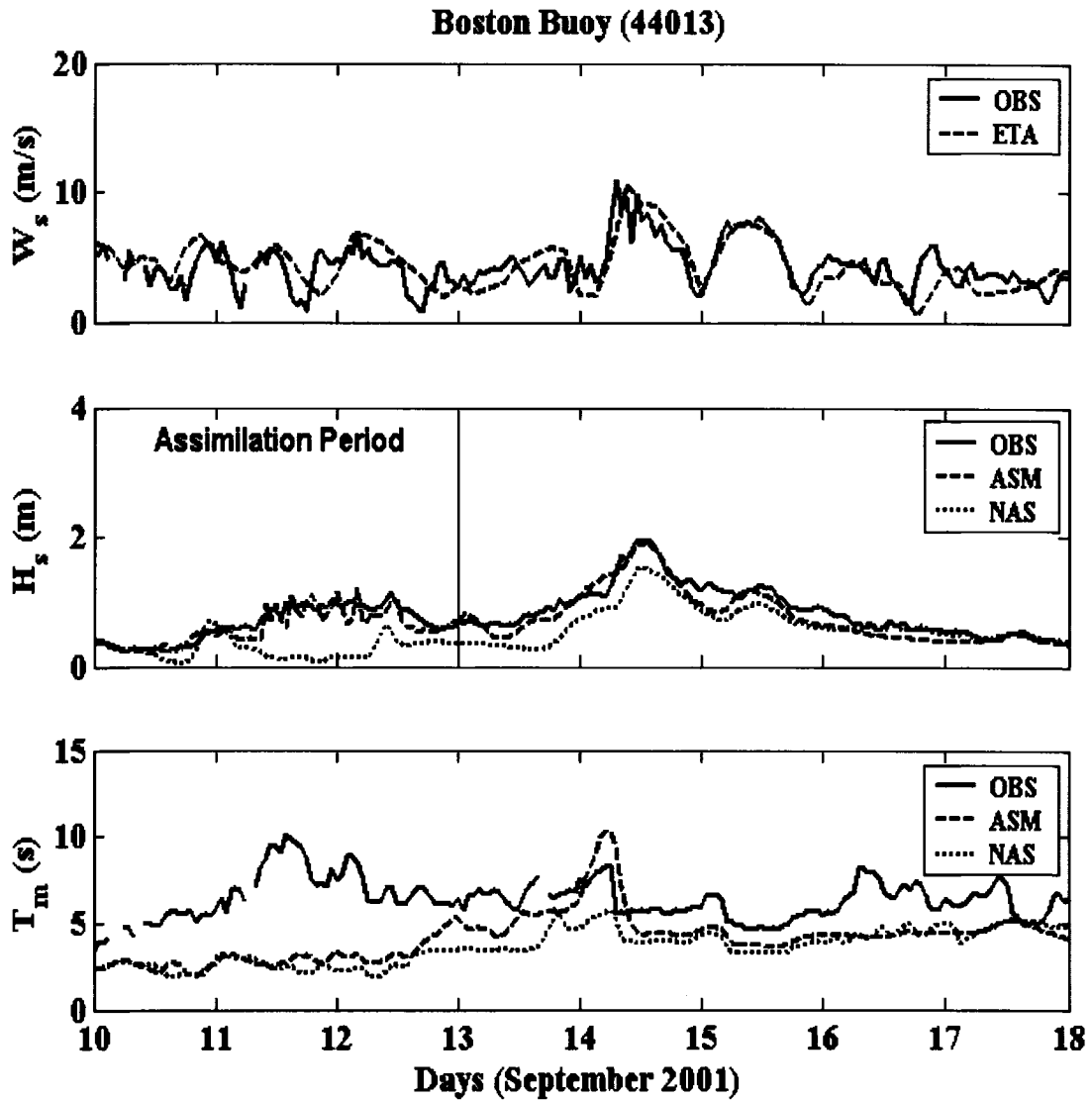
- a. Observed (OBS) and predicted wind speed (top panel), significant wave height (middle panel) and mean wave period (bottom panel) for an 8-day period in September 2001 at buoy 44005. ETA represents ETA model predicted wind speed; ASM and NAS represent SWAN results with and without buoy data assimilation, respectively.

b.



- b. Observed (OBS) and predicted wind speed (top panel), significant wave height (middle panel) and mean wave period (bottom panel) for an 8-day period in September 2001 at buoy 44007. ETA represents ETA model predicted wind speed; ASM and NAS represent SWAN results with and without buoy data assimilation, respectively.

c.



c. Observed (OBS) and predicted wind speed (top panel), significant wave height (middle panel) and mean wave period (bottom panel) for an 8-day period in September 2001 at buoy 44013. ETA represents ETA model predicted wind speed; ASM and NAS represent SWAN results with and without buoy data assimilation, respectively.

buoy locations. This probably indicates that the significant improvements in the predicted wave heights at the three buoy locations have resulted from the assimilation of the observed wave conditions at the outside two buoys (i.e. 44008 and 440013) at an hourly interval during the first 72 hours of the assimilation instead of the regular 3-hour interval. It can be also seen from Figure 3.11 that although the model went back to underpredicting the wave height around the end of the day on the 15th, additional improvements in the model predictions occurred few hours later at the three buoy locations.

The inter-comparison of the observed and computed wave heights, Figure 3.12, shows that the model predicted wave heights obtained with data assimilation are less scattered compared to those obtained without data assimilation. This is also shown by the statistical analysis provided in Table 3.6, which also indicates that the data assimilation have reduced the scatter index by more than 19% and 23% at the locations of buoys 44005 and 44013, respectively.

Storm 4: For the simulated period, the observed and computed wind and wave conditions are shown in Figure 3.13 at the locations of the three Gulf of Maine wave buoys. Forced only by the predicted wind field and the boundary conditions the model largely underpredicted the significant wave heights after the first day of the simulation at three buoy locations. The significant underpredictions have lasted for about 4 days at buoy location 44005 and about 2 days at the locations of buoys 44007 and buoy 44013 (Figure 3.13). These underpredictions could result from apparent underpredictions in the forcing

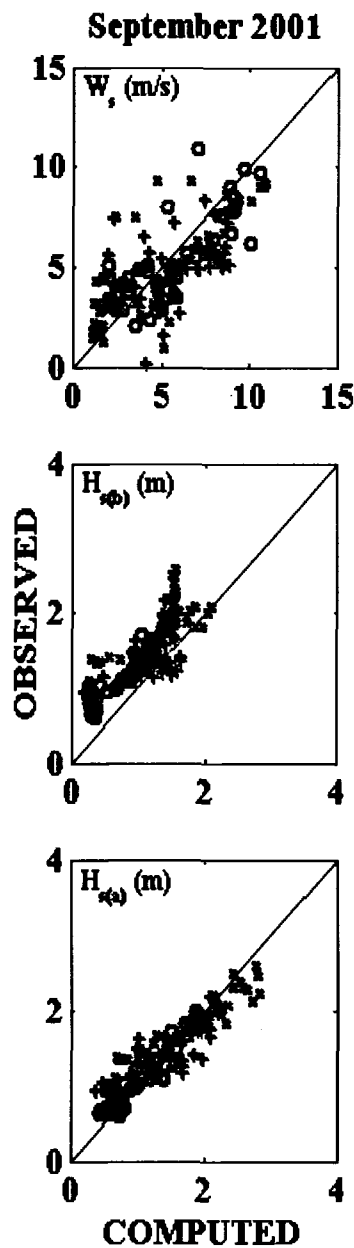


Figure 3.12: September 2001 inter-comparisons of observed and ETA model computed wind speeds (top panel), observed and SWAN computed significant wave heights without buoy data assimilation (middle panel); and observed and SWAN computed significant wave heights with data assimilation (bottom panel) for 48 hours after assimilation switched off. (x), (+) and (o) represent buoys 44005, 44007 and 44013, respectively.

Wind Speed				
Gauge	Bias	RMSE	SI	Cor.
#	(m/s)	(m/s)	(%)	(.)
44005	0.13	1.93	39.39	0.61
44007	0.72	2.40	45.35	0.55
44013	0.14	1.60	32.02	0.68

Significant Wave Height (Boundary)				
Gauge	Bias	RMSE	SI	Cor.
#	(m)	(m)	(%)	(.)
44005	-0.54	0.62	38.96	0.61
44007	-0.18	0.37	24.55	0.75
44013	-0.37	0.39	35.31	0.65

Significant Wave Height (Assimilation)				
Gauge	Bias	RMSE	SI	Cor.
#	(m)	(m)	(%)	(.)
44005	-0.05	0.31	19.61	0.80
44007	0.15	0.33	21.90	0.78
44013	-0.04	0.14	12.84	0.87

Table 3.6: Statistical analysis of computed wind speeds and significant wave heights at three buoy locations for 48 hours period after assimilation switched off in September 2001. SI = Scatter Index, Cor. = Correlation (see Appendix for formulas).

a.

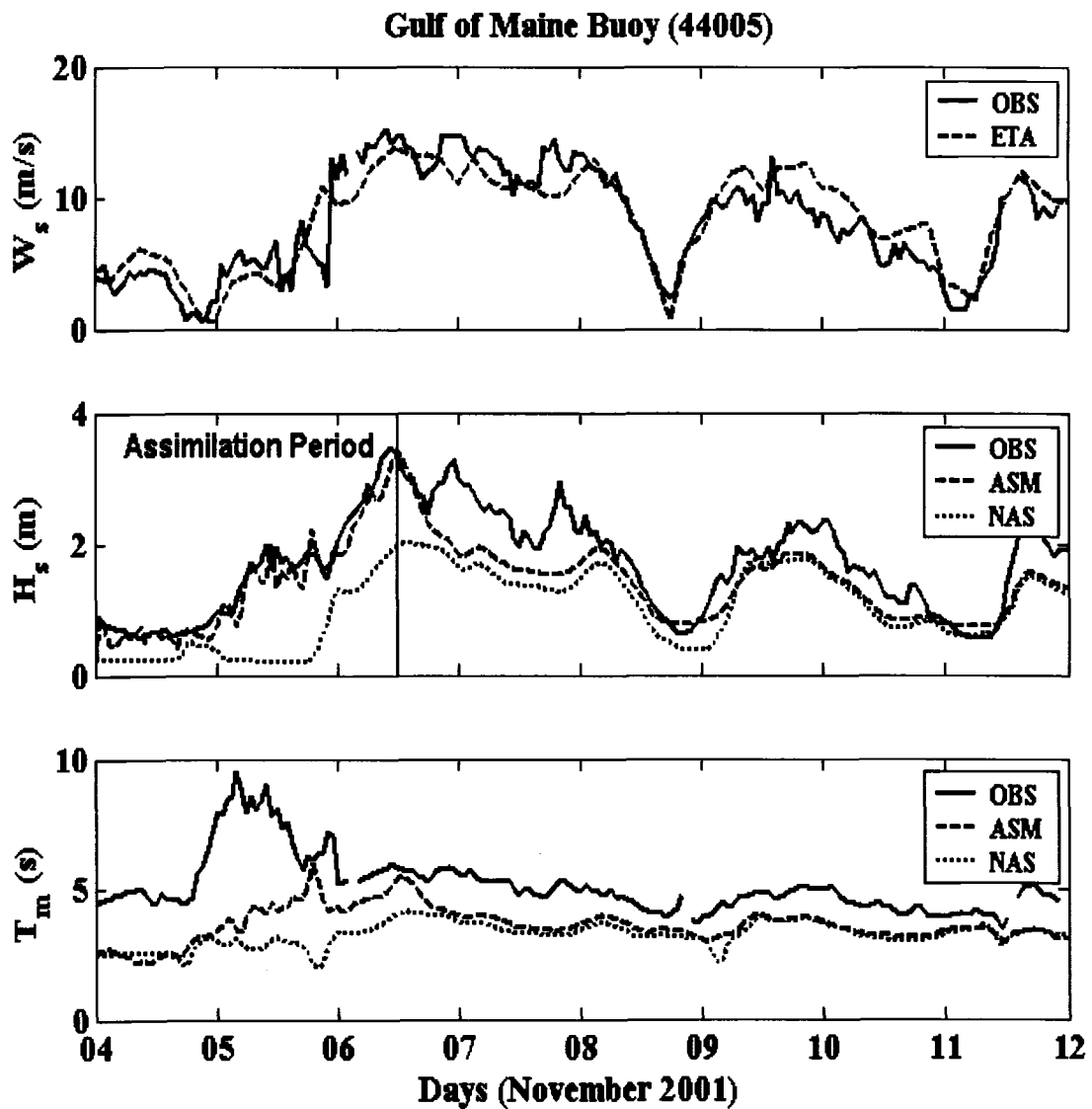
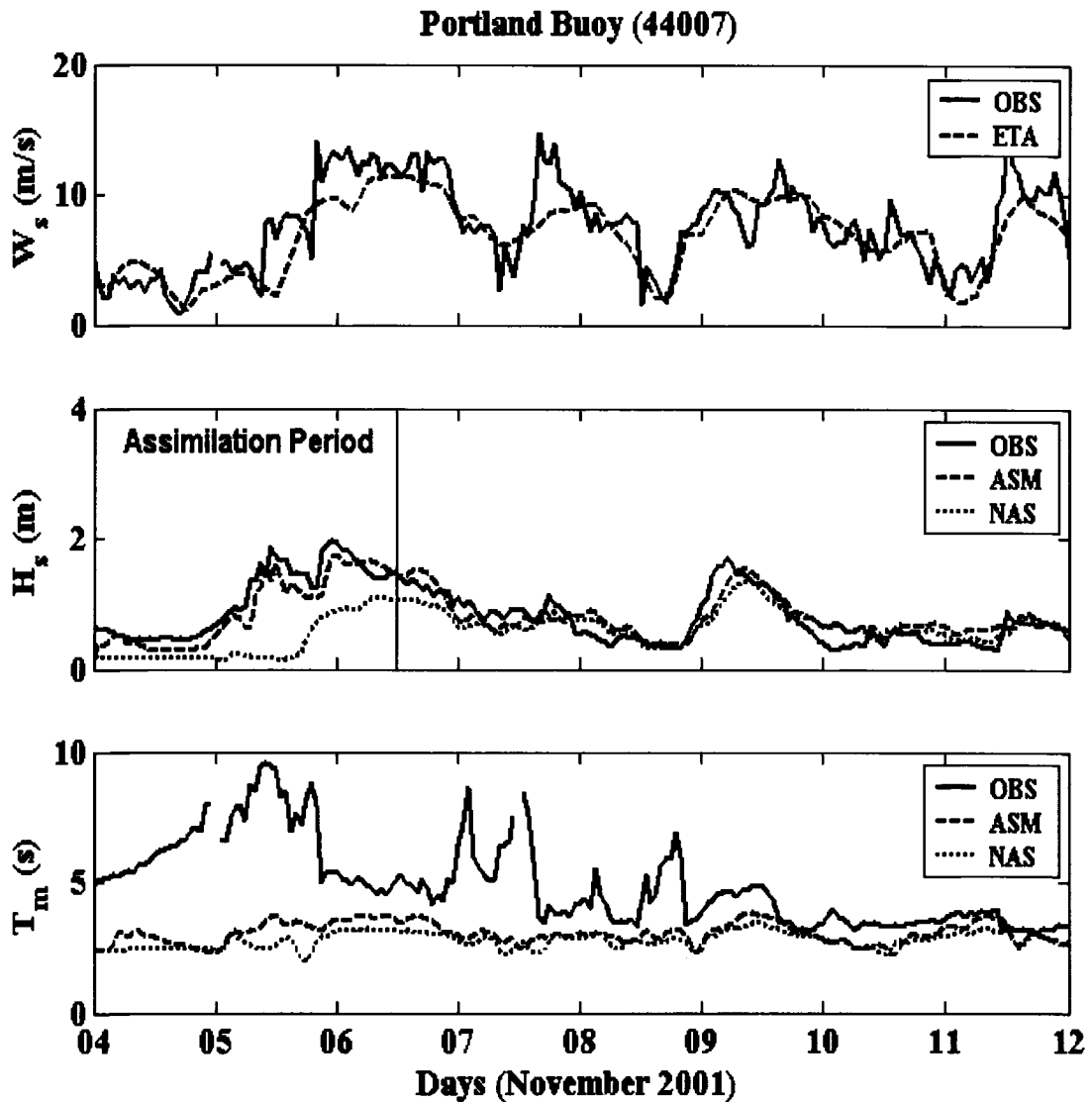


Figure 3.13: Observed (OBS) and predicted wind speed (top panel), significant wave height (middle panel) and mean wave period (bottom panel) for an 8-day period in November 2001 at three buoy locations.

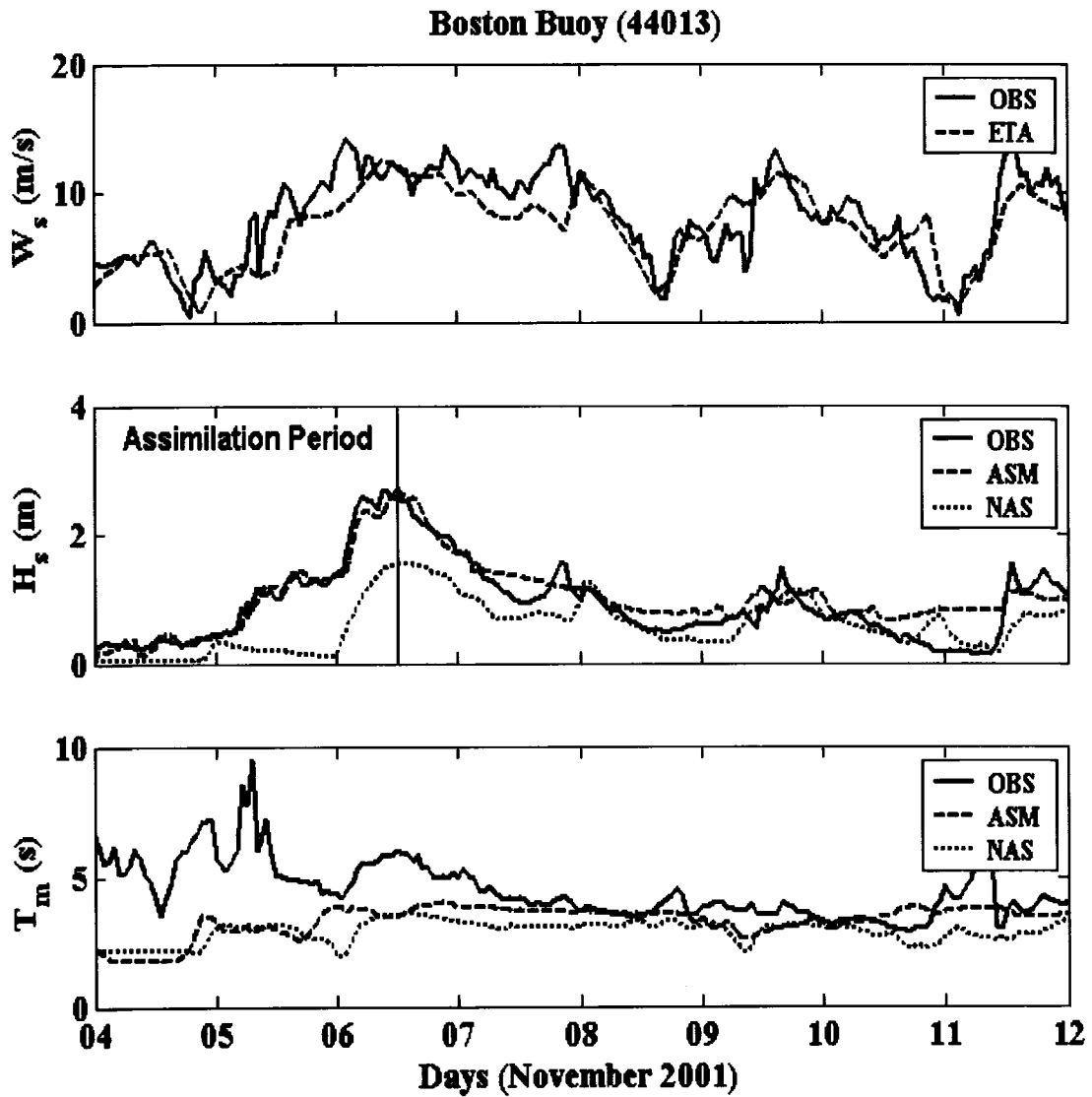
- a. Observed (OBS) and predicted wind speed (top panel), significant wave height (middle panel) and mean wave period (bottom panel) for an 8-day period in November 2001 at buoy 44005. ETA represents ETA model predicted wind speed; ASM and NAS represent SWAN results with and without buoy data assimilation, respectively.

b.



- b. Observed (OBS) and predicted wind speed (top panel), significant wave height (middle panel) and mean wave period (bottom panel) for an 8-day period in November 2001 at buoy 44007. ETA represents ETA model predicted wind speed; ASM and NAS represent SWAN results with and without buoy data assimilation, respectively.

c.



- c. Observed (OBS) and predicted wind speed (top panel), significant wave height (middle panel) and mean wave period (bottom panel) for an 8-day period in November 2001 at buoy 44013. ETA represents ETA model predicted wind speed; ASM and NAS represent SWAN results with and without buoy data assimilation, respectively.

wind field during this period. Possible contribution from inadequate boundary conditions can not be ruled out. It is noticed that a large mismatch also occurs between the observed and the model predicted mean wave period during the first 3 days of the simulation at the three buoy locations. Model predictions beyond November 7th are in less disagreement with the observed conditions at the three buoy locations mainly because fewer underpredictions occur in the predicted wind fields.

The observed significant wave heights at the three buoy locations were assimilated into the model in an hourly basis for the first 60 hours of the simulation period. The results shown in Figure 3.13 indicate that significant improvements in the model wave height predictions were obtained at the end of each hour during the assimilation period at the three buoy locations. Minor improvements in the predicted mean wave period were also achieved near the end of the assimilation periods especially at buoy 44005 location. After the assimilation has been switched off on the noon time of the 6th, the effect of the agreement between the observed and model computed wave conditions lasted for only 6 hours at buoy 44005 (Figure 3.13a). Beyond that, the model still largely underpredicts the wave heights for more than 24 hours at this location. This underprediction can be attributed to the underpredicted wind field (Figure 3.13a). Some minor improvements in the wave heights predictions occur at this location during the 8th of November. Improvements in wave height predictions at buoy locations 44007 and 44013 have lasted for about 12 hours after switching off the assimilation. At buoy location 44007, model predictions beyond the 6th are almost similar to those obtained without data assimilation. Wave heights over predictions occur at buoy location 44013

during most of the period between the 7th and the 12th. The mismatches between the peak periods obtained with assimilation and those obtained without assimilation over most of this period probably indicates that the wave height overpredictions did not result from local effects. The underpredicted wind field during most of the period between the 7th and the 9th at this location might also support this argument.

The inter-comparisons between the observed and computed wave heights with and without data assimilation (Figure 3.14) indicate that over the 48 hours following the assimilation period the model computed wave heights obtained with data assimilation are less scattered compared to those obtained without assimilation. Results in Table 3.7 indicate that, the data assimilation have reduced the significant wave height scatter index at buoys 44005 and 44013 locations by more than 12% and 24% respectively.

3.4.4 Spatial scale of assimilation impact

The results presented in the above subsections (3.4.2 and 3.4.3) allowed for quantifying the temporal scale of the assimilation effect. In this subsection an attempt to quantify the scale of the assimilation influence on spatial domain is made. Differences in SWAN results obtained with and without assimilation, for storm 1 in the above subsection, are examined at different time steps. Figure 3.15 shows contour plots of the values obtained by subtracting SWAN computed significant wave heights without assimilation from SWAN computed wave heights with assimilation.

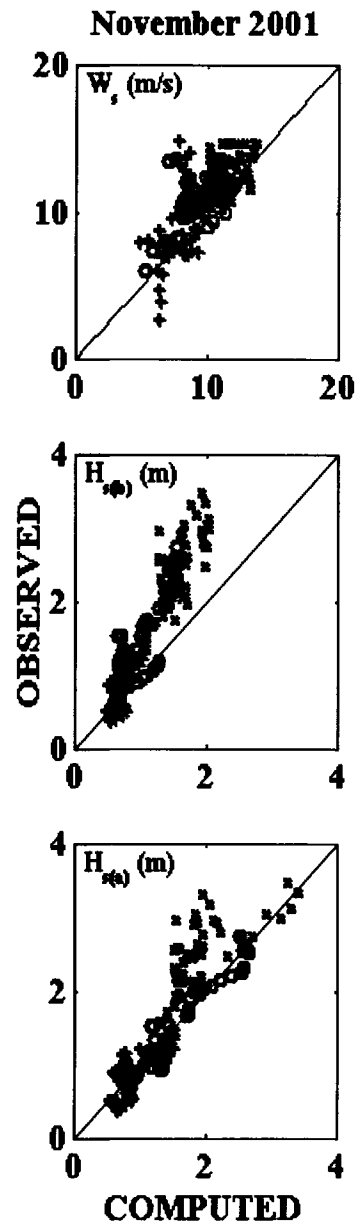


Figure 3.14: November 2001 inter-comparisons of observed and ETA model computed wind speeds (top panel), observed and SWAN computed significant wave heights without buoy data assimilation (middle panel); and observed and SWAN computed significant wave heights with data assimilation (bottom panel) for 48 hours after assimilation switched off. (x), (+) and (o) represent buoys 44005, 44007 and 44013, respectively.

Wind Speed				
Gauge	Bias	RMSE	SI	Cor.
#	(m/s)	(m/s)	(%)	(.)
44005	-0.94	1.66	13.22	0.87
44007	-0.82	2.13	22.75	0.77
44013	-1.48	2.24	20.55	0.79

Significant Wave Height (Boundary)				
Gauge	Bias	RMSE	SI	Cor.
#	(m)	(m)	(%)	(.)
44005	-0.90	0.96	38.84	0.61
44007	-0.13	0.24	27.30	0.73
44013	-0.43	0.54	38.00	0.62

Significant Wave Height (Assimilation)				
Gauge	Bias	RMSE	SI	Cor.
#	(m)	(m)	(%)	(.)
44005	-0.54	0.67	26.88	0.73
44007	0.01	0.21	23.24	0.77
44013	0.08	0.19	13.57	0.86

Table 3.7: Statistical analysis of computed wind speeds and significant wave heights at three buoy locations for 48 hours period after assimilation switched off in November 2001. SI = Scatter Index, Cor. = Correlation (see Appendix for formulas).

a.

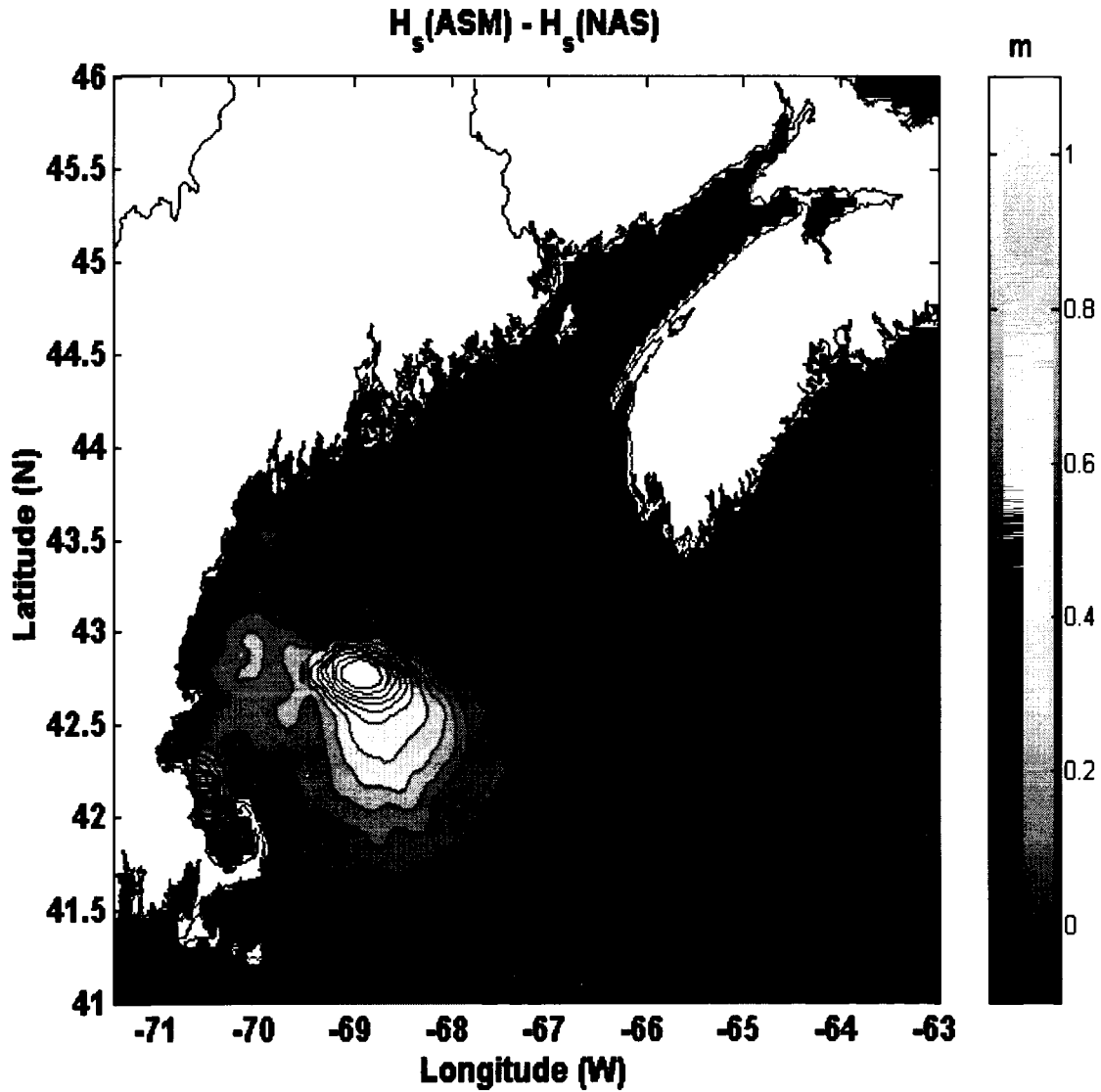
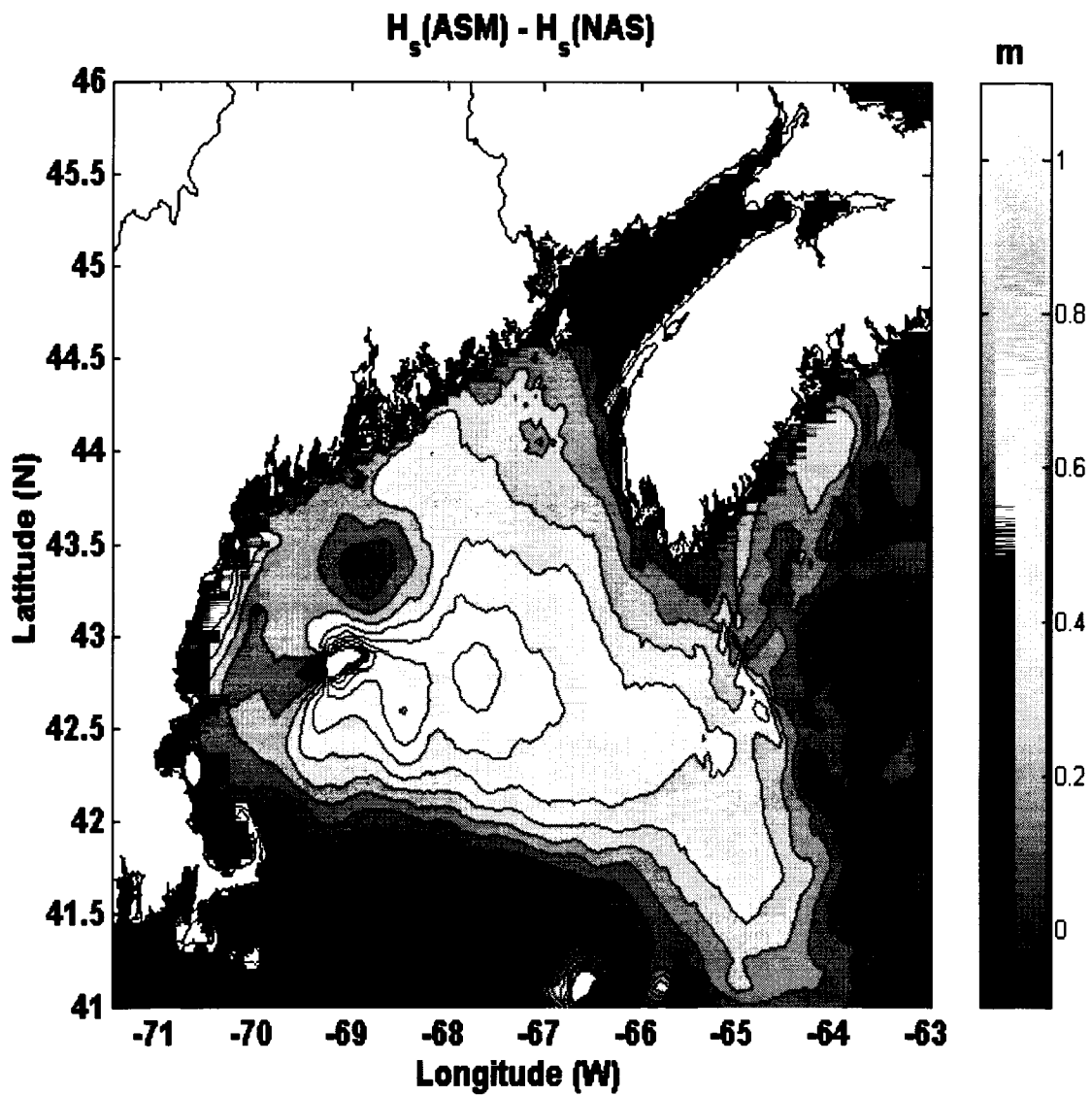


Figure 3.15: Differences between “with assimilation” significant wave heights and “without assimilation” significant wave heights obtained from SWAN at different times.

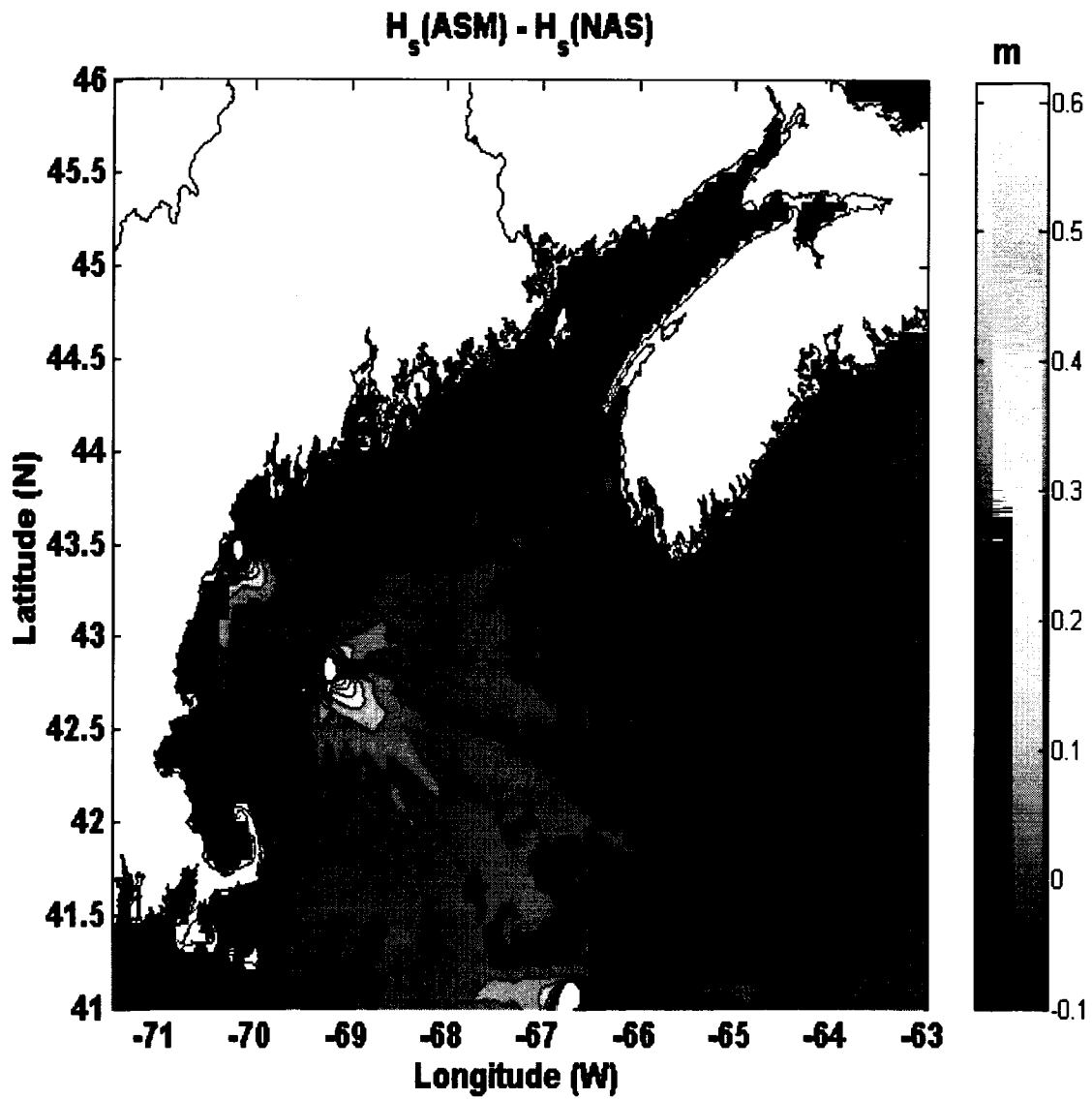
- a. Difference between “with assimilation” significant wave heights and “without assimilation” significant wave heights obtained from SWAN at 12 hours after the simulations start times.

b.



b. Difference between “with assimilation” significant wave heights and “without assimilation” significant wave heights obtained from SWAN at 72 hours after the simulations start times.

c.



- c. Difference between “with assimilation” significant wave heights and “without assimilation” significant wave heights obtained from SWAN at 120 hours after the simulations start times.

The results obtained 12 hours after the start of the runs, shown in Figure 3.15a, indicate that the effect of the assimilation at buoy 44005 has a spatial scale of more than 1° in both longitudinal and latitudinal directions. The longitudinal scale is almost twice the longitudinal range of influence (0.54° per Table 3.3) for this buoy location. However, the latitudinal spatial scale is about five times larger than the latitudinal range of influence (0.18°). This indicates that the assimilation effect at this buoy location has propagated with the waves as they were forced by the northwesterly winds shown in Figure 3.8. At the location of buoy 44013, the spatial scale of the assimilation effect is of the order of about 0.5° , Figure 3.15a. This scale is about double the assimilation ranges of influence (longitudinal and latitudinal) for this buoy. For buoy 44007, Figure 3.15a, the spatial scale of the assimilation is less pronounced compared with the other two Gulf of Maine buoys. This is probably not surprising, considering the fact that the assimilation latitudinal range of influence for this buoy is significantly smaller compared with that for the other two bayous.

Figure 3.15b shows the results obtained 72 hours after the runs started. The results indicate that the effect of the assimilation has spread all over the Gulf of Maine with the exception of the Bay of Fundy region. The effect has also extended well in the southeast direction toward the Georges Bank. These results probably suggest that the most significant effect is due to assimilating buoy 44005 observed wave data. This effect is to be expected since buoy 44005 is located fairly distant from coastlines unlike the two other Gulf of Maine buoys (44007 and 44013).

After 120 hours from the runs start times, similar to the temporal scale, the spatial scale of the assimilation has faded by a considerable amount (Figure 3.15c). Although the assimilation was switched off 48 hours earlier, its effect around buoy 44005 and buoy 44007 can still be seen. It can be also seen from Figure 3.15c that the effect of the assimilation became considerably smaller in comparison with the effect obtained during the assimilation period. Note that the scales in Figure 3.15 are different. Figure 3.15c also shows that for the location of buoy 44013, the results obtained with and without the assimilation are almost equal which can be also seen from Figure 3.7c.

Further evidence for the significance of the effect of assimilation in spatial scale can be seen from the results for storm 4 (subsection 4.3.3) which showed that while data at buoy 44007 were not available for assimilation in this case; significant improvements in wave height predictions can be still seen at this buoy location. Obviously, these improvements have resulted from the assimilation made at other buoy locations. It must be noted here that the spatial scale of the assimilation effect is largely controlled by the assimilation longitudinal and latitudinal ranges of influence. This indicates that using ranges of influence different than those given in Table 4.3 will most likely yield differences in the spatial scale of the effect of assimilation.

3.5 Summary and Conclusions

The research presented in this chapter was motivated by a desire to develop a high resolution operational wave forecasting system for the Gulf of Maine. Such a system is

essentially needed for obtaining reliable wave predictions for the Gulf of Maine nearshore areas at an adequate resolution. The system is based on the state-of-the-art numerical wave model SWAN which accounts for physical mechanisms that affect the wave evolution in both deep and shallow waters. Attempts are made, in this research, to improve the prediction quality of the SWAN-based system through the assimilation of observed wave data at buoys located inside and outside the Gulf of Maine into the wave model. The research mainly investigates the extent to which wave buoy data can be cross validated and assimilated using SWAN model.

In the developed system, the wave model is forced by the ETA predicted wind field which is routinely provided by the National Center for Environmental Predictions (NCEP) obtained in three hours interval. For boundary conditions the system had to rely on wave predictions from the coarser grid wave model WW3 also provided routinely by NCEP. A boundary conditions scheme had to be developed for converting WW3 parametric wave predictions along SWAN domain open boundaries into 2D wave spectra in an operational basis. Data assimilation scheme has also been developed for operationally assimilating the observed significant wave heights at the five buoy locations into the hindcast model simulations. This simple scheme adjusts only the energy levels of the SWAN predicted 2D wave spectra at grid points within the range of influence of each buoy.

The operation of the developed system has been experimentally replicated in a sample case presented in this study. Results obtained for this sample case showed that an

improvement in wave model forecast was achieved at buoy location 44005 as a result of the implementation of the data assimilation scheme. The statistical analysis of the model results have shown that the data assimilation reduced the predicted wave height scatter index by more than 13% in the first 48 hours of the model forecast at the location of buoy 44005. The relaxation time for the effect of assimilation is approximately 36 hours at this buoy location. The data assimilation has a minimal effect at the location of buoys 44007 and 44013, which can be attributed to a significant underprediction of the wind field. This leads to a significantly shorter relaxation time at these two buoy locations.

SWAN model was also used, in this study, to simulate Gulf of Maine seasonal maximum wave conditions observed in the year 2001. To substitute for the un-archived wave predictions by WW3, another boundary conditions scheme had to be developed specifically for this study case. This boundary conditions scheme is based on the continuous assimilation of the observed wave data at the two buoys located outside the Gulf of Maine. In some of the simulated cases in this study, SWAN was able to reproduce most of the changes in the observed wave conditions at the locations of the three buoys inside the Gulf of Maine. In other cases, however, significant differences between model results and observed wave conditions were found. These differences were partially attributed to the mismatch between observed and predicted wind field, while other mismatches may have resulted from an adequate representation of the boundary conditions. For the assimilation-based boundary conditions only the energy levels of the predicted spectra are corrected, while no corrections to the energy distribution over the frequency domain are made. Since the wave period (frequency) is in

fact a controlling factor for wave dissipation, boundary conditions based on poorly distributed spectral energies yield poor wave predictions.

Attempts were made to improve the quality of the model predictions, in three of the seasonal maximum wave conditions simulations, through the assimilation of observed wave data at five buoy locations. Buoy data have been assimilated in an hourly basis into the model simulation for the first 60 or 72 hours before the assimilation scheme is switched off. Results obtained at the end of each hour during the assimilation period showed improvement in wave height model predictions at the locations of three Gulf of Maine buoys. After the assimilation schemes was turned off, the improvements in the wave height predictions were maintained for more than 2 days at one or more buoy locations, while in other cases the relaxation time for the assimilation effect was as short as few hours. For all cases, the data assimilation has reduced the predicted wave height scatter index in the first 48 hours following the assimilation by more than 10% and 20% at the locations of buoys 44005 and 44013 respectively. The overall minimal improvement at buoy location 44007 was not surprising since the largest scatter index in predicted wind speeds always occur at this location.

In addition to the significant temporal scales that have been seen for the assimilation effect, the spatial scales were also shown to be significant. Both scales are probably controlled to large extents by the selection of the assimilation range of influence around each buoy. The effect of assimilation on spatial scale could be seen at the location of one of the Gulf of Maine buoys for which no data were available for

assimilation. Comparisons of the differences between SWAN results obtained with and without assimilation have shown how significant the effect of the assimilation can be on the spatial scale. The comparisons made at different time step during and after the assimilation have also shown the temporal variability in the spatial scale of the assimilation effect.

The concluding remarks provided below intended to answer the following two major questions, relevant to the future of high resolution wave forecasting in the Gulf of Maine. (1) How significant is the impact of the wave data assimilation technique used on the quality of SWAN model predictions?, and (2) Is the assimilation of the observed wave height data sufficient or is the assimilation of other types of observation (e.g. spectral data), which requires higher level of sophistication, needed?.

The data assimilation scheme used in this study had a significant impact in improving the quality of significant wave height predictions. Minor improvements in the predicted mean wave periods occasionally occurred. To a large extent, differences between observations and the model predictions have resulted from mismatches between the observed and predicted wind fields (e.g. buoy 44007). The difference between the two wind fields shortens the relaxation time of the assimilation, hence reducing its effect. This is due to the fact that waves in the model (as in the real world) are mainly controlled by the forcing wind field.

The assimilation of the observed wave heights at the two buoys located outside the Gulf of Maine have not always served adequately as boundary conditions for SWAN model simulations. This is mainly because the assimilation technique used in this study adjusts only the total wave energy levels of the model predicted wave spectra, without the capability of adjusting the energy distribution over the frequency domain. The implementation of the boundary conditions scheme which provides full 2D spectral boundary is probably essential to overcome this limitation.

Correcting the wind field and the use of a more sophisticated assimilation scheme will improve the quality of model predictions. However, the implementation of such techniques in an operational system will be computationally expensive. Nevertheless, expected improvement from any computationally expensive technique will shortly fade away if the model is forced, in the forecast mode, with inaccurately predicted wind fields or boundary conditions. Therefore, no matter how sophisticated the assimilation scheme, the wave model will produce poor results if is forced by poorly predicted wind fields or boundary conditions.

This research has demonstrated that a simple data assimilation scheme that uses only the observed significant wave height to correct the energy level of the predicted full 2D wave spectrum may improve the quality of wave forecasting model predictions. The effect of the assimilation is seen in the model predictions with relaxation times up to 2 days. This suggests that a simple and computationally inexpensive assimilation scheme is sufficient.

In conclusion, the research presented in this chapter has shown that data assimilation would be of greater benefit to high resolution operational wave prediction systems for the Gulf of Maine. Additional studies are necessary to evaluate the applicability and robustness of the Gulf of Maine operational wave prediction system developed in this study.

Chapter Four

SUMMARY AND CONCLUDING REMARKS

Applications of the several existing numerical wave models, nowadays, fall under two major categories: one is practical and the other is scientific. In practical applications models are used as reliable tools to provide near future wave predictions, wave climatology or extreme wave statistics for specific regions. Scientific applications of wave models involve the investigation of methods to improve the model performance, the simulations of extreme cases that rarely occur in the real world and the development of better understanding of physical mechanisms associated with the waves and the way they interact in specific field experiments.

Obviously, models have to go through extensive validation/verification procedures before they can be used in practical applications to provide wave predictions. For the outer ocean wave models, the length scale of the wind-induced changes is large and the combination of the available buoy and satellite data in the domain are generally sufficient for model validation. In coastal areas, however, spatial variability induced by

geometric irregularities can be greater and more complex. Yet, most model domains will have little or no data for validation/calibration. Satellite data close to the coast are not reliable and buoys, if at all present, are too localized to provide a proper representation of the complete wave scattering problem. Even when data are available, they would most likely contain the effects of physical mechanisms not modeled. It is obvious that unlike regional tidal/circulation models, it is difficult to validate or calibrate a regional coastal wave model used in an ocean observing system. In order to invest faith in the predictions, it is therefore necessary to validate the models whenever the opportunity exists and, if satisfactory results are obtained, to apply them at other desired sites in the hope that the predictions are reliable.

In the first part of this thesis, two wave transformation models, SWAN and CGWAVE, were used to simulate wave conditions at the Field Research Facility (FRF), Duck (North Carolina). The domain of interest (FRF) contains a greater number of measurements than are normally available and therefore provided great opportunity for the verification of the two models. The motivation was to examine how well these models reproduce observations and to determine the level of consistency between the two models. Stationary wave conditions pertaining to three different storm-induced bathymetric representations were modeled. It was found that SWAN and CGWAVE reproduced the observed wave behavior to a large extent, but CGWAVE results tended to be somewhat smaller than the SWAN results and the measurements. The differences were attributed to nonlinear wave-wave interactions and breaking. Otherwise the models showed a high level of consistency. Once verified, the two models were also used to

explore other mechanisms reported in the recent literature were it was able to qualitatively confirm observational findings of other researchers regarding wave breaking, triad wave-wave interactions, and wave directional spreading at this site. SWAN and CGWAVE were also used in a quantitative-qualitative sense to investigate the effect of the piles of the FRF research pier on obliquely approaching waves as they pass under the pier during an event that has been studied by other researchers. In contrast to the suggestion made by the other researchers, the results of SWAN and CGWAVE indicated that research pier legs did not have significant effect on the observed wave conditions for the investigated event. The analysis and results presented in this part of the thesis have demonstrated that when the modeled physics are commensurate with what is occurring in the field, numerical wave models provide fairly reasonable and compatible predictions.

Traditionally, numerical wave models were run without the use of actual wave observations to improve the overall quality of the model results. The limited numbers of wave buoy observations were only useful for model validation/verification studies since, for many cases, these buoys are too localized for their measurements to provide a proper representation of the complete wave scattering problem. The significant increase in both spatial and temporal coverage of wave observations, which occurred over the last two decades, is mainly attributed to the wave measurements made available by satellite mounted instruments such as the Synthetic Aperture Radar (SAR) and Wave Altimeter. This dramatic increase in wave observations was utilized for improving the quality of wave model predictions via data assimilation techniques. Although many previous

studies have demonstrated that data assimilation considerably improves wave models predictions, most of these studies; however; have shown that the obtained improvement fades away shortly after turning off the data assimilation scheme. This is mainly due to the fact that waves in the model (and also in the real world) are primarily controlled by the forcing wind field.

The research presented in the second part of this thesis was motivated by the desire to develop a high resolution operational wave forecasting system for the Gulf of Maine. The system is based on the numerical wave model SWAN which accounts for physical mechanisms associate with wave evolution in both deep and shallow waters. The major goal of this research was to examine the impact of buoy data assimilation on the quality of SWAN model predictions for the Gulf of Maine. The extent to which buoy data can be cross validated and assimilated using the wave model was investigated. The data assimilation scheme used in this study had a significant impact in improving the quality of significant wave height predictions. To a large extent, differences between observations and the model predictions have resulted from mismatches between the observed and predicted wind fields (e.g. buoy 44007). The difference between the two wind fields shortens the relaxation time of the assimilation, hence reducing its effect. The assimilation of the observed wave heights at the two buoys located outside have not always served adequately as boundary conditions for SWAN model simulations. This is mainly because the assimilation technique used in this study adjusts only the total wave energy levels of the model predicted wave spectra, without the capability of adjusting the energy distribution over the frequency domain. The implementation of the boundary

conditions scheme which provides full 2D spectral boundary is probably essential to overcome this limitation. Correcting the wind field and the use of a more sophisticated assimilation scheme will improve the quality of model predictions. However, the implementation of such techniques in an operational system will be computationally expensive. Nevertheless, expected improvement from any computationally expensive technique will shortly fade away if the model is forced, in the forecast mode, with inaccurately predicted wind fields or boundary conditions. Therefore, no matter how sophisticated the assimilation scheme, the wave model will produce poor results if is forced by poorly predicted wind fields or boundary conditions. This research has demonstrated that a simple data assimilation scheme that uses only the observed significant wave height to correct the energy level of the predicted full 2D wave spectrum may improve the quality of wave forecasting model predictions. The effect of the assimilation is seen in the model predictions with relaxation times up to 2 days. This suggests that a simple and computationally inexpensive assimilation scheme is sufficient. It can be concluded from this study that data assimilation would be of greater benefit to high resolution operational wave prediction systems for the Gulf of Maine. Additional studies are necessary to evaluate the applicability and robustness of the Gulf of Maine operational wave prediction system developed in this study.

The major contributions of the research presented in this thesis are:

1. In the model validation study presented in the first part of this thesis, scientific model application allowed to explore other mechanisms reported in the recent literature;

the results were either consistent with some observations or they shed more light on others .

2. The second part of the research presented in this thesis represents, to the best of the author's knowledge, one of the earliest studies involving wave data assimilation using SWAN model. The results indicate that even a simple data assimilation scheme can have significant impact on wave forecasting in practical model applications.

REFERENCES

- Battjes, J. A. and Janssen J., 1978. "Energy Loss and Set-Up Due to Breaking of Random Waves." Proc. 16th Int. Conf. Coastal Engineering, ASCE, 569-587.
- Battjes, J. A., 1994. "Shallow Water Wave Modelling." Proc. Int. Sympos.: Waves-Physical and Numerical Modelling, Vancouver, 1-23.
- Bauer, E., Hasselmann, S., Hasselmann, K. and Graber, H. C., 1992. "Validation and Assimilation of Seasat Altimeter Wave Heights Using the WAM Wave Model." *J. Geophys. Res.*, 97, C8, 12671-12682.
- Bondzie, C. and Panchang V. G., 1993. "Effects of Bathymetric Complexities and Wind Generation in a Coastal Wave Propagation Model." *Coastal Engg.*, 21, 333-336.
- Booij, N., Holthuijsen, L. H. and Ris, R. C., 1996. "The "SWAN" Wave Model for Shallow Water." Proc. 25th Int. Conf. Coastal Engineering, ASCE, 668-676.
- Booij, N., Holthuijsen, L. H., Doorn N., and Kieftenburg, A. T. M. M., 1997. "Diffraction in a Spectral Wave Model." Ocean Wave Measurements and Analysis: Proc. 3rd Int. Sympos., Waves97, ASCE, 243-255.
- Booij, N., Ris, R. C. and Holthuijsen, L. H., 1999. "A Third-Generation Wave Model for Coastal Regions, 1, Model Description and Validation." *J. Geophys. Res.*, 104, C4, 7649-7666.
- Bova, S. W., Breshears, C. P., Cuicchi, C., Demirbilek, Z. and Gabb, H. A., 2000. "Dual level Parallel Analysis of Harbor Wave Response Using MPI and OpenMPI. Internat. " *J. High Performance Computing Applic.* v14, 1, 49-64.

Breivik, L. A., Reistad, M., Schyberg, H., Sunde, J., Krogstad, H. E. and Jonsen, H., 1998. "Assimilation of ERS SAR Wave Spectra in an Operational Wave Model." *J. Geophys. Res.*, 103, C4, 7887-7900.

Chawla, A., Ozkan-Haller, H. T. and Kirby J. T., 1998. "Spectral Model for Wave Transformation and Breaking Over Irregular Bathymetry." *J. Wtrwy, Port, Coast, Ocean. Engg.*, 124, 843-855.

Chen, H. S. and Houston J. R., 1986. "Calculation of Water Level Oscillation in Coastal Harbors." Instruc. Repr. CERC-87-2, Coastal Engr. Research Center, WES, Vicksburg, Mississippi, 39108.

Chen, Y., Guza, R. T. and Elgar, S., 1997. "Modeling Spectra of Breaking Surface Waves in Shallow Water." *J. Geophys. Res.*, 102, C11, 25035-25046.

Dally, W. R., Dean, R. G. and Dalrymple, R. A., 1985. "Wave Height Variation Across Beaches of Arbitrary Profile." *J. Geophys. Res.*, 90, C6, 11917-11927.

Dean, R. G., and Dalrymple, R.A., 1984 "*Water Wave Mechanics for Engineers and Scientists.*" Prentice-Hall, Inc., New Jersey

Demirbilek, Z. and Panchang, V. G., 1998. "CGWAVE: A Coastal Surface Water Wave Model of the Mild Slope Equation." Tech. Rept. CHL-98-26, US Army Corps of Engineers, Waterways Expt. Station, Vicksburg, Mississippi, 39180.

Dickson, S. M., 1999. "The Role of Storm-Generated Combined Flows in Shoreface and Inner Continental Shelf Sediment Erosion, Transport, and Deposition.", Ph.D. Thesis, The Graduate School, University of Maine, UMI Microform 9926402.

Dunlap, E. M., Olsen, R. B., Wilson, L., De Margerie, S. and Lalbeharry, R., 1998. "The Effect of Assimilating ERS-1 Fast Delivery Wave Data into the North Atlantic WAM Model.", *J. Geophys. Res.*, 103, C4, 7901-7915.

Ebersole, B. A., Cialone, M. A. and Parter, M. D., 1986. "Regional Coastal Processes Numerical Modeling System: Report 1,: RCPWAVE – A Linear Wave Propagation Model for Engineering Use." Tech. Rept. CERC-86-4, Coastal Engg. Research Center, WES, Vicksburg, Mississippi, 39108.

Elgar, S., Guza, R. T., Herbers, T. H. C., Raubenheimer, B. and Gallagher, E. L., 1997. "Spectral Evolution of Shoaling and Breaking Waves on a Barred Beach." *J. Geophys. Res.*, 102, C7, 15797-15805.

Elgar, S., Guza, R. T., O'Reilly, W. C. O., Raubenheimer, B. and Herbers, T. H. C., 2001. "Wave Energy an Direction Observed Near a Pier." *J. Wtrwy., Port, Coast, Ocean. Engg.*, 127, 1, 1-6.

Gallagher, E. L., Elgar, S. and Guza, R. T., 1998. "Observation of Sand Bar Evolution on a Natural Beach." *J. Geophys. Res.*, 103, C2, 3203-3215.

Gilhousen, W. R., Meindl, E. A., Changery, M. J., Franks, P. L., Burgin, M. G. and McKittrick, D. A., 1990. "Climatic Summaries for NDBC Buoys and Stations." National Weather Service, National Data Buoy Center Update 1, NSTL, Mississippi.

Herbers, T. H. C., Elgar, S. and Guza, R. T., 1999. "Directional Spreading of Waves Nearshore." *J. Geophys. Res.*, 104, C4, 7683-7693.

Herbers, T. H. C., Russnogle, N. R. and Elgar, S., 2000. "Spectral Energy Balance of Breaking Waves within the Surf Zone." *J. Phys. Oceaogr.*, 30, 2723-2737.

Holthuijsen, L. H., Booij, N., Van Endt, M., Caires, S. and Guedes Soares, C., 1996. "Integral Control Data Assimilation in Wave Predictions." Proc. 25th Int. Conf. Coastal Engineering, ASCE, 725-753.

Holthuijsen, L. H., Booij, N., Ris, R. C., R., Haagsma, IJ. G., Kieftenburg, A. T. M. M. and Kriezi, E. E., 2000. "SWAN Cycle III Users' Manual." For SWAN version 40.11, Unauthorized Electronic Version, Delft Univ. Techn..

Howd, P. A. and Birkemeier, W. A., 1987. "Storm-Induce Changes During Duck85." Coastal Sediments'87, ww Div./ ASCE, New Orleans, LA, 834-847.

Janssen, P. A. E. M., Lionello, P., Reistad, M. and Hollingsworth, A., 1989, " Hind-Casts and Data Assimilation Studies with WAM Model During the SEASAT Period." *J. Geophys. Res.*, 94, 973-993.

Jensen, R. E., 1983. "Atlantic Coast Hindcast, Shallow-Water Significant Wave Information." U.S. Army Corps of Engineers, WES, Report 9, Vicksburg, Mississippi.

Kaihatu, J. and Kirby J. T., 1995. "Nonlinear Transformation of Waves in Finite Water Depth. *Phys. Fluids.*, 7(8), 1903-1914.

Kirby, J. T. and Ozkan, H. T., 1994. "Combined Refraction/Diffraction Model for Spectral Wave Conditions." CARC Rept. No, 94-04, University of Delaware.

Komen, G. J., Cavaleri, L., Donlean, M., Hasselmann, K., Hasselmann, S. and Janssen, P. A. E. M. 1994. "*Dynamics and Modeling of Ocean Waves.*" Cambridge University Press.

Lionello, P., Günther, H. and Janssen P. A. E. M., 1992. "Assimilation of Altimeter Data in a Global Third Generation Model." *J. Geophys. Res.*, 97, C8, 14453-14474.

Massel, S. R., 1996. "Ocean Surface Waves: their Physics and Predictions." Advanced Series on Oce. Engg., Vol. 11, World Scientific.

Mei, C. C., 1983. "The Applied Dynamics of Ocean Surface Waves." Wiley, New York.

Miller, H. C., Birkemeier, W. A. and Dewall, A. E., 1983. "Effects of CERC Research Pier on Nearshore Processes." Coastal Structures '83, US Army Coastal Engineering Research Center, 769-784.

Panchang, V. G., Ge, W., Pearce, B. R. and Briggs, M. J., 1990a. "Numerical Simulation of Irregular Wave Propagation Over a Shoal." *J. Wtrwy., Port, Coast, Ocean. Engg.*, 116, 3, 324-340.

Panchang, V. G., Pearce, B. R. and Puri, K. K., 1990b. "Hindcast Estimate of Extreme Wave Conditions in the Gulf of Maine." *Applied Oce. Res.*, Vol. 12, No. 1, 43-49.

Panchang, V. G., Xu, B. and Demirbilek, Z., 1998. "Wave Prediction Models for Coastal Engineering Applications." Ch. 4 in: *Developments in Offshore Engineering*, Ed. J. B. Herbich, Gulf Publishing, Houston, TX, 163-194.

Panchang, V. G., Chen, W., Xu, B., Schlenker, K., Demirbilek, Z. and Okihiro, M., 2000. "Exterior Bathymetric Effects in Elliptic Harbor Wave Models *J. Wtrwy., Port, Coast, Ocean. Engg.*, 126, 2, 71-78.

Panchang, V. G. and Demirbilek, Z., 2001. "Simulation of Waves in Harbors Using Two Dimensional Elliptic Equation Models." *Advances in Coastal & Ocean Engineering*, vol. 7. (World Scientific), pp 125-162.

Pearce, B. R., & Panchang, V. G., 1985. "A Method for the Investigation of Steady State Wave Spectra in Bays *J. Wtrwy., Port, Coast, Ocean. Engg.*, 111, 4, 629-644.

Resio, D. T., 1993. "STWAVE: Wave Propagation Simulation Theory, Testing and Application." Department of Oceanography , Ocean Engineering, and Environmental Science, Florida Institute Techn.

Ris, R. C., 1997. "Spectral Modeling of Wind Waves in Coastal Areas." Commun. On Hydraulics and Geotechnical Engineering, Rep. No. 97-4, Delft Univ. Techn..

Ris, R. C., Booij, N., Holthuijsen, L. H., Padilla-Hernandez, R., Haagsma, IJ. G., 1998. "SWAN Cycle II Users' Manual." For SWAN version 30.75, Unauthorized Electronic Version, Delft Univ. Techn..

Ris, R. C., Holthuijsen, L. H. and Booij, N., 1999. "A Third-Generation Wave Model for Coastal Regions, 2, Verification." *J. Geophys. Res.*, 104, C4, 7667-7681.

Siddabathula, M. and Panchang V. G., 1996 "Quality Control of Geosat Wave Data for Engineering Applications." Proc. 25th Int. Conf. Coast. Engg., Orlando, Sept 1996, 81-94.

Sorensen, R. M., 1993. "*Basic Wave Mechanics for Coastal and Ocean Engineers.*" Wiley, New York.

Tang, Y. and Ouellet Y., 1997. "A New Kind of Nonlinear Mild-Slope Equation for Combined Refraction-Diffraction of Multifrequency Waves." *Coastal Engg.*, 31, 3-36.

Thieler, E. R., Pilkey, O. H., Young, R. S., Bush, D. M. and Chai, F., 2000. "The Use of Mathematical Models to Predict Beach Behavior for Coastal Engineering: A Critical Review." *J. Coastal Res.*, 16, 1, 48-70.

Thompson, E. F., Chen, H. S. and Hadley, L. L., 1996. "Validation of Numerical Model for Wind Waves and Swell in Harbors." *J. Wtrwy, Port, Coast, Ocean. Engg.*, 122, 5, 245-256.

Tolman, H. L., 1989: "The Numerical Model WAVEWATCH: a Third Generation Model for the Hindcasting of Wind Waves on Tides in Shelf Seas." Commun. Hydraulic and Geotechnical Engg, Delft Univ. of Techn., ISSN 0169-6548, Rep. No. 89-2.

Voorrips, A. C., Herbsbach, H., Koek, F. B., Komen, G. J., Makin, V. K. and Onvlee, J. R. N., 1996. "Wave Prediction and Data Assimilation at the North Sea." KNMI memo OO-96-04.

Young, I. R., 1999. "*Wind Generated Ocean Waves.*" Elsevier Ocean Engineering Book Series, Vol. 2. Elsevier Sci. Ltd, Oxford

Zhao, L., Panchang, V. G., Chen, W., Demirbilek, Z. and Chhabbra, N., 2001. "Simulation of Breaking Effects in a Two-dimensional Harbor Wave Prediction Model." *Coastal Engg.*, v42, 4, 359-373.

Zundel, A. K., Fugal, A. L., Jones, N. L., and Demirbilek, Z., 1998. "Automatic Definition of Two-dimensional Coastal Finite Element Domains." 693-700, in: *Hydroinformatics98, Proc. 3rd Int. Conf. Hydroinformatics.* Ed. V. Babovic and L. C. Larsen. A. A. Balkema, Rotterdam.

Appendix

STATISTICAL PARAMETERS

For time series of length (N) the observed (obs) and model computed (com) wind or wave parameter (X) are used to calculate the bias according to the following relation:

$$Bias = \frac{1}{N} \sum_1^N (X_{com} - X_{obs}) \quad (A.1)$$

The root mean square of the error (RMSE) is calculated as follows:

$$RMSE = \sqrt{\left[\frac{1}{N} \sum_1^N (X_{com} - X_{obs})^2 \right]} \quad (A.2)$$

Normalizing the RMSE by the mean of the observations yield the scatter index (SI):

$$SI = \frac{RMSE}{\bar{X}_{obs}} \times 100 \quad (A.3)$$

The correlation is calculated as follows:

$$Cor = 1 - \frac{RMSE}{\bar{X}_{obs}} \quad (A.4)$$

BIOGRAPHY OF THE AUTHOR

Khalid M. Zubier was born in Jeddah, Saudi Arabia, on June 22, 1968. He grew up in Jeddah where he graduated from Raudhat Al-Ma'aref School in 1985. He attended King Abdulaziz University, Jeddah and Graduated in 1990 with a B.Sc. degree in Marine Physics. After graduation Khalid was appointed a position in the Marine Physics Department, King Abdulaziz University, and was sponsored by the University to pursue his graduate education in the United States.

Khalid came to Maine in 1992 and joined the Oceanography Department, at The University of Maine, right after he attended a semester in the University's Intensive English Institute. Khalid pursued his M.S. in Oceanography under the supervision of Dr. Neal Pettigrew. Right after Khalid received his M.S. degree in Oceanography from The University of Maine in 1997 he started pursuing his Ph.D. degree in Oceanography at the School of Marine Sciences, The University of Maine under the supervision of Dr. Vijay Panchang. Upon the completion of his Ph.D. degree requirements in the United States, Khalid will return back to his home country, Saudi Arabia, where he will join the Marine Physics Department, King Abdulaziz University as an Assistant Professor. Khalid is a candidate for the Doctor of Philosophy degree in Oceanography from The University of Maine in August, 2002.